COMBATING BACTERIAL INFECTIONS WITH *IN-SITU* DETECTION AND ANTIBIOTIC TECHNOLOGY

BY

PAUL JAMES RENICK

DISSERTATION

Submitted in partial fulfillment of the requirements
for the degree of Doctor of Philosophy in Quantitative Biology at
The University of Texas at Arlington
August 2020

Arlington, Texas

Supervising Committee:

Liping Tang, Supervising Professor
Mike Roner, Supervising Professor
He Dong
Joseph Boll
Woo-Suk Chang
Lei Shi

ABSTRACT

COMBATING BACTERIAL INFECTIONS: UNDERSTANDING DEVICE INFECTIONS, NOVEL *IN SITU* DETECTION AND NEW ANTIBIOTIC TECHNOLOGY

Paul James Renick, Ph.D.

The University of Texas at Arlington, 2020

Supervising Professors: Liping Tang and Mike Roner

Currently, there is a looming crisis in the field of antibacterial drug therapy. The emergence of antibacterial drug resistance because of poor antibacterial stewardship, coupled with booming elderly populations, economic disparity and climate change leading to societal instability is undoing the successes of the 20th century in combating infectious disease. New approaches and methods are needed to reverse these trends. My dissertation focuses on three key areas: (1) develop a better understanding of device-related biofilm infections, (2) the use of a bacterial specific D-glutamine positron emission tomography tracer for the direct visualization of infection, and (3) the development of an acid-activated antimicrobial strategy. Each of these areas represents an opportunity to reverse the negative trends of the past few decades. A greater understanding of device-related biofilm infections can provide insight to new treatment modalities, direct imaging of infection will allow more accurate diagnosis of infection and help drive preclinical drug discovery by being able to non-invasively track therapy efficacy, while low pH-activated antimicrobial peptides serve as an example of emerging technologies to directly combat resistance under specific conditions found in infections. These are examples of next-generation ideas applied to the development of antibacterial agents, enhanced imaging tools for diagnosis and targeted antibacterial therapies.

ACKNOWLEDGEMENTS

I would like to thank my Supervising Committee for their patience and guidance during my doctoral studies. I also would like to thank my collaborators from the University of Texas Southwestern for their help, input and support with my project

Lastly, I would like to acknowledge the support of my co-workers and management at Smith+Nephew for providing advice and support.

Chapter 2 is reprinted by permission from Springer Nature (Springer International Publishing) Racing for the Surface: Pathogenesis of Implant Infection and Advanced Antimicrobial Strategies, by Bingyun Li, Fintan Moriarty, Thomas Webster, Malcolm Xing (Eds.)

Chapter 5 is reproduced with permission from Journal of Material Chemistry B

DEDICATION

I would like to dedicate my dissertation to my family whose love and support has been critical through my dissertation, especially my children, Hayley and Luka, who have been my inspiration. I also appreciate the support of my friends who provided support throughout the entire experience. I greatly appreciate the support, mentoring and encouragement of my supervisory committee, Drs. Tang, Roner, Chang, Dong, Boll and Shi. Finally, my coworkers and friends in the Smith+Nephew Biologics R&D group and my management who helped make this happen. I could not have done this without all of you.

TABLE OF CONTENTS

LIST OF FIGURES

LIST OF TABLES

LIST OF ABBREVIATIONS

AMP	Antimicrobial peptide
AUC/MIC	Area under the inhibitory curve over MIC
BPA	Bacterial protease activity
CD	Circular dichroism
CO2	Carbon dioxide
Cmax/MIC	peak level divided by MIC
CsCN	Azanylidynemethane;cesium
CRP	C-reactive protein
CT	Computerized tomography
DAA	D-amino acids
DNA	Deoxyribonucleic acid
eDNA	Extracellular deoxyribonucleic acid
EPS	Extracellular polymeric matrix
ESR	Erythrocyte sedimentation rate
FISH	Fluorescent in situ hybridization
Gln or Q	Glutamine
His or H	Histidine
H&E	Haemotoxylin and eosin
HCN	Hydrogen cyanide
Lys or K	Lysine
kDa	Kilodalton
Leu or L	Leucine
MALDI-TOF	Matrix assisted laser desorption/Ionization time-of-flight mass spectrometry

MIC	Minimum inhibitory concentration
MDP	Multidomain peptide
MRI	Magnetic resonance imaging
MRSA	Methicillin resistant *Staphylococcus aureus*
MTT	3-(4,5-dimethylthiazol-2-yl)-2,5-diphenyltetrazolium bromide
OSEM3D/MAP	Ordered subsets expectation maximization
PABA	Para-aminobenzoic acid
PBS	Phosphate buffered saline
PCR	Polymerase chain reaction
PCT	Procalcitonin
PEG	Polyethylene glycol
PET	Positron emission tomography
PGLA	D, L, -lactic-co-glycolic acid
PK/PD	Pharmacokinetic/pharmacodynamic
PIA	Polysaccharide intracellular adhesion
QS	Quorum sensing
RBC	Red blood cell
ROS	Reactive oxygen species
SACs	Surface active compounds
SANs	Self-assembling nanofibers
SEM	Scanning electron microscopy
SFDI	Spatial frequency domain imaging
SPECT	Single photon emission computed tomography
SUV	Standardized uptake unit
TA	Toxin-antitoxin
TSB	Trypticase soy broth

TEM	Transmission electron microscopy
T/MIC	Time above MIC
UV	Ultraviolet
W	Tryptophan
WBC	White blood cell
X-ray	Radiography

CHAPTER 1

INTRODUCTION

Currently medicine is facing a crisis in our armamentarium to fight bacterial diseases. While great strides have been made in combating infectious disease via vaccination, antibiotics, and sanitation, approximately eighty years-ago the first reports of drug resistance emerged (1-3). The emergence of drug-resistant pathogens has led some to state that we are entering the post-antibiotic era and return to pre-1920's morbidity and mortality from infectious disease. The antimicrobial resistance burden on world healthcare systems, coupled with the rise of older and elderly populations in developed nations, poor antibacterial stewardship, the impact of climate change, and geopolitical instability of a multipolar world pessimistically predicts a coming medical crisis in infectious disease (4-6).

Considering the issues stated above, I wanted to take a look at technologies that could help in the fight on antibiotic resistance. At a superficial level, this could be regarded as increasing our knowledge of infectious disease and resistance development. Since resistance development is tied to the use of antibiotics, I thought about how antibiotics are prescribed. The first time a patient is prescribed antibiotics it is usually in the context of empiric therapy(7, 8). In most cases, especially critical care cases where immediate intervention is required, empiric therapy results in the use of broad spectrum agents against a methodical "best-guess" of pathogen based on clinical presentation, past physician experience, and past clinical outcomes. With this as a starting point I identified that areas that I believed would make a meaningful impact in combating resistance. With this as a starting point I identified that areas that I believed would make a meaningful impact in combating resistances. In medical devices many the infections are caused bacterial biofilms(9). A better understanding of these types of biofilm infections would allow for the development of new technologies for the prevention and treatment of biofilm device-related infections. A second area for improvement would be *in situ* confirmation of

infection and diagnosis of infection. If technologies can be developed to either provide more information to guide empiric therapy or to identify bacteria from these *in situ* methods. As part of my graduate work, I helped author a review of the current wound diagnosis technology, including innovative methods of non-invasive diagnosis. Additionally, in collaboration with UTSW, we developed a bacterial specific positron emission tomography based on the utilization of D amino acids by bacteria. Better diagnosis will ideally result more judicious and appropriate use of antibiotics which will ideally reduce the emergence of antibiotic resistance. Finally, the development of new antibiotics that are efficacious, designed with the knowledge of the resistance problem and have less-side effects would be beneficial to combating antimicrobial resistance. Designing antibiotics around known resistance mechanisms has expanded the utility of several classes of antibiotic such as penicillins, cephalosporins and quinolones. The advent of delivery technologies such as PGLA microbeads and nanotechnology(10, 11) could improve dosing and limit the exposure of the host microbiome to antibiotics. The host microbiome is placed under the same selective pressure as pathogens and can serve as a reservoir of resistance factors that can be spread via horizontal gene transfer(12). Some of these delivery technologies using targeting approaches can also reduce the risk of antibiotic associated adverse events(13, 14) improving patient safety as well as effecting only the pathogens.

Over the course of my graduate studies, I have explored these three areas that can help reverse the negative trends of the past decades in the publications listed below for my article-based dissertation.

#1. Renick P, Tang L. 2020. Device-Related Infections, p 171-188. In Li B, Moriarty TF, Webster T, Xing M (ed), Racing for the Surface: Pathogenesis of Implant Infection and Advanced Antimicrobial Strategies doi:10.1007/978-3-030-34475-7_7. Springer International Publishing.

Medical devices have been a life changing development in medicine with roles in restoring mobility, vision, bodily functions, regulation of bodily functions and enable easy and relatively painless introduction of drugs and nutrients. One of the main caused of medical device failure is the establishment of biofilm infections on these devices, resulting in significant patient morbidity and mortality. Bacteria exploit the localized inflammation and surface conditioning by host proteins to infect these devices by non-specific and specific ligand binding. Once established the local concentration of bacteria forms a biofilm, a colonial organization of bacteria encased in an exopolysaccharide matrix. The presence of this matrix provides physical protection from the environment, emergent drug resistance properties and an ideal environment for horizontal gene transfer of drug resistance. These factors make treating biofilm extremely difficult and will require new approaches for control and eradication.

Drawing on my own experience working in this field and a review of up to date literature, I wrote a review with Dr. Tang on device related infection exploring the role of biofilm in device related infection.

#2. Renick PJ, Mulgaonkar A, Co CM, Wu C-Y, Pennington J, Sherwood A, Velazquez A, Quan B, Oz OK, Tang L, Sun X. Development of D-glutamine-derived PET tracer for diagnosing bacterial infection *in vivo*. (to be submitted).

The second article focuses on the exploration of improved detection modalities, I have collaborated with the Sun lab at UTSW in the development of [^{11}C]-D-glutamine positron emission tomography tracers to directly detect the presence of both gram-positive and gram-negative myositis. Body of work shared here details the development and synthesis of the tracer and the mouse myositis infection model that was used to validate the ability of the tracer that is specific for the detection of bacterial infection.

I was the key lead on both the microbiology and the development of the dual infection in the *in vivo* mouse myositis model used for tracer development. My additional roles in the collaboration were experimental design, data analysis and training of both UTSW and UTA students on both the microbiology and animal methods.

#3 Li Shuxin, Renick PJ, Senkowsty, J, Nair, AM, Tang L. (2020). "Diagnostics for Wound Infections" Advances in Wound Care. Ahead of Print.

I was a co-author of a review publication by Shuxin Li under Dr. Liping Tang covering the diagnostics of wound infections. The review show-cased the current methods used to detect wound infection and provided insight to the strengths and limitations of those methods. Additionally, new technologies for use in this field were explored.
My contribution to the review was to provide information regarding the microbiological methods discussed and information on *in situ* visualization of wound infection using nuclear medicine and molecular methods.

#4. Chen W, Li S, Renick P, Yang S, Pandy N, Boutte C, Nguyen KT, Tang L, Dong H. 2019. Bacterial acidity-triggered antimicrobial activity of self-assembling peptide nanofibers. Journal of Materials Chemistry B 7:2915-2919.

There has been a dearth of antibacterial agents developed recently and from 2003-2017 there were only 4 truly novel classes of antibacterial agents (linezolid, daptomycin, fidaxomicin and monoclonal antibodies for *B. anthracis*) that were approved for clinical use with many approved agents were improvements on existing classes. A strategy for new agent development focuses on the development of multidomain antimicrobial peptides form self-assembling nanofibers in basic and neutral pH, only disaggregating and becoming active in acidic conditions. This new

method for delivery also has the potential to reduce side-effects such as hemolysis and cytotoxicity since they only activate under acidic conditions.

My role in this body of work was to perform *in vitro* efficacy screening of a library of these peptides, evaluating the antimicrobial activity at physiological and acidic pH. I also was responsible for modifying the testing methods under the nonstandard conditions need to evaluate the activity at acidic pH.

References

1. Lobanovska M, Pilla G. 2017. Penicillin's Discovery and Antibiotic Resistance: Lessons for the Future? Yale J Biol Med 90:135-145.

2. Davies J, Davies D. 2010. Origins and evolution of antibiotic resistance. Microbiol Mol Biol Rev 74:417-33.

3. Aminov RI. 2010. A brief history of the antibiotic era: lessons learned and challenges for the future. Front Microbiol 1:134.

4. Connolly MA, Heymann DL. 2002. Deadly comrades: war and infectious diseases. The Lancet 360:s23-s24.

5. Raoult D. 1998. Infectious disease. Return of the plagues. The Lancet (British edition) 352 Suppl 4:SIV18.

6. Letendre K, Fincher CL, Thornhill R. 2010. Does infectious disease cause global variation in the frequency of intrastate armed conflict and civil war? Biological Reviews 85:669-683.

7. Beović B. 2019. Empiric Antimicrobial Therapy. http://esgap.escmid.org/?page_id=389. Accessed March 15.

8. MacDougall C. 2019. Guidelines for Empiric Antimicrobial Therapy | Infectious Diseases Management Program at UCSF. https://idmp.ucsf.edu/guidelines-empiric-antimicrobial-therapy. Accessed March 15.

9. Malone M, Bjarnsholt T, McBain AJ, James GA, Stoodley P, Leaper D, Tachi M, Schultz G, Swanson T, Wolcott RD. 2017. The prevalence of biofilms in chronic wounds: a systematic review and meta-analysis of published data. J Wound Care 26:20-25.

10. Gaspar LMdAC, Dórea ACS, Droppa-Almeida D, de Mélo Silva IS, Montoro FE, Alves LL, Macedo MLH, Padilha FF. 2018. Development and characterization of PLGA nanoparticles containing antibiotics. Journal of nanoparticle research : an interdisciplinary forum for nanoscale science and technology 20:1-9.

11. Radovic-Moreno AF, Lu TK, Puscasu VA, Yoon CJ, Langer R, Farokhzad OC. 2012. Surface charge-switching polymeric nanoparticles for bacterial cell wall-targeted delivery of antibiotics. ACS nano 6:4279-4287.

12. Leónidas Cardoso L, Durão P, Amicone M, Gordo I. 2020. Dysbiosis individualizes the fitness effect of antibiotic resistance in the mammalian gut. Nature Ecology & Evolution doi:10.1038/s41559-020-1235-1.

13. Geller AI, Lovegrove MC, Shehab N, Hicks LA, Sapiano MRP, Budnitz DS. 2018. National Estimates of Emergency Department Visits for Antibiotic Adverse Events Among Adults—United States, 2011–2015. Journal of General Internal Medicine 33:1060-1068.

14. Tamma PD, Avdic E, Li DX, Dzintars K, Cosgrove SE. 2017. Association of Adverse Events With Antibiotic Use in Hospitalized Patients. JAMA Internal Medicine 177:1308-1315.

CHAPTER 2

DEVICE RELATED INFECTIONS

COMPLETE REFERENCE:

RENICK, P. AND L. TANG (2020). DEVICE-RELATED INFECTIONS. RACING FOR THE SURFACE: PATHOGENESIS OF IMPLANT INFECTION AND ADVANCED ANTIMICROBIAL STRATEGIES. B. LI, T. F. MORIARTY, T. WEBSTER AND M. XING. (ED), SPRINGER INTERNATIONAL PUBLISHING: 171-188.

Device-Related Infections

Abstract Device-related infection is responsible for a quarter of all health-care-associated infections and can even compromise device function. These infections are caused by the colonization of microorganisms during the implantation processes. Unfortunately, the treatment option for device-related infection is limited. To make the situation worse, some of these organism's form biofilms that cover the device surface notably weakening the effectiveness of antimicrobial treatments. This chapter summarizes our current understanding of the pathogenesis of device-related infection. It also discusses our knowledge of the processes governing the formation, regulation, and resistance of biofilms. Finally, we introduce several new methods developed for diagnosing and treating biofilm infections on medical devices.
Keywords Medical device, infection, extracellular polymeric substances, biofilm, protein, biomaterials, fibrinogen, implants, hydrophobic, quorum sensing, surface-active compounds, diagnosis

Introduction

Medical devices have transformed health care significantly improving the lives of patients. The incorporation of medical devices to treatment have restored mobility, regulated or restored body functions and permitted easy and relatively painless drug delivery. Examples of these devices include: as cardiac implants (pacemakers, vascular grafts, cardiac valves), central and peripheral vascular catheters, endotracheal tubes, contact lenses, tissue fillers/breast implants, orthopedic and prosthetic implants and urinary catheters (1). Unfortunately, implanting devices can result in the introduction of normally benign flora or pathogenic organisms resulting in

infection and compromising device function. This represents significant burden on the healthcare systems and causes significant morbidity and mortality. Device-related infections account for 25.6% of all health-care-associated infections in the US(2) and a 6.4% prevalence in England with 1,000,000 reported per year(3). The routes of infection include surgical implantation procedures, placement of devices in extended contact with mucous membranes and hematogenous seeding(4, 5). Causative organisms include gram-positive bacteria such as *Staphylococcus aureus, Staphylococcus epidermidis*, Coagulase-negative *Staphylococci, Streptococcal* species, *Enterococcus faecalis* and Enterococcal species. *S. aureus* and S. *epidermidis* are known to make up the majority of prosthetic implant infections(2, 3). Commonly isolated gram-negative species include *Pseudomonas aeruginosa, Escherichia coli, Proteus miriabilis* and *Klebsiella pneumoniae*(1, 3, 6). In addition to bacteria, yeasts, especially Candida species can play a role in these infections(6).

Further complicating device infection is the formation of biofilms by the infecting organisms. A biofilm is a highly organized aggregate of bacteria (or yeast) attached to a surface or each other that secretes hydrated extracellular polymeric substances (EPS). The EPS is comprised of polysaccharides, extracellular DNA, and proteins. Biofilms are known to exhibit community behavior, communicating and regulation gene expression in the biofilm by quorum sensing molecules. The biofilm aggregate represents a defense against hostile environments (chemotherapy, immune response and predation) enabling the survival of the microorganisms in the biofilm(7-14). Biofilm formation on devices occurs in several steps: attachment to conditioned implant surfaces, microcolony formation, maturation and dispersal. A graphical summary of these traits is shown in Figure. 1.

Implant Surface Conditioning

Immediately after implantation, medical devices are rapidly coated with host proteins, specifically plasma proteins that condition the surfaces of the implants. Most of the implant devices are hydrophobic attracting proteins like albumin, immunoglobulin IgG and fibrinogen. Once in contact with these surfaces, the proteins can either maintain a configuration similar to the configuration in the liquid phase or, due to conditions in the local environment, unfold and denature exposing occult epitopes to the immune system enhancing inflammation at the implant site (15). An example of this is the binding and conformational change of the serum protein fibrinogen. In Tang et al (20), it was demonstrated that fibrinogen underwent a time-dependent conformational change, exposing the occult sequences P1 and P2. These epitopes enhanced the recruitment of phagocytic cells to the implant, increasing levels of inflammatory cytokines, suggesting that these two epitopes are linked to fibrotic reactions (16). In this background of inflammation and surface coating, bacteria have developed a means to exploit and bind to these host proteins that coat implanted materials. Figure 2 shows an image of S. aureus biofilm that has formed on a host-conditioned catheter segment.

Bacterial Adhesion to Surfaces

Bacterial adhesion is a two-step process with a primary adhesion step (“docking”) and a secondary adhesion step (“locking”) (17). The first stage of adhesion is random with the organism arriving at the surface by chance. This process occurs by physiochemical interactions (hydrophobic, electrostatic, van der Waals forces, temperature and hydrodynamic forces). These interactions are reversible and can be altered by environmental conditions and depend on the net sum of attractive and repulsive forces over a critical proximity to the surface (17).

Overall, electrostatic interactions favor repulsion based on bacterial and surface negative charges, while hydrophobic interactions drive primary adhesion (17, 18). The secondary adhesion or “Locking” is facilitated by receptor-ligand reactions between the bacteria and the surface. This step of adhesion is permanent unless disrupted by mechanical and physical means. Once this secondary binding is complete, the process of biofilm formation begins (2, 8, 17). Figure 2 shows a scanning electron microscopy (SEM) established biofilm on a Teflon-coated catheter segment.

Binding to abiotic surfaces by bacteria is driven by nonspecific means such as electrostatic, hydrophobic and hydrophilic interactions mentioned above but different mechanisms come into play on conditioned surfaces (2, 8, 17-19). In the case of device-related infections, the bacteria encounter surfaces that are preconditioned by host proteins. Bacteria have developed a wide array of adhesion that can exploit collagen, fibronectin, fibrinogen, and lectin and can express a variety of surface-active compounds (SACs) to aid in attachment (17, 18, 20). *S. epidermidis* has been demonstrated to have competitive binding for fibronectin with heparin (19) and the ability of *S. aureus* to bind to a variety of epitopes including fibrinogen, collagen and bone sialoprotein is well documented (20-23). There is evidence that suggests *E. coli* and *Pseudomonas aeruginosa* can alter their surface hydrophobicity by the secretion of SACs (18). *Pseudomonas aeruginosa* expresses PA-IL and PA-IIL which recognize host glycans (24). (24).Other bacteria cell surface features that initiate or aid in binding include flagella, lipopolysaccharides (LPS), fimbriae, mycolic acids and lipopolysaccharides (8). Additionally, their context and environmental conditions can result in distinct adhesion coming into play to aid with surface attachment. The El Tor strain of *Vibrio cholera* when in contact with borosilicate uses a mannose-sensitive hemagglutinin not associated with pathogenicity to bind to these surfaces. In contrast with this, when the bacteria comes in contact to chitin, a virulence-associated toxin-coregulated pilus is used to attach and begin biofilm formation (25). Another feature of some of these adhesions is that they are transcriptionally regulated and are

expressed either during the planktonic or sessile phases of life. Polysaccharide intercellular adhesion (PIA) expressed by *S. epidermidis* is an example of these transcriptionally regulated inhibitors. Interruption of the icxADBC operon controlling the expression of PIA results in impaired adherence mutants, while expression in a deficient strain enables attachment to surfaces (17, 26-28). The binding of organisms to surfaces can also promote the adhesion of other organisms to the surface and each other (29). For example, Leung et al. demonstrated in an *in vitro* biofilm model that colonization of biliary stents by *E. coli* enhances the binding of *Enterococcus* (29).

Biofilm Formation

After adhesion to the surface, bacteria form microcolonies composed of single and multiple species of bacteria, alter their phenotypes to a sessile existence and begin to express EPS. The maturing biofilm develops stratified structures with nutrient channels and differing zones of metabolic rates and genomic expression giving rise to a situation analogous to tissues in higher organisms (30, 31). As the high densities of cells limit the rate of growth and nutrients (31), biofilms display altruistic and cooperative properties (32). In multispecies biofilms, different species can utilize alternative catabolic pathways and feed off the metabolites of other species (32, 33). The resulting microenvironments with the developing biofilm result in different growth responses and gene expression by the bacteria ultimately resulting in structurally complex mature biofilms (30). Environmental stresses placed on the forming biofilm can speed the development of the biofilm. In both *S. aureus* and *S. epidermidis*, the main polysaccharide in the matrix is PIA, which is expressed via the icxADBC operon. In response to environmental stresses such as antibiotic treatment, osmolarity, alcohols, low oxygen, low nutrients and heat lead to increased expression of PIA and more rapid matrix development (2, 26, 27). The rate of liquid flow and sheer stress also can result in modifications to the amount of the matrix

produced depending on the vascularization and location in the body. Increased levels of PIA are present in *S. epidermidis* catheter infections compared to other lower shear environments (2). After maturation, complex signaling within biofilms can result in the dispersal of planktonic bacteria and can occur actively or passively (10, 31, 34). Passive dispersal of biofilms occurs because of abrasion, fluid shear (erosion and sloughing), predator grazing and medical intervention (30, 31, 34). Active dispersal is initiated by the biofilms in response to environmental or signaling cues. These cues include changes in nutrient levels, quorum-sensing molecules, chemical signals and cyclic dimeric guanosine monophosphate (GMP) (34). Active biofilm dispersion allows the bacteria to colonize other surfaces and serves as a survival mechanism (30, 31, 34).

Quorum Sensing and Biofilm Regulation

Bacteria regulate physical processes and cooperative efforts via small molecule autoinducers that are expressed at a basal level during growth in a process known as quorum sensing (QS) (8, 10, 35-37). These molecules allow coordination of a response in a population dependent manner by the activation or repression of gene expression. The localized QS molecules are directly related to the population density and only induce behavior in locally high concentrations of bacteria (35, 36, 38). Currently, there are three classes of QS molecules with example systems and functions showing in Table 1. For a more comprehensive review of these systems, see references (35-39).

QS molecules are known to play a role in biofilm formation and regulate societal traits such as competence, sporulation, virulence factors, structural formations, dispersion, antimicrobial expression, fratricide, bioluminescence and symbiosis (36, 39). QS molecules are reported to be involved in altruistic cooperative group benefits even when confronted with other bacteria that would exploit this altruism. An example would be a trade off in growth rates where slow

rates with a high yield are ultimately better for the population than a fast growth rate with low yield. The higher yields suggest a more efficient use of resources even at the expense of individual bacteria (32, 36). The modulation of virulence factors by QS molecules implicates them in the biofilm formation and infection processes. Multiple species of bacteria do not express virulence factors until a critical concentration of bacteria is reached allowing them to collectively avoid the host immune system (39-42). While QS systems can be extremely precise, there is also a certain degree of leakiness in these communication systems allowing cross-talk between species (35). In cystic fibrosis infections, *P. aeruginosa* can upregulate virulence factors in response to intercepting AI-2 signals from nonpathogenic oropharyngeal flora (41). Another cystic fibrosis pathogen, *Burkholderia cepacia*, can intercept *P. aeruginosa* QS signals and up-regulate its virulence factors to establish infection (37, 41). Species crosstalk between *Haemophilus influenzae* and *Moraxella catarrhalis* can help establish chronic infections and resistance in polymicrobial otitis media (43).

The EPS Matrix

The essential part of the biofilm is the production of an EPS matrix which comprises roughly 90% of the biomass of the biofilms (44). The EPS represents both a habitat and a fortress for the bacteria encased within. The organization of the matrix depends on the structural components within the matrix and the metabolic activity occurring within the biofilm (13). The largest component of the matrix is water comprising up to 97% of the matrix with the remaining bulk of the materials being composed of soluble components like polysaccharides, proteins and eDNA. Insoluble matrix components include amyloids, cellulose, pili, flagella and fimbriae (9). The physical distances between microcolonies during the initial formation result in voids that ultimately become pore and channels which facilitate nutrient and liquid transport within the biofilm (9, 13). The formation of the matrix results in emergent properties that help the biofilms

survive in the environment. The matrix provides localized gradients allowing for different populations of bacteria to survive various niches and utilize different metabolic pathways for survival. The material of the matrix also functions to absorb resources from the surrounding environment. The matrix also serves to sequester secreted enzymes resulting in a de facto external digestive system. This environment enables social behavior between bacterial species, both cooperative and competitive (13, 33, 36). Since the matrix is a semi-solid gel, the matrix can also form a skin and retain water protecting the biofilm from dehydration. Its gel like nature also allows the migration of bacteria in the biofilm and in some cases can represent population efforts that parallel the division of labor (9, 13). A key advantage of matrix formation is tolerance and resistance from chemotherapy, host defenses and predation by *Protista (45).*

Biofilm Resistance

One of the prime advantages of the EPS matrix is the protection from antimicrobials, the immune system and predators. In some cases, it has been noted that to affect biofilms sometimes up to 1000-fold or more, antibiotics are required to kill the planktonic form of the same bacteria (46). Biofilm resistance is a multifactorial process involving the biology, chemistry and physics of the biofilm (11). The factors that have been associated with the increase in antibiotic resistance are gradients (oxygen, nutrients, slowed agent diffusion, etc.) stress responses, gene expression (resistance factors), dormancy and tolerance (3, 7, 8, 10-13, 31, 47, 48). Gradients present in the biofilm can result from the diffusion of agents into the biofilm resulting in sublethal concentrations of antibiotics selecting for resistance. Gradients in nutrients and oxygen lead to zones of decreased metabolism and dormant bacteria (13, 48). The slowing metabolism of these phenotypes can affect antimicrobials that require active cellular metabolism for efficacy (49-51). The enzyme sequestering effects of the matrix can lead to antimicrobial deactivation and the matrix components can complex with antimicrobials leading to chelation

and precipitation of these agents (13). Close proximity of bacteria in a biofilm facilitate horizontal gene transfer of resistance mechanisms, especially under conditions of environmental stress (2, 7, 52). In addition, preexisting drug resistance could be present in biofilms. One of the most used agents to treat biofilm infections is the ansamycin antibiotic rifampicin. While highly efficacious, this RNA synthesis targeting agent requires a single mutation in the *rpoB* gene to confer resistance. In vitro resistance determination studies have found that the frequency of mutation conferring rifampin resistance is between 10^{-7} and 10^{-8} (53-55). Base on this frequency, if the biofilm being treated has a population of 10^{9} cfu, then by random chance there are approximately 10-100 bacteria that have the mutation conferring rifampicin resistance. Thus, monotherapy treatment with antibiotics will result in enrichment of the mutant population and addressing this requires extended therapy with drug cocktails to avoid this enrichment (56-58). A final source of biofilm resistance is the subpopulation of persister cells that develop in biofilms. This cell phenotype can survive high levels of antibacterials while lacking any specific resistance mechanisms (7, 47, 59). These dormant cells can survive blocking the activity of antibacterials by depriving them of targets through metabolic inactivity and remain dormant (47). Eventually when environmental conditions permit, these cells will emerge from dormancy and proliferate. The exact mechanisms of persister formation are unknown but current theories center on toxin and antitoxin systems (TA) (47, 60). The 5 classes of TA systems are composed of a stable protein toxin that disrupts an essential metabolic function and a labile antitoxin which is coded in an operon (see Table 2).

This arrangement results in tight co-transcription and translation (60, 61). One of the key drivers of persister formation is environmental stress, especially antibiotic treatment. It is believed that the TA system activity is modulated by the (p)ppGpp signaling nucleotide and that persister cells can spontaneously form in bacterial populations (61).

Biofilms are also highly resistant to clearance by the immune system. When a device is implanted, especially internal implants, the procedure can result in localized acute and chronic

inflammation which can lead to a foreign body reaction. The implantation results in localized acute and chronic inflammation plus a foreign body reaction to the implant (2, 15, 16). Ultimately a fibrous capsule forms around the implant resulting in a zone of suppressed immune response know as a *locus minoris resistentiae* which can increase the chance of infection and biofilm formation (2, 62, 63). Studies have also uncovered that biomaterial implants can also alter immune cell responses. The implanted biomaterial can activate the complement system, platelets and neutrophils. Chronic inflammatory responses may lead to neutrophil exhaustion, depletion of oxidative species and "frustrated phagocytosis" while other demonstrate that leukocytes can react and then penetrate the biofilm (2). Studies performed in animal models with *S. aureus* suggest that the immune response may skew from the traditional pro-inflammatory response to a pro-fibrotic response. The *S. aureus* biofilm was able to alter macrophage responses towards an anti-inflammatory response with significant reductions in IL-1β, TNF-α, CXCL2 and CCL2 expression (2, 14). In addition to dampening the inflammation, *S. aureus* biofilms have been shown to change macrophage responses to the M2 phenotype and immune suppressive T cell response by increased expression *Arg1* (64, 65). *S. aureus* can also induce dysfunction and death in macrophages via various toxins, including Leukocidin (64). *Pseudomonas aeruginosa* biofilms have been found to suppress neutrophils disrupting the response and reducing neutrophil oxidation potential (66).

Diagnosis of Biofilm Infections on Medical Devices

Diagnosis of infections on biofilm infected devices is commonly determined using traditional microbial growth means. For orthopedic devices, the device itself is sampled with three to six biopsies of the surrounding tissues (67). Sonication of the devices or samples to remove the adherent bacteria has proven to be superior to identifying delayed and late infections compared to a tissue sample, histology and synovial culture (2, 3, 46, 68, 69). In most cases, removal of

the device or sampling of the surface and associate materials (respiratory secretions, urine samples, etc.) are used to confirm the presence of a biofilm (67). These conventional methods are not without drawback. The main challenge is that it is difficult to survey the presence of small colony variants in biofilms on different regions of medical implants. To overcome such limitations, several new methods have been investigated in recent years. For example, indirect methods of diagnosis have been successfully used to confirm implant infection including immunoglobulin assays, the inflammatory marker C-reactive protein and histopathological evaluation of samples (70). Other diagnostic methods include PCR (which can also screen for drug resistance markers) (3, 70), next generation sequencing, fluorescent in situ hybridization (FISH), Matrix Assisted Laser Desorption/Ionization Time-of-Flight Mass Spectrometry (MALDI-TOF) mass spectroscopy and assay of α-defensin levels in the synovial fluid (2, 67).

Of recent interest has been the incorporation of nuclear medicine in visualization of infected implanted devices and foci of infection. These methods have included computerized tomography (CT) magnetic resonance imaging (MRI), ultrasound, and radionucleotide methods such as Single Photon Emission Computed Tomography (SPECT) and Positron Emission Tomography (PET). Current applications include combinations of both screening modalities to generate anatomical information via CT scanning with the labeling data from either SPECT or PET (SPECT/CT or PET/CT) (71-73). CT imaging utilizes X-rays to generate three dimensional slices of the target while SPECT incorporates the gamma ray emissions from a radioisotope to show specific areas of interest via the radiolabel's interactions with the target (see Figure 3). PET looks for the localization of specific radioisotope accumulation and measures the emission of gamma photons from positron annihilations at 511 KeV which results in these photons moving in opposite directions. The impact of these photons on detectors, result in a simultaneous detection event that can be used to construct a three-dimensional image of the areas where the radioisotopes have accumulated. Many of the combination systems are already

available from commercial vendors and have seen use clinically (71, 72, 74-76). SPECT/CT has been used to visualize a wide variety of infections including osteomyelitis, prosthetic joint infections, mixed infections, infectious endocarditis and infected cardiac implant devices (72). Currently, PET has been used to image tumors in cancer patients indirectly by using radiolabels on metabolites that have enhanced uptake in tumors or white blood cells (WBCs) migrating to the site of the tumor (see Table 3) (77-80). While these methods have been shown to work, many rely on indirect measurements looking at a paired response to infection, such as metabolite update and infiltration of immune cells and modulators (79, 81, 82). More direct approaches have recently been successfully attempted using tagged antibodies, antimicrobials and molecules that are utilized by the infecting pathogens including the differentiation between gram-positive and gram-negative infections (75, 83-90). While targeting by antimicrobials and immune cells is a proven approach, it must be considered that labeled agents of this type could generate a skewed or no signal based on killing of the target. An approach taken by Ordonez et al. (91) has used *in silico* screening to identify radiolabeled molecules that are specifically taken up by bacteria and are not antimicrobial. There results identified ten promising leads that identified three lead candidates (Para-aminobenzoic acid or PABA, D-mannitol and D-sorbital) that were successful in *in vivo* testing, specifically identifying infection sites in a murine model of myositis.

Both the SPECT and PET methods have limitations to their use that must be accounted for in the final interpretation of the results and to prevent misdiagnosis. With the indirect visualization of infection, distinctions between sterile inflammation and actual infection must be made with the approach of infection specific tracers allowing this differentiation (75, 85, 89). In the cases of combined systems (SPEC/CT and PET/CT) allowances must be made for the proximity of the two independent screening modalities in the physical design of the device (92) and CT measurements have to take into account photon attenuation and correction for scattering. An example of successful imaging is shown in the SPECT/CT scan in Figure 3 from

two different patients with suspected prosthetic hip infections. The top image is the emission of the tracer administered to both patients while the second image is the traditional CT scan. The final set of images is the superposition of both SPECT and CT images. By the combination of these results, the clinicians were able to specifically identify that the infection was limited to either the soft tissue and posterior aspect of the prothesis or the peri-prosthetic soft tissue. This fusion of the imaging technology has further allowed the identification of the cortical, corticomedullary and subperiosteal foci of chronic osteomyelitis with a specificity value of 89% and a sensitivity of 100% (72, 93). These results would allow for a targeted intervention if surgery and debridement would be required or allow non-invasive monitoring of efficacy of pharmaceutical treatment.

Treatment of Biofilm Infections on Medical Devices

Treatment for device-related infections vary with the type of device and the location. In the case of peripheral devices, the easiest course is to remove the device and treat the infection with antibiotics (67). In some cases, central venous catheters can be kept in place and treated using antimicrobial lock out therapy typically with combinations of disinfectants and antibiotic at elevated levels above the minimum inhibitory concentration (MIC). With implanted devices such as prosthetic joints, the timing of the detection is critical. Infections occurring within three weeks of surgery can be treated with antibiotic therapy with a 70-90% success rate. For delayed or late infections, the device is usually removed to ensure that the biofilm is eradicated. The gold standard treatment is a two-stage surgical procedure where the infected device is removed, and the devitalized tissue is debrided. An antibiotic-impregnated filler is placed in the wound and at least six weeks of antimicrobial therapy is carried out (94). At the completion of antibiotic therapy, the new sterile device is implanted. The success rate for the two-stage procedure is 93-100% (2, 46, 70). Antibiotic therapy for the treatment of these infections is typically a

combination therapy of rifampin, a fluoroquinolone followed by a glycopeptide (2, 70, 94, 95). Other options in the combination therapy include daptomycin, linezolid, tigecycline, cephalosporins and carbapenems (67), amoxicillin and trimethoprim-sulfamethoxazole (46).

Due to increasing rates of antimicrobial resistance mechanisms and the inherent resistance of biofilms, some novel approaches to dealing with biofilm infection are being explored. Therapy using bacteriophages and cocktails of bacteriophages are being used against biofilms including phages that lyse the target bacteria and phage encoded enzymes to dissolve the EPS matrix (96). Phages were used as successful therapeutic agents by the former Soviet Union and Eastern European countries (97). In 2017, a personalized cocktail targeting drug resistant *Acinetobacter baumannii* successfully cleared a persistent infection in a clinical setting illustrating the utility of this therapeutic approach (98). The incorporation of phage therapy also has been reported to enhance the efficacy of antibiotics against *S. aureus* biofilms in vitro (99). Another novel therapeutic approach being explored is the use of antimicrobial peptides (AMPs). AMPs are small positively charged peptides secreted by virtually every type of organisms to combat pathogens (100-102). The AMP Database as of 2019 contains a total of 3055 entries from all the kingdoms of life (Protista, Archaebacteria, Eubacteria, Plants, Fungi and Animals) (103). The mode of action of these ubiquitous agents is through membrane disruption and depolarization but recently evidence has been mounting that there are additional targets within bacteria such as translation, transcription and replication that are affected by these peptides (100, 101, 104). Currently, there are several classes of AMPs used clinically as systemic and topical agents including colistin, polymyxin B, nisin and bacitracin in addition to synthetic AMPs in development (104-106).

A challenge posed by is the modification of the environment around the wound is that it typically becomes anoxic and mildly acidic (pH 5.0). Acidic pH values can both enhance or inhibit the activity of antibiotics (107, 108). The MICs for gentamicin against *S. aureus* increase as pH decreases while the opposite holds true for oxacillin (109). In purulent wounds, the

bactericidal activity of ciprofloxacin and imipenem is inhibited (110). A novel approach to adapting agents to this acidic environment is the design targeted delivery systems that only activate in these mildly acidic conditions. A pH activated targeted delivery system has been tried using poly (D, L, -lactic-co-glycolic acid) (PGLA) nanoparticles that were laced with PEG to prevent non-specific interactions. To provide specificity to the target bacteria, a poly-L-lysine was incorporated that becomes a positively charged cationic moiety by gaining electrons at an acidic pH. This technology was successfully used to deliver vancomycin to *S. aureus* in an in vitro system (110). The targeted delivery concept has also been applied to AMPs. Modification of the Cardin and Weintraub heparin-binding sequences (AKKARA and ARKKAAKA) with histidines yielded membrane damaging antimicrobials that only were activated under acidic conditions and were active against Gram negative, Gram positive and yeast (111). A similar approach has shown in vivo efficacy against *H. pylori* infection, a causative organism in the generation of stomach ulcers. This pH responsive polypeptide AMP was designed with a random distribution of positive and negative residues which, under a physiological pH adopted a non-toxic, inactive random configuration. When exposed to acidic conditions, the AMP transitioned to the antimicrobial helical configuration (112).

Conclusion and Summary

Device-related infection remains to be a major burden on the healthcare system. With the recent improved knowledge on the pathogenesis of bacterial infection, we may be able to develop new methods for the detection of bacterial activities and eradication of biofilm-encapsulated microorganisms surrounding implanted medical devices. Equally important is the need for more studies to explore the possibility of designing medical device surfaces that can reduce bacterial colonization while restoring “normal” anti-microbial responses of immune cells. It is our belief

that such a biological response-oriented approach will help in the creation of next generation medical devices with significantly improved safety and functionality.

References

1. Lebeaux D, Ghigo J-M, Beloin C. 2014. Biofilm-Related Infections: Bridging the Gap between Clinical Management and Fundamental Aspects of Recalcitrance toward Antibiotics. Microbiology and Molecular Biology Reviews 78:510-543.
2. Arciola CR, Campoccia D, Montanaro L. 2018. Implant infections: adhesion, biofilm formation and immune evasion. Nature Reviews Microbiology 16:397-409.
3. Percival SL, Suleman L, Vuotto C, Donelli G. 2015. Healthcare-associated infections, medical devices and biofilms: risk, tolerance and control. Journal of Medical Microbiology 64:323-334.
4. Akgün D, Müller M, Perka C, Winkler T. 2018. An often-unrecognized entity as cause of recurrent infection after successfully treated two-stage exchange arthroplasty: hematogenous infection. Archives of Orthopaedic and Trauma Surgery 138:1199-1206.
5. Dennison T, Alentorn-Geli E, Assenmacher AT, Sperling JW, Sánchez-Sotelo J, Cofield RH. 2017. Management of acute or late hematogenous infection after shoulder arthroplasty with irrigation, débridement, and component retention. Journal of Shoulder and Elbow Surgery 26:73-78.
6. Donlan RM. 2001. Biofilms and Device-Associated Infections. Emerging Infectious Diseases 7:277.
7. Davies D. 2003. Understanding biofilm resistance to antibacterial agents. Nature Reviews Drug Discovery 2:114-122.
8. Donlan RM. 2002. Biofilms: microbial life on surfaces. Emerging infectious diseases 8:881-890.

9. Flemming H-C, Wingender J. 2010. The biofilm matrix. Nat Rev Micro 8:623-633.
10. Hall-Stoodley L, Costerton JW, Stoodley P. 2004. Bacterial biofilms: from the Natural environment to infectious diseases. Nature Reviews Microbiology 2:95.
11. Stewart P. 2018. How Bacteria in Biofilms Withstand Antibiotics. Montana Biofilm Science and Technology Meeting 2018.
12. Stewart PS, Franklin MJ, Williamson KS, Folsom JP, Boegli L, James GA. 2015. Contribution of stress responses to antibiotic tolerance in Pseudomonas aeruginosa biofilms. Antimicrobial agents and chemotherapy 59:3838-3847.
13. Flemming H-c, Wingender J, Szewzyk U, Steinberg P, Rice SA, Kjelleberg S. 2016. Biofilms: an emergent form of bacterial life. Nature Reviews Microbiology 14:563-575.
14. Thurlow LR, Hanke ML, Fritz T, Angle A, Aldrich A, Williams SH, Engebretsen IL, Bayles KW, Horswill AR, Kielian T. 2011. Staphylococcus aureus biofilms prevent macrophage phagocytosis and attenuate inflammation in vivo. Journal of immunology (Baltimore, Md : 1950) 186:6585-6596.
15. Liping T, Paul T, Wenjing H. 2008. Surface Chemistry Influences Implant Biocompatibility. Current Topics in Medicinal Chemistry 8:270-280.
16. Tang L, Hu W. 2005. Molecular determinants of biocompatibility. Expert Review of Medical Devices 2:493-500.
17. Dunne WM, Jr. 2002. Bacterial adhesion: seen any good biofilms lately? Clinical microbiology reviews 15:155-166.
18. Neu TR. 1996. Significance of bacterial surface-active compounds in interaction of bacteria with interfaces. Microbiological Reviews 60:151-166.
19. Arciola CR, Bustanji Y, Conti M, Campoccia D, Baldassarri L, Samorì B, Montanaro L. 2003. Staphylococcus epidermidis–fibronectin binding and its inhibition by heparin. Biomaterials 24:3013-3019.

20. Patti JM, Allen BL, McGavin MJ, Höök M. 1994. MSCRAMM-MEDIATED ADHERENCE OF MICROORGANISMS TO HOST TISSUES. Annual Review of Microbiology 48:585-617.

21. Herrmann M, Vaudaux PE, Pittet D, Auckenthaler R, Lew PD, Schumacher-Perdreau F, xe, oise, Peters G, Waldvogel FA. 1988. Fibronectin, Fibrinogen, and Laminin Act as Mediators of Adherence of Clinical Staphylococcal Isolates to Foreign Material. The Journal of Infectious Diseases 158:693-701.

22. Foster TJ, Geoghegan JA, Ganesh VK, Höök M. 2014. Adhesion, invasion and evasion: the many functions of the surface proteins of Staphylococcus aureus. Nature Reviews Microbiology 12:49-62.

23. Herman-Bausier P, El-Kirat-Chatel S, Foster TJ, Geoghegan JA, Dufrêne YF. 2015. Staphylococcus aureus Fibronectin-Binding Protein A Mediates Cell-Cell Adhesion through Low-Affinity Homophilic Bonds. mBio 6:e00413-15.

24. Imberty A, Wimmerová M, Mitchell EP, Gilboa-Garber N. 2004. Structures of the lectins from Pseudomonas aeruginosa: insights into the molecular basis for host glycan recognition. Microbes and Infection 6:221-228.

25. Watnick PI, Fullner KJ, Kolter R. 1999. A role for the mannose-sensitive hemagglutinin in biofilm formation by Vibrio cholerae El Tor. Journal of bacteriology 181:3606-3609.

26. Mack D, Riedewald J, Rohde H, Magnus T, Feucht HH, Elsner HA, Laufs R, Rupp ME. 1999. Essential functional role of the polysaccharide intercellular adhesin of Staphylococcus epidermidis in hemagglutination. Infection and immunity 67:1004-1008.

27. Mack D, Nedelmann M, Krokotsch A, Schwarzkopf A, Heesemann J, Laufs R. 1994. Characterization of transposon mutants of biofilm-producing Staphylococcus epidermidis impaired in the accumulative phase of biofilm production: genetic identification of a hexosamine-containing polysaccharide intercellular adhesin. Infection and immunity 62:3244-3253.

28. Li H, Xu L, Wang J, Wen Y, Vuong C, Otto M, Gao Q. 2005. Conversion of Staphylococcus epidermidis strains from commensal to invasive by expression of the ica locus encoding production of biofilm exopolysaccharide. Infection and immunity 73:3188-3191.

29. Leung JW, Liu YL, Desta T, Libby E, Inciardi JF, Lam K. 1998. Is there a synergistic effect between mixed bacterial infection in biofilm formation on biliary stents? Gastrointestinal Endoscopy 48:250-257.

30. Costerton JW, Lewandowski Z, Caldwell DE, Korber DR, Lappin-Scott HM. 1995. MICROBIAL BIOFILMS. Annual Review of Microbiology 49:711-745.

31. SCosterton JW, Stewart PS, Greenberg EP. 1999. Bacterial Biofilms: A Common Cause of Persistent Infections. Science 284:1318-1322.

32. Kreft J-U. 2004. Biofilms promote altruism. Microbiology 150:2751-2760.

33. Kuramitsu HK, He X, Lux R, Anderson MH, Shi W. 2007. Interspecies interactions within oral microbial communities. Microbiology and molecular biology reviews : MMBR 71:653-670.

34. Kaplan JB. 2010. Biofilm dispersal: mechanisms, clinical implications, and potential therapeutic uses. Journal of dental research 89:205-218.

35. Hawver LA, Jung SA, Ng W-L, Shen A. 2016. Specificity and complexity in bacterial quorum-sensing systems. FEMS microbiology reviews 40:738-752.

36. Li Y-H, Tian X. 2012. Quorum sensing and bacterial social interactions in biofilms. Sensors (Basel, Switzerland) 12:2519-2538.

37. de Kievit TR, Iglewski BH. 2000. Bacterial quorum sensing in pathogenic relationships. Infection and immunity 68:4839-4849.

38. Miller MB, Bassler BL. 2001. QUORUM SENSING IN BACTERIA. Annual Review of Microbiology 55:165.

39. Le KY, Otto M. 2015. Quorum-sensing regulation in staphylococci—an overview. Frontiers in Microbiology 6.

40. Antunes LCM, Ferreira RBR, Buckner MMC, Finlay BB. 2010. Quorum sensing in bacterial virulence. Microbiology (Reading, England) 156:2271-2282.

41. Juhas M, Eberl L, Tümmler B. 2005. Quorum sensing: the power of cooperation in the world of Pseudomonas. Environmental Microbiology 7:459-471.

42. Sircili MP, Walters M, Trabulsi LR, Sperandio V. 2004. Modulation of Enteropathogenic Escherichia coli Virulence by Quorum Sensing. Infection and Immunity 72:2329-2337.

43. Armbruster CE, Hong W, Pang B, Weimer KED, Juneau RA, Turner J, Swords WE. 2010. Indirect pathogenicity of Haemophilus influenzae and Moraxella catarrhalis in polymicrobial otitis media occurs via interspecies quorum signaling. mBio 1.

44. Kostakioti M, Hadjifrangiskou M, Hultgren SJ. 2013. Bacterial biofilms: development, dispersal, and therapeutic strategies in the dawn of the postantibiotic era. Cold Spring Harbor perspectives in medicine 3:a010306-a010306.

45. Matz C, McDougald D, Moreno AM, Yung PY, Yildiz FH, Kjelleberg S. 2005. Biofilm formation and phenotypic variation enhance predation-driven persistence of Vibrio cholerae. Proceedings of the National Academy of Sciences of the United States of America 102:16819-16824.

46. Hogan S, Stevens NT, Humphreys H, O'Gara JP, O'Neill E. 2015. Current and future approaches to the prevention and treatment of staphylococcal medical device-related infections. Current pharmaceutical design 21:100.

47. Lewis K. 2007. Persister cells, dormancy and infectious disease. Nature Reviews Microbiology 5:48-56.

48. Roberts ME, Stewart PS. 2004. Modeling Antibiotic Tolerance in Biofilms by Accounting for Nutrient Limitation. Antimicrobial Agents and Chemotherapy 48:48-52.

49. English BK. 2014. Limitations of beta-lactam therapy for infections caused by susceptible Gram-positive bacteria. Journal of Infection 69:S5-S9.

50. Hausler WJ. 1996. Antibiotics in Laboratory Medicine, 4 ed, vol 29. Wilkins & Wilkins, Baltimore, MD.

51. Stevens DL, Gibbons AE, Bergstrom R, Winn V. 1988. The Eagle Effect Revisited: Efficacy of Clindamycin, Erythromycin, and Penicillin in the Treatment of Streptococcal Myositis. The Journal of Infectious Diseases 158:23-28.

52. Savage VJ, Chopra I, O'Neill AJ. 2013. Staphylococcus aureus Biofilms Promote Horizontal Transfer of Antibiotic Resistance. Antimicrobial Agents and Chemotherapy 57:1968-1970.

53. Curry SR, Marsh JW, Shutt KA, Muto CA, O'Leary MM, Saul MI, Pasculle AW, Harrison LH. 2009. High frequency of rifampin resistance identified in an epidemic Clostridium difficile clone from a large teaching hospital. Clinical infectious diseases : an official publication of the Infectious Diseases Society of America 48:425-429.

54. Morosini M-I, Baquero M-R, Sánchez-Romero JM, Negri M-C, Galán J-C, Campo Rd, Pérez-Díaz JC, Baquero F. 2003. Frequency of Mutation to Rifampin Resistance in *Streptococcus pneumoniae* Clinical Strains: *hexA* and *hexB* Polymorphisms Do Not Account for Hypermutation. Antimicrobial Agents and Chemotherapy 47:2064-2064.

55. O'Neill AJ, Chopra I, Cove JH. 2001. Mutation frequencies for resistance to fusidic acid and rifampicin in Staphylococcus aureus. Journal of Antimicrobial Chemotherapy 47:647-650.

56. Croes S, Beisser PS, Neef C, Bruggeman CA, Stobberingh EE. 2010. Unpredictable Effects of Rifampin as an Adjunctive Agent in Elimination of Rifampin-Susceptible and -Resistant Staphylococcus aureus Strains Grown in Biofilms. Antimicrobial Agents and Chemotherapy 54:3907-3912.

57. Floss HG, Yu T-W. 2005. Rifamycin-mode of action, resistance, and biosynthesis. Chemical reviews 105:621.

58. Wichelhaus TA, Böddinghaus B, Besier S, Schäfer V, Brade V, Ludwig A. 2002. Biological Cost of Rifampin Resistance from the Perspective of Staphylococcus aureus. Antimicrobial Agents and Chemotherapy 46:3381-3385.

59. Singh R, Ray P, Das A, Sharma M. 2009. Role of persisters and small-colony variants in antibiotic resistance of planktonic and biofilm-associated Staphylococcus aureus: an in vitro study. Journal of Medical Microbiology 58:1067-1073.

60. Wood TK, Knabel SJ, Kwan BW. 2013. Bacterial Persister Cell Formation and Dormancy. Applied and Environmental Microbiology 79:7116-7121.

61. Wen Y, Behiels E, Devreese B. 2014. Toxin–Antitoxin systems: their role in persistence, biofilm formation, and pathogenicity. Pathogens and Disease 70:240-249.

62. Bouvresse S, Chiras J, Bricaire F, Bossi P. 2006. Pott's disease occurring after percutaneous vertebroplasty: An unusual illustration of the principle of locus minoris resistentiae. Journal of Infection 53:e251-e253.

63. Chan ED, Po-Marn K, Kevin F, Anthony PD, Iseman MD. 2001. Vertebral Osteomyelitis Due to Infection with Nontuberculous Mycobacterium Species after Blunt Trauma to the Back: 3 Examples of the Principle of Locus Minoris Resistentiae. Clinical Infectious Diseases 32:1506-1510.

64. Scherr T, Heim C, Morrison J, Kielian T. 2014. Hiding in Plain Sight: Interplay between Staphylococcal Biofilms and Host Immunity. Frontiers in Immunology 5.

65. Prabhakara R, Harro JM, Leid JG, Harris M, Shirtliff ME. 2011. Murine Immune Response to a Chronic Staphylococcus aureus Biofilm Infection. Infection and Immunity 79:1789.

66. Jesaitis AJ, Franklin MJ, Berglund D, Sasaki M, Lord CI, Bleazard JB, Duffy JE, Beyenal H, Lewandowski Z. 2003. Compromised Host Defense on Pseudomonas aeruginosa

Biofilms: Characterization of Neutrophil and Biofilm Interactions. The Journal of Immunology 171:4329-4339.

67. Høiby N, Bjarnsholt T, Moser C, Bassi GL, Coenye T, Donelli G, Hall-Stoodley L, Holá V, Imbert C, Kirketerp-Møller K, Lebeaux D, Oliver A, Ullmann AJ, Williams C, Biofilms ESGf, Consulting External Expert Werner Z. 2015. ESCMID guideline for the diagnosis and treatment of biofilm infections 2014. Clinical Microbiology and Infection 21:S1-S25.

68. Vasoo S. 2018. Improving the Diagnosis of Orthopedic Implant-Associated Infections: Optimizing the Use of Tools Already in the Box. Journal of clinical microbiology 56.

69. Xu Y, Larsen LH, Lorenzen J, Hall-Stoodley L, Kikhney J, Moter A, Thomsen TR. 2017. Microbiological diagnosis of device-related biofilm infections. APMIS 125:289-303.

70. Parikh MS, Antony S. 2015. A comprehensive review of the diagnosis and management of prosthetic joint infections in the absence of positive cultures. Journal of Infection and Public Health 9:545-556.

71. Ady J, Fong Y. 2014. Imaging for infection: from visualization of inflammation to visualization of microbes. Surgical infections 15:700-707.

72. Erba PA, Israel O. 2014. SPECT/CT in infection and inflammation. Clinical and Translational Imaging 2:519-535.

73. Granov A, Tiutin L, Schwarz T. 2013. Positron Emission Tomography, 1. Aufl.;1st; ed. Springer Berlin Heidelberg, Berlin, Heidelberg.

74. Palestro CJ, Love C. 2017. Role of Nuclear Medicine for Diagnosing Infection of Recently Implanted Lower Extremity Arthroplasties. Seminars in Nuclear Medicine 47:630-638.

75. Sellmyer MA, Lee I, Hou C, Weng C-C, Li S, Lieberman BP, Zeng C, Mankoff DA, Mach RH. 2017. Bacterial infection imaging with [^{18}F]fluoropropyl-trimethoprim. Proceedings of the National Academy of Sciences 114:8372-8377.

76. Signore A, Glaudemans AWJM, Gheysens O, Lauri C, Catalano OA. 2017. Nuclear Medicine Imaging in Pediatric Infection or Chronic Inflammatory Diseases. Seminars in Nuclear Medicine 47:286-303.

77. Koglin N, Mueller A, Berndt M, Schmitt-Willich H, Toschi L, Stephens AW, Gekeler V, Friebe M, Dinkelborg LM. 2011. Specific PET Imaging of x_c^--Transporter Activity Using a 18F-Labeled Glutamate Derivative Reveals a Dominant Pathway in Tumor Metabolism. Clinical Cancer Research 17:6000-6011.

78. Krasikova RN, Kuznetsova OF, Fedorova OS, Belokon YN, Maleev VI, Mu L, Ametamey S, Schubiger PA, Friebe M, Berndt M, Koglin N, Mueller A, Graham K, Lehmann L, Dinkelborg LM. 2011. 4-[18F]Fluoroglutamic Acid (BAY 85-8050), a New Amino Acid Radiotracer for PET Imaging of Tumors: Synthesis and in Vitro Characterization. Journal of Medicinal Chemistry 54:406-410.

79. Vallabhajosula S, Solnes L, Vallabhajosula B. 2011. A Broad Overview of Positron Emission Tomography Radiopharmaceuticals and Clinical Applications: What Is New? Seminars in Nuclear Medicine 41:246-264.

80. Wang L, Zha Z, Qu W, Qiao H, Lieberman BP, Plössl K, Kung HF. 2012. Synthesis and evaluation of 18F labeled alanine derivatives as potential tumor imaging agents. Nuclear Medicine and Biology 39:933-943.

81. Shukla AK, Kumar U. 2006. Positron emission tomography: An overview. Journal of medical physics 31:13-21.

82. Vaquero JJ, Kinahan P. 2015. Positron Emission Tomography: Current Challenges and Opportunities for Technological Advances in Clinical and Preclinical Imaging Systems. Annual review of biomedical engineering 17:385-414.

83. Ankrah AO, Glaudemans AWJM, Maes A, Van de Wiele C, Dierckx RAJO, Vorster M, Sathekge MM. 2018. Tuberculosis. Seminars in Nuclear Medicine 48:108-130.

84. Kouijzer IJE, Mulders-Manders CM, Bleeker-Rovers CP, Oyen WJG. 2018. Fever of Unknown Origin: the Value of FDG-PET/CT. Seminars in Nuclear Medicine 48:100-107.

85. Neumann KD, Villanueva-Meyer JE, Mutch CA, Flavell RR, Blecha JE, Kwak T, Sriram R, VanBrocklin HF, Rosenberg OS, Ohliger MA, Wilson DM. 2017. Imaging Active Infection in vivo Using D-Amino Acid Derived PET Radiotracers. Scientific Reports 7:7903.

86. Nielsen KM, Kyneb MH, Alstrup AKO, Jensen JJ, Bender D, Schønheyder HC, Afzelius P, Nielsen OL, Jensen SB. 2016. 68Ga-labeled phage-display selected peptides as tracers for positron emission tomography imaging of Staphylococcus aureus biofilm-associated infections: Selection, radiolabelling and preliminary biological evaluation. Nuclear Medicine and Biology 43:593-605.

87. Ordonez AA, Jain SK. 2018. Pathogen-Specific Bacterial Imaging in Nuclear Medicine. Seminars in Nuclear Medicine 48:182-194.

88. Rice SL, Roney CA, Daumar P, Lewis JS. 2011. The Next Generation of Positron Emission Tomography Radiopharmaceuticals in Oncology. Seminars in Nuclear Medicine 41:265-282.

89. Salmanoglu E, Kim S, Thakur ML. 2018. Currently Available Radiopharmaceuticals for Imaging Infection and the Holy Grail. Seminars in Nuclear Medicine 48:86-99.

90. Weinstein EA, Ordonez AA, DeMarco VP, Murawski AM, Pokkali S, MacDonald EM, Klunk M, Mease RC, Pomper MG, Jain SK. 2014. Imaging Enterobacteriaceae infection in vivo with ^{18}F-fluorodeoxysorbitol positron emission tomography. Science Translational Medicine 6:259ra146-259ra146.

91. Ordonez AA, Weinstein EA, Bambarger LE, Saini V, Chang YS, DeMarco VP, Klunk MH, Urbanowski ME, Moulton KL, Murawski AM, Pokkali S, Kalinda AS, Jain SK. 2017. A Systematic Approach for Developing Bacteria-Specific Imaging Tracers. Journal of nuclear medicine : official publication, Society of Nuclear Medicine 58:144-150.

92. Livieratos L. 2015. Technical Pitfalls and Limitations of SPECT/CT. Seminars in Nuclear Medicine 45:530-540.

93. Horger M, Eschmann SM, Pfannenberg C, Storek D, Dammann F, Vonthein R, Claussen CD, Bares R. 2003. The value of SPET/CT in chronic osteomyelitis. European Journal of Nuclear Medicine & Molecular Imaging 30:1665-1673.

94. Chaussade H, Uçkay I, Vuagnat A, Druon J, Gras G, Rosset P, Lipsky BA, Bernard L. 2017. Antibiotic therapy duration for prosthetic joint infections treated by Debridement and Implant Retention (DAIR): Similar long-term remission for 6 weeks as compared to 12 weeks. International journal of infectious diseases : IJID : official publication of the International Society for Infectious Diseases 63:37-42.

95. Sendi P, Zimmerli W. 2012. Antimicrobial treatment concepts for orthopaedic device-related infection. Clinical Microbiology and Infection 18:1176-1184.

96. Chan BK, Abedon ST. 2015. Bacteriophages and their enzymes in biofilm control. Current pharmaceutical design 21:85.

97. Sulakvelidze A, Alavidze Z, Morris JG, Jr. 2001. Bacteriophage therapy. Antimicrobial agents and chemotherapy 45:649-659.

98. Schooley RT, Biswas B, Gill JJ, Hernandez-Morales A, Lancaster J, Lessor L, Barr JJ, Reed SL, Rohwer F, Benler S, Segall AM, Taplitz R, Smith DM, Kerr K, Kumaraswamy M, Nizet V, Lin L, McCauley MD, Strathdee SA, Benson CA, Pope RK, Leroux BM, Picel AC, Mateczun AJ, Cilwa KE, Regeimbal JM, Estrella LA, Wolfe DM, Henry MS, Quinones J, Salka S, Bishop-Lilly KA, Young R, Hamilton T. 2017. Development and Use of Personalized Bacteriophage-Based Therapeutic Cocktails To Treat a Patient with a Disseminated Resistant Acinetobacter baumannii Infection. Antimicrobial agents and chemotherapy 61:e00954-17.

99. Dickey J, Perrot V. 2019. Adjunct phage treatment enhances the effectiveness of low antibiotic concentration against Staphylococcus aureus biofilms in vitro. PLOS ONE 14:e0209390.

100. Strempel N, Strehmel J, Overhage J. 2015. Potential application of antimicrobial peptides in the treatment of bacterial biofilm infections. Current pharmaceutical design 21:67.

101. Jenssen H, Hamill P, Hancock REW. 2006. Peptide antimicrobial agents. Clinical microbiology reviews 19:491-511.

102. Zasloff M. 2002. Antimicrobial peptides of multicellular organisms. Nature 415:389-395.

103. Li X, Wang Z, Wang G. 2015. APD3: the antimicrobial peptide database as a tool for research and education. Nucleic Acids Research 44:D1087-D1093.

104. Li Y, Xiang Q, Zhang Q, Huang Y, Su Z. 2012. Overview on the recent study of antimicrobial peptides: Origins, functions, relative mechanisms and application. Peptides 37:207-215.

105. Hermsen ED, Sullivan CJ, Rotschafer JC. 2003. Polymyxins: Pharmacology, pharmacokinetics, pharmacodynamics, and clinical applications, vol 17, p 545-562. Elsevier Inc, United States.

106. Landman D, Georgescu C, Martin DA, Quale J. 2008. Polymyxins Revisited. Clinical Microbiology Reviews 21:449-465.

107. Thomas J, Linton S, Corum L, Slone W, Okel T, Percival SL. 2012. The affect of pH and bacterial phenotypic state on antibiotic efficacy. Int Wound J 9:428-35.

108. Yang L, Wang K, Li H, Denstedt JD, Cadieux PA. 2014. The influence of urinary pH on antibiotic efficacy against bacterial uropathogens. Urology 84:731.e1-7.

109. Baudoux P, Bles N, Lemaire S, Mingeot-Leclercq M-P, Tulkens PM, Van Bambeke F. 2007. Combined effect of pH and concentration on the activities of gentamicin and

oxacillin against Staphylococcus aureus in pharmacodynamic models of extracellular and intracellular infections. Journal of Antimicrobial Chemotherapy 59:246-253.

110. Bryant RE, Mazza JA. 1989. Effect of the abscess environment on the antimicrobial activity of ciprofloxacin. The American Journal of Medicine 87:S23-S27.

111. Kacprzyk L, Rydengård V, Mörgelin M, Davoudi M, Pasupuleti M, Malmsten M, Schmidtchen A. 2007. Antimicrobial activity of histidine-rich peptides is dependent on acidic conditions. Biochimica et Biophysica Acta (BBA) - Biomembranes 1768:2667-2680.

112. Xiong M, Bao Y, Xu X, Wang H, Han Z, Wang Z, Liu Y, Huang S, Song Z, Chen J, Peek RM, Jr., Yin L, Chen L-F, Cheng J. 2017. Selective killing of Helicobacter pylori with pH-responsive helix–coil conformation transitionable antimicrobial polypeptides. Proceedings of the National Academy of Sciences of the United States 114:12675-12680.

Figures

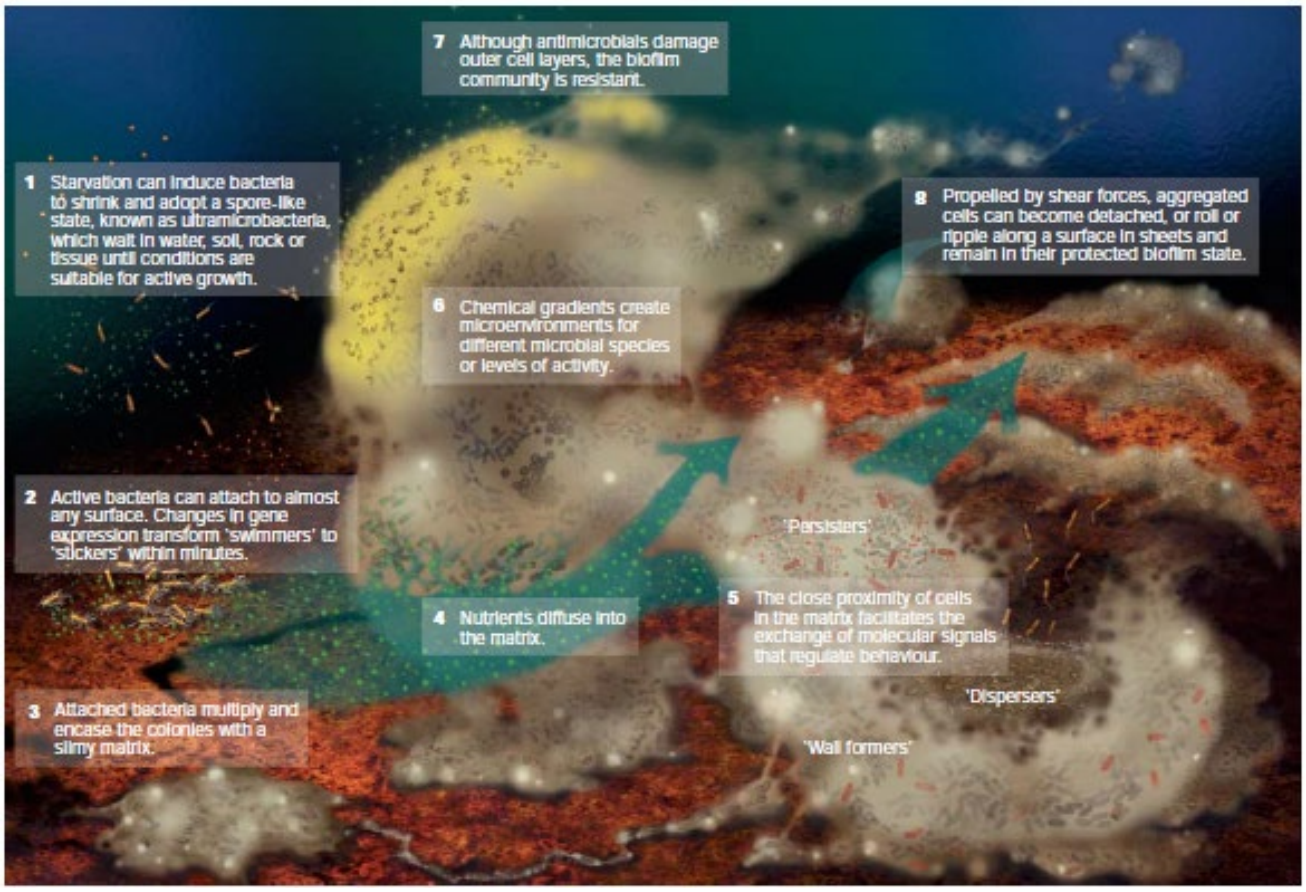

Figure 1. A summary of the complexity of biofilms illustrating the colonial and organized nature of this type of infection. Reprinted by permission from Springer Nature, Nature Reviews Microbiology , Hall-Stoodely et al .2004 (10) Copyright 2004

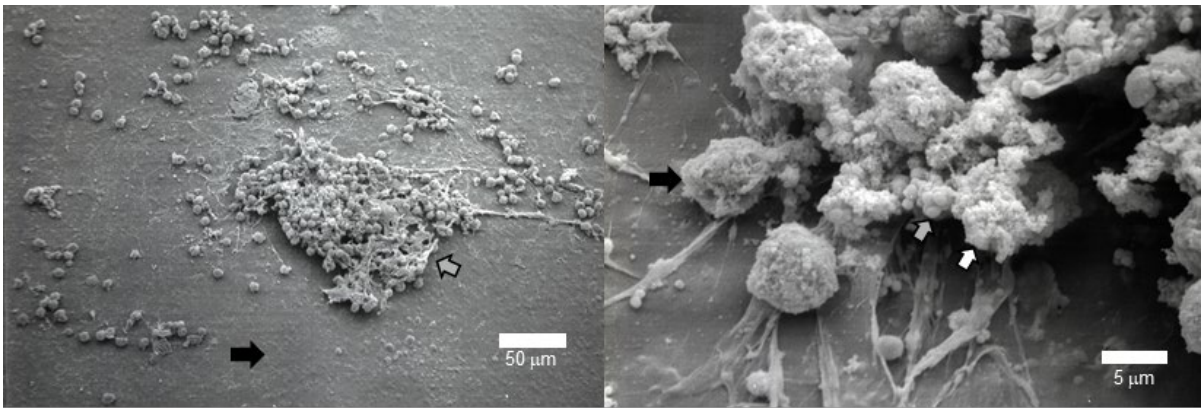

Figure 2. SEM images of Staphylococcus aureus biofilms on the surface of Teflon coated catheters established in a mouse model of biofilm infection. The panel on the left shows the biofilm (grey arrow) adhered to the catheter surface (black arrow). The right-hand image shows the individual staphylococci (grey arrow matrix (white arrow) and host immune cells (black arrow).

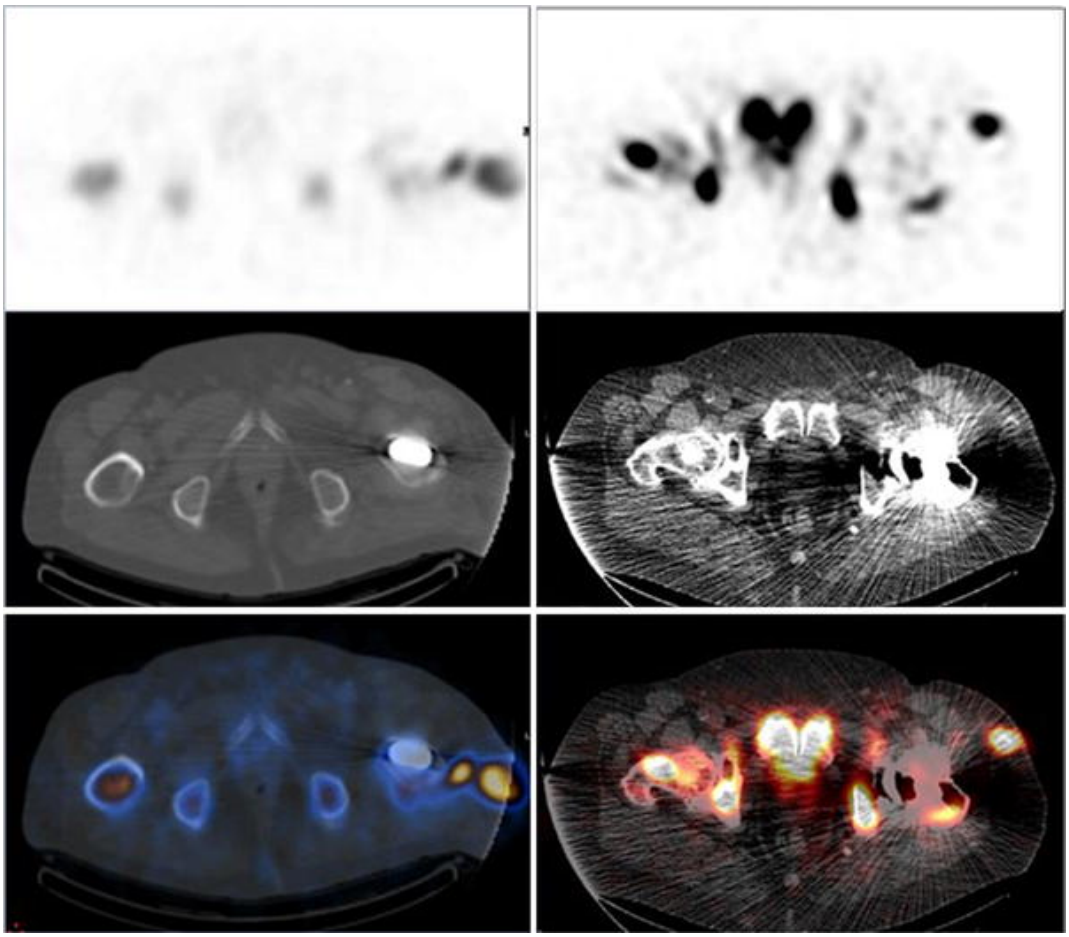

Figure. 3 SPECT/CT images of infections in two patients with prosthetic hip infections. The upper panels show the emission while the middle panels show the CT images while the bottom panels show the superimposed images of 99mTC-HMPAO WBC uptake. Reprinted by permission from Springer Nature, Clinical and Translational Imaging, Erba et al. (72)

Tables

Table 1 The three classes of quorum sensing molecules used by bacteria.

Bacteria	Signaling molecule	Example system	Function
Gram negative	Acyl Homoserine Lactones	*LuxI/LuxR*	Bioluminescence
Gram positive	Small peptides	*Agr*	Virulence factors
Both gram negative and gram positive	AI-2	*LuxS*	Interspecies communication

The AI-2 signaling molecules are unique in that they allow for cross-species communication.

Table 2: The five toxin-antitoxin systems with their regulatory elements and mechanisms of actions (61).

Type	Regulatory Element	Mechanism of Action
I	sRNA	Binding to toxin mRNA preventing ribosome binding
II	Protein	DNA binding that suppresses toxin transcription
III	RNA-protein complex	Toxin function inhibited by interaction with pseudoknots antitoxin RNA
IV	Protein	Blocking of toxin target site on cytoskeletal proteins
V	Endoribonuclease	Cleavage of toxin mRNA

All these systems are believed to play an active role in the generation of persister populations in biofilms.

Table 3: PET radiolabels used to detect inflammation and infection. These have been used successfully to identify tumors or infection.

Tracer	Abbreviation	Diagnosis	Reference
^{18}F-fluorodeoxyglucose (FDG)	^{18}F-FDG	Tuberculosis *S. aureus* biofilm infection Bacterial infection	Ankarh et al. (2017) Garrido et al. (2014) Neumann et al. (2017) Ordonez et al. (2018) Palestro et al. (2017) Sathekge et al. (2017) Signore et al. (2017)
^{18}F-labeled glutamate analogs	BAY 94-9392 BAY 85-8050	Cancer	Koglin et al. (2011) Krasikova et al. 2011
Labeled White blood cells	^{111}In-WBCs ^{99m}Tc-WBC	Bacterial infection	Neumann et al. (2017) Signore et al. (2017) Erba et al. (2014)
D-[methyl-^{11}C]-methionine	[^{11}C]-D-Met	Bacterial infection	Neumann et al. (2017)
^{68}Ga-labled phage display peptides	^{68}Ga-A9-K-DOTA	*S. aureus* biofilm	Nielsen et al. (2016)
[^{18}F]-fluoropropyl-trimethoprim	[^{18}F]-FPTMP	Bacterial infection	Sellymer et al. (2017)
2-[^{18}F]-fluorodeoxysorbital	^{18}F-FDS	Bacterial infection	Weinstein et al. (2014)

These have been used successfully to identify tumors or infection.

CHAPTER 3

DEVELOPMENT OF D-GLUTAMINE-DERIVED PET TRACER FOR DIAGNOSING BACTERIAL INFECTION *IN VIVO*

Complete reference

Renick PJ, Mulgaonkar A, Co CM, Wu C-Y, Pennington J, Sherwood A, Velazquez A, Quan B, Oz OK, Tang L, Sun X. Development of D-glutamine-derived PET tracer for diagnosing bacterial infection *in vivo*. (to be submitted).

Abstract

D-amino acid imaging has been exploited in recent years for bacterial imaging *in vivo*, since D-amino acids can only be metabolized by bacteria, but not mammalian cells. Among all amino acids, it is well established that glutamine plays a pivotal role in controlling the growth and biofilm formation of many bacteria. Given the essential nature of glutamine's pivotal role in bacterial survival, cell growth, biofilm formation, and even virulence, here we report a new positron emission tomography (PET) imaging approach using D-5-[11C]glutamine (D-[5-11C]-Gln) for potential clinical assessment of bacterial infection through a comparative study with its L-isomer counterpart, L-[5-11C]-Gln. Both tracers were synthesized from the appropriate enantiomeric precursor of tert-Butyl-2-((tert-butoxycarbonyl) amino)-4-Iodobutanoate by [^{11}C]HCN trapping and cyanation followed by hydrolysis and purification to generate the glutamine enantiomers. Using PET imaging, our results show that L-[^{11}C]Gln tracer had substantially higher systemic levels compared to D-[^{11}C]gln tracer in both healthy and infected animals. Interestingly, the uptake of L-[^{11}C]gln tracer are found to be higher than the uptake of D-[^{11}C]gln tracer in most organs, except kidney. Most importantly, our results show that PET imaging with D-5-[^{11}C]glutamine, but not L-5-[^{11}C]glutamine, is capable of diagnosing both E. coli and MSRA infection using murine dual-infection myositis models. Furthermore, D-5-[^{11}C]glutamine PET imaging was shown to be capable of significantly differentiating active bacterial infection from sterile inflammation. These results support strong translational potential of D-5-[^{11}C]glutamine PET imaging for noninvasive detection of bacterial infectious diseases in humans.

Keywords

D amino acid, metabolic imaging, glutamine, bacterial infection, positron emission tomography

Introduction

In recent years, increased research efforts have been placed to design PET probes

based on differences in host versus bacterial *in vivo* consumption of D-amino acids (DAAs). Although DAAs can be acquired through dietary intake and through *in vivo* conversion by host amino acid racemases[1-3], humans predominantly use only the L form of the twenty two amino acids. The only systems in humans that utilize DAAs (D-serine, D-aspartate, D-alanine and D-cysteine) by mammalian cells is limited to the central nervous and endocrine systems and, to date, they are known to only use D forms of serine, aspartate, alanine, and cysteine

In contrast, bacteria can utilize both enantiomeric types of all amino acids (D and L forms) via specialized amino acid transport proteins[4-6]. By taking advantage of this differential uptake capability, several studies have successfully exploited DAAs, such as D-[^{11}C]methionine and D-[^{11}C]alanine, as PET probes and demonstrated their potential for clearly distinguishing between sterile inflammation and infection caused by gram-positive and gram-negative bacteria in animal models[7-9]. Previous work has exploited the use of DAAs in bacterial cell wall, specifically D-methionine and D-alanine. D-methionine is incorporated into the C-terminus of peptidoglycan by transpeptidase reactions carried out by penicillin binding protein in addition to incorporation into peptidoglycan muropeptides. D-alanine is incorporated into the peptide chains in the cytoplasmic peptidoglycan synthesis steps by D-alanine ligase. D-glutamine plays a dual role in the synthesis of peptidoglycan either as a substrate the formation of D-glutamate or is directly incorporated by transpeptidase reactions. Glutamine uptake also plays a unique and critical role in bacterial infection by affecting the expression of bacterial virulence expression and biofilm production[10-12]. However, the feasibility of developing D-glutamine probe for detection bacterial infection has not been evaluated and was the main objective of this work.

The L-isomer of gln radiolabeled with ^{18}F (half-life = 110 min) or ^{11}C (half-life = 20 min) has been evaluated in preclinical and clinical studies for cancer imaging[13-15]. However, to the best of our knowledge, there have been no such published reports for radiolabeled D-gln. While radiolabeling the gln molecule with ^{11}C radionuclide is a significant advantage by maintaining its native chemical form for *in vivo* evaluations, the challenges faced due to the short half-life

of ^{11}C, coupled with complex synthesis procedures maybe the reason for lack of published data in humans for this tracer's isomers. A fully automated synthesis and purification of a clinical grade of L-5-[^{11}C]glutamine (L-[^{11}C]gln) was developed by our group[16] and the same process was used to producing a D-5-[^{11}C]glutamine tracer.

Here we reported successful synthesis of D-[^{11}C]gln using a reliable and feasible method with excellent potential for future clinical application. We first assessed the "normal" metabolism of both D-gln tracer and L-gln tracer in different organs of healthy animals. Using a modified neutropenic mouse myositis model infected with *Escherichia coli* and *Staphylococcus aureus*, we subsequently evaluated the efficacy of using either D-gln tracers or L-gln tracers to distinguish bacterial colonization and sterile inflammation. The use of neutropenic animals simulates our worst-case patient scenario, representing patients that are critically ill with reduced immune function. Our results showed preferential accumulation of D-gln tracer, but not L-gln tracer, at the site with live bacterial colonization, allowing us to distinguish these foci from sterile inflammation.

Results

Automated Synthesis of the D and L isomers of [^{11}C]Gln: Both D-[^{11}C]gln and L-[^{11}C]gln were fabricated to assess their potential as metabolism imaging tracers for diagnosing bacterial infection. While the synthesis of L-[^{11}C]gln was based on modifications of previous literature[17-19], this is the first reported synthesis of the D isomer of glutamine (Figure 4. Automated synthesis involved the production of [^{11}C]HCN, azeotropic drying of 18-C-6/CsHCO3 solution, [^{11}C]HCN trapping, and [^{11}C] cyanation of eithter the R or S form of *tert*-Butyl-2-((tert-butoxycarbonyl) amino)-4-Iodobutanoate precursor to generate the tracers. Both D and L isomers of clinical grade [^{11}C]gln were reproducibly synthesized with high efficiency (n = 9), > 90% radiochemical purity (Figure 5 and Figure 6 for HPLC analyses) and a radiochemical yield of approximately 33.5 ± 16.0 % and 34.9 ± 11.3 % for the D and L 5-[^{11}C]gln, respectively (data were decay corrected from total collected H^{11}CN activity). Both

these tracers were synthesized reproducibly with > 99% enantiomeric radiochemical purity (n = 9).

[^{11}C]Gln Tracer Biodistribution: The metabolism of [^{11}C] D-gln and [^{11}C] L-gln tracer was evaluated in both healthy and infected mice by comparing the biodistribution of the tracers.

In healthy animals, whole body quantification of the PET data show that L-[^{11}C]gln tracer had substantially higher systemic levels compared to D-[^{11}C]gln tracer (Figure 7). When specific organs are quantified this trend is reflected by significantly (*P*-values < 0.05) elevated uptake of L-[^{11}C]gln the brain, heart, thyroid, lung, liver, bone and muscle of the healthy animals (Figures 3). An exception to this trend is the lower renal uptake of the L-[^{11}C]gln tracer when compared to the D-[^{11}C]gln tracer (p-value < 0.001). Similar differential uptakes of both L-[^{11}C]gln tracer and D-[^{11}C]gln tracer by various organs were found in infected animals (Figure 8).

PET Imaging in Infected Mice: The feasibility of D-[11C]gln tracer and L-[11C]gln tracer for infection detection was investigated. The infected mice were scanned from 20 to 40 min p.i. (static PET scans) and then analyzed. By compare the visual PET images, we find that the foci of *S. aureus* and *E. coli* can be easily identified in animals treated with D-[11C]gln tracer, but not L-[11C]gln tracer (Figure 8). Quantification of absolute tracer uptake showed that the uptake of D-[^{11}C]gln by the *S. aureus* and *E. coli* foci was significantly higher (~ 2 fold) than the heat-killed bacteria and the muscle background (p-values <0.0001 and 0.0004, respectively). There was no significant difference of L-[^{11}C]gln tracer uptake values between the infection foci, heat-killed bacteria or background muscle (Figure 8). Furthermore, the infection-to-muscle background contrast for both the infectious foci was obviously distinguishable after PET imaging with D-[^{11}C]gln; whereas, this was not the case for the L-[^{11}C]gln PET signal (Figure 8).

***Ex vivo* analysis of the dual infection models post-imaging**. Post-imaging tissues were harvested for *ex vivo* analysis by histology and recovery of viable bacteria. Histology confirms the presence of bacteria in the infection foci for both *S. aureus* and *E. coli*, while the heat-killed biopsy samples show no evidence of intact bacteria in the tissues (Figure 9) confirming that the heat-killed bacteria were not viable and had been lysed. Confirmation of an active infection was further confirmed by recovery of viable *S. aureus* and *E. coli* from the infection foci, with median recoveries of 6.23 and 7.23 $\log_{10}$ cfu/sample, respectively (Figure 9). No bacteria were recovered from the heat-killed foci. Additional samples (liver, heart and blood) were taken, processed and showed low to no recovered *S. aureus* or *E. coli* counts indicating the myositis infections were predominantly confined to the infection sites (Figure 11).

Discussion

Pathogen-specific metabolic imaging has gained increasing popularity for use in the diagnosis of infection. As our hypothesis is based on the incorporation of our D-[^{11}C]gln tracer into the bacteria peptidoglycan and nitrogen assimilation pathways essential for biofilm formation and bacterial virulence, an automatic production of the radiotracer with high enantiomeric purity was essential. To the best of our knowledge, this is the first reported synthesis of D-[^{11}C]gln based on an modified method use to generate L-[^{11}C]gln[17-19] with >90% radiochemical purity.

The D-[^{11}C]gln tracer has a biodistribution similar to the L-[^{11}C]gln tracer in both healthy and infected animals. These results suggest that infection status does not affect the metabolism of both tracers by different organs. Furthermore, the higher uptake of L-isomer than that of D-isomer in many vital organs confirms the exclusive uptake of L-isomer by mammalian cells as described earlier. The data also indicate the D-tracer is excreted via the renal system which is

consistent with elimination of L-glutamine from the body[20-22]. Most importantly and in support of our hypothesis, PET imaging shows that D-[^{11}C]gln tracer, but not L-[^{11}C]gln, have significantly high accumulation in the infection foci of both *S. aureus* and *E. coli* foci *in vivo*. It should be noted that neutropenic animal model was used in this study to simulate clinical immune compromised patient condition as established in earlier studies[23-25]. The induction of neutropenia has been shown to minimize the impact of innate immunity on establishing an infection commonly found in immunocompromised patient population[26-28] .

Glutamine plays a significant role in the metabolism of bacterial thus providing multiple avenues to exploit as tracer for the detection of infection. Glutamine is a critical substrate for glutamate which is used in peptidoglycan synthesis, a metabolite bridging carbon and nitrogen metabolism and has a role in triggering the expression of virulence factors[12, 29-30]. Specifically, D-Gln can be incorporated by transpeptidase reactions into the cell wall of gram-positive and gram-negative bacteria[31-33]. Glutamine is an essential amino acid in the assimilation of nitrogen and provides a bridge to carbon metabolism[34-36] . The regulation and detection of glutamine has also been implicated in the expression of virulence factors and biofilm formation. For example, inhibition of glutamine synthesis (GS) and lack glutamine uptake results in reduced fitness and ability to cause infection in bacteria including *Listeria, Staphylococci, Streptococci, Enterococcus, Salmonella and Bacillus*[10-11, 37]. The ability to detect the presence of glutamine in the environment serves as a trigger in some bacteria for the expression of virulence factors[10] and to help maintain resistance factors[37]. Glutamine uptake and synthesis also plays a role in biofilm formation. The transition from single celled bacteria to commensal aggregate in biofilm requires glutamine for survival and growth.[38-40].

While there are many exciting findings on D-[^{11}C]gln tracer present here, many questions related to the clinical potential of the tracer has yet to be answered. For example, the minimal detection level of the D-5-[^{11}C]gln tracer needs to be determined. Currently, we can successfully

image infections with ~10^6-10^7 bacteria and these levels are consistent with bacterial counts isolated from infections in humans[41-43]. Nevertheless, for sucessful monitoring of antibacterial therapies a lower limit would need to be determined to prevent prematurely stopping treatment. Furthermore, it is not clear whether the presence of high numbers of commensal bacteria such as the gut[44-46] would interfere D-5-[^{11}C]gln PET imaging.

The overall data has shown that the D-5-[^{11}C]gln tracer has potential as an infection-specific PET probe, with capability to distinguish active gram-positive and gram-negative bacterial infections from host-specific sterile inflammatory responses. The central nature of glutamine in affecting biofilm formation and virulence factor regulation makes it uniquely suited for labeling of bacterial infections. Our results support the combination of PET D-5-[^{11}C]gln tracer with other imaging techniques like CT or MRI would provide a critical quantitative measures of infection and anatomical data that could guide intervention and real-time monitoring of therapy with improved therapeutic outcomes.

Methods

Radiotracer production: Carbon-11 labeled carbon dioxide ([^{11}C]CO_2) was produced by the ^{14}N(p,α)^{11}C reaction with 16.5 MeV proton beam from a GE PETtrace 880® Cyclotron using a commercial N_2 target containing 1% O_2 as target material in the UT Southwestern Medical Center Cyclotron and Radiochemistry Facility (Dallas, TX). The automated synthesis of D-5-[^{11}C]-Gln (**3**, Scheme 1) was performed in Synthra MeI plus® synthesizer which involved the following four major steps (see Figure 1): **1)** Production and trapping of [^{11}C]hydrogen cyanide ([^{11}C]HCN), **2)** [^{11}C]cyanation of precursor **1**, **3)** Hydrolysis of intermediate **2**, and **4)** Purification and formulation of the final product.

Briefly, the prepared [^{11}C]CO_2 is sent to the synthesizer, trapped in the CO_2-trap and cooled to -190 °C using liquid nitrogen. It is converted to [^{11}C]CH_4 and then to [^{11}C]HCN by coupled gas reactions. The [^{11}C]HCN is sent to a reaction vessel and reacted with a mixture of 18-Crown-6

and $CsHCO_3$ in dimethyl formamide to produce [^{11}C]CsCN. The precursor is reacted with the intermediate at 90°C for 8 min, followed by cooling to 35 °C. The intermediate mixture containing **2** (see Figure 1) is diluted with sterile water for injection (SWI), purified using an Oasis® HLB Light cartridge, and eluted with anhydrous acetonitrile to a second reaction vessel. Here, the intermediate is heated to 70°C under nitrogen flow and vacuum for 2 min, and then at 90°C for 1 min, followed by drying under vacuum for 3 min without nitrogen flow. The vessel is then cooled to 50°C and a mixture of TFA/sulfuric acid is added to the intermediate. The reaction temperature is then raised to 90°C for 5 min to form the crude product **3** (see Figure 1), followed by cooling. The crude product is then diluted with SWI, passed through a column packed with Ag11-A8 ion exchange resin, and eluted with SWI into a formulation vial containing 23.4% sodium chloride for injection. The final product is sterilized inside the dispensing hot cell using a 0.22 μm sterilizing filter. The samples are then withdrawn for quality control testing prior to use in any study. Quality control analysis was performed by radio-high performance liquid chromatography (radio-HPLC; Agilent Technologies) analysis using Supelco Astec Chirobiotic™ T Chiral column, 250 × 4.6 mm, 5 μL (Phenomenex) with 70% ethanol in water as the mobile phase. The UV Analysis was performed at 210 nm at the flow rate of 1 mL/min. A CsI (Th) scintillation probe radiation detector was used for the analysis.

Animals: CD-1® IGS female 6 – 8 weeks old (28 – 33 g weight) mice (Charles River Laboratories) were used for the study. Throughout the experiment, the animals were housed in laminar flow cages maintained at 22 ± 2 °C, 50 – 60% relative humidity, under a 12-hour light:12-hour dark cycle. The mice were permitted free access to autoclaved tap water and commercial normal chow food[47] throughout the experiment. All animal experiments were approved by the University of Texas Southwestern Institutional Animal Care and Use

Committee in compliance with the United States Public Health Service Standards and National Institute of Health guidelines.

Murine Myositis Model: The infection models were carried out in an ABSL-2 animal facility with the approval the University of Texas Southwestern Institutional Animal Care and Use Committee. Mice were rendered neutropenic by intraperitoneal injection with 150 mg/kg and 100 mg/kg of cyclophosphamide (Sigma-Aldrich) at 5 days and 1 day prior to infection. The day before the study, inoculum of *Staphylococcus aureus* (MRSA ATCC® 33592) and *Escherichia coli* (ATCC® 8739) were prepared by selection of 5-10 colonies from a trypticase soy agar stock agar (TSA) plate were passed into trypticase soy broth (TSB) and incubated overnight at 37.0°C with shaking. On the day of the infection, the cultures were pelleted and washed three times to remove spent medium and toxins and resuspended in fresh TSB adjusted to approximately 1.0 x 10^8 cfu/mL by OD600nm using the calibration factor of 1.0 OD600nm equaling 0.9 x 10^8 cfu/mL for MRSA and 1.0 OD600nm equaling 4.30 x 10^8 cfu/mL, respectively. Both calibration factors were determined in growth curve experiments to link an OD600 to a cfu/mL value. Heat-killed cultures were prepared in the same manner but followed by autoclaving to ensure the bacteria were killed. Inoculum counts (cfu) for each strain were serially diluted in an 8 point 1:10 series and spotted (10 µL, 4 replicates) for colony counts[48-49] on TSA. Heat-killed samples were plated in a similar manner to confirm sterility. Counts were performed after overnight growth at 37.0°C. The mice had their hind limbs and the shoulders of the fore limbs were shaved and were then anesthetized using ~2% isoflurane. The shaved limbs and shoulders were sterilized with alcohol swabs and the mice challenged with a 10 µL intramuscular injection of the ~10^8 cfu/mL inoculum (~10^6 cfu/mL final) into the anterior cranial tibialis of each of the hind limb muscles (MRSA to the right leg and *E. coli* to the left leg). Heat-killed pathogen controls were injected in a similar manner in the right shoulder (deltoid/trapezius) of the animal. The animals

were monitored until they recovered from anesthesia and had access to food and water. The infections were allowed to establish for a twelve hour period prior to imaging

PET Imaging: The mice were imaged at baseline (before infection) and 12 - 18 hours after infection. Mice were anesthetized and maintained under 1.5 - 2% isoflurane for the scan duration. PET/CT imaging was performed using the Siemens Inveon PET/CT Multimodal Scanner (Siemens Medical Solutions, Knoxville, TN) with a custom-made imaging bed capable of simultaneously imaging two mice. Mice were injected with 9 - 11 µCi/g (mouse body weight) of the radiotracer and PET imaging was performed 20 minutes post-injection, for a scan duration of 20 minutes (static PET scans). The optimal imaging window of 20 minutes post-injection was determined in a pilot study where the mice were dynamically scanned from 0-60 min p.i. (data not shown). A CT was first acquired for attenuation correction. CT images were reconstructed from 180 projections (140 ms exposure, 80 KVp tube voltage and 500 µA current) over a full 360° gantry rotation using the Feldkamp algorithm with a Shepp-Logan Filter and slight noise reduction. PET images were reconstructed into a single frame using the 3D Ordered Subsets Expectation Maximization (OSEM3D/MAP) algorithm. Random coincidence correction, attenuation correction, and scatter correction were applied during the reconstruction of the final PET images. PET and CT images were co-registered in Inveon Acquisition Workplace (Siemens Medical Solutions, Knoxville, TN) for PET quantification. Regions of interest (ROI) were drawn manually, including the regions in all planes containing the tissue. The target activity was calculated as Standardized Uptake Value normalized to body weight (SUV).

Statistical Analysis: All statistical analyses were made using GraphPad Prism® software (version 8). L versus D form isomer organ uptake in the biodistribution studies was done by

unpaired t-test with Welch's correction and an alpha value of 0.05. Multiple comparisons of the uptake in infection foci was performed using analysis of variance with Welch's correction and an alpha value of 0.05.

Pathogen Recoveries: At the end of the *in vivo* imaging study, mice were humanely euthanized and the infected hind limbs and control right shoulders were recovered by reflecting the skin over the sites and aseptically removing the muscles, followed by homogenization in 2 mL sterile phosphate buffered saline (PBS). Between samples, the homogenizer aggregate was sterilized by an isopropanol wash, followed by two sterile water rinses. Between samples containing different bacteria, there were three isopropanol washes and three sterile water rinses. The homogenates were brought to a final volume of 10 mL with sterile cold PBS, then 0.2 mL added to row A of a 96 well sterile round bottom plate. The plated samples serially diluted in an 8 point 1:10 series by transferring 20 µL of sample to the next row (with 180 µL sterile PBS) and mixed. This process was repeated until the eight dilution was reached (row H) The plates were then spotted (10 µL in duplicate) for colony counts on TSA plate using the spot (or drop) plate method [48-49]. The spots were dried at room temperature and then the plates were incubated overnight at 37 °C in and the colonies were then counted for processing the CFU count for each sample. Colony counts were converted to log cfu/mL using the following equation:

$$Log_{10}\frac{cfu}{mL} = [(colony\ count)(dilution\ of\ count)(plate\ dilution\ factor)(spot\ dilution\ factor)]$$

Where the dilution of the count is the least dilute sample dilution with countable colonies, the plate dilution factor is the dilution from the sample tube to the 96 well plate (10mL/ 0.2 mL = 50) and the spot dilution factor is the dilution from the 96 well plate to the TSA plate (0.2 mL/0.01mL = 20). Based on these dilutions, the limit of detection of this method was 3.0 $\log_{10}$ CFU/m.

Histology: Upon necropsy, limb musculature samples were collected, grossly trimmed for orientation, and fixed in twenty-volumes of 10% neutral-buffered formalin for 48 hours with agitation. Samples were submitted to UT Southwestern's Histopathology Core for further processing[50]. The Core dehydrated, cleared, and infiltrated limb musculature with paraffin prior to rotary microtomy. On resulting serial sections made of step-levels through the muscle, routine hematoxylin and eosin stain was performed, as well as a variation Brown & Brenn Histologic Gram Stain. Regressive H&E was performed on a Sakura DRS-601 x-y-z staining robot utilizing Leica Selectech Reagents, and the Gram Stain performed manually. In brief, serial sections destined for gram staining were deparaffinized to water and stained for 2 minutes with 1% crystal violet. Following distilled water rinse, sections were mordanted in Gram's Iodine for 5 minutes and again rinsed in distilled water. Slides were individually decolorized with acetone, rinsed in distilled water, and aggregated in basic fuchsin for 5-10 minutes. Slides were rinsed in distilled water and differentiated in Gallego's Solution, prior to rapid sequential decolorization through distilled water, acetone, picric acid, and acetone. Slides were finally cleared through acetone-xylene and coverslips affixed with permanent mounting media.

Acknowledgements

The authors would like to acknowledge the help with provided by the Cyclotron Research Program at UTSW. CC acknowledges the financial support from the National Heart, Lung and Blood Institute with the award number NIH T32 HL134613. The content is solely the responsibility of the authors and does not necessarily represent the official views of the National Institutes of Health

References

1. Bastings, J. A. J. J.; van Eijk, M. H.; Olde Damink, W. S.; Rensen, S. S., d-amino Acids in Health and Disease: A Focus on Cancer. *Nutrients* **2019,** *11* (9). DOI: 10.3390/nu11092205.

2. Kiriyama, Y.; Nochi, H., D-Amino Acids in the Nervous and Endocrine Systems. *Scientifica* **2016,** *2016*, 6494621-9. DOI: 10.1155/2016/6494621.

3. Taniguchi, M.; Konya, Y.; Nakano, Y.; Fukusaki, E., Investigation of storage time-dependent alterations of enantioselective amino acid profiles in kimchi using liquid chromatography-time of flight mass spectrometry. *Journal of Bioscience and Bioengineering* **2017,** *124* (4), 414-418. DOI: https://doi.org/10.1016/j.jbiosc.2017.04.019.

4. Burkovski, A.; Krämer, R., Bacterial amino acid transport proteins: occurrence, functions, and significance for biotechnological applications. *Applied Microbiology and Biotechnology* **2002,** *58* (3), 265-274. DOI: 10.1007/s00253-001-0869-4.

5. Hosie, A. H. F.; Poole, P. S., Bacterial ABC transporters of amino acids. *Research in Microbiology* **2001,** *152* (3), 259-270. DOI: https://doi.org/10.1016/S0923-2508(01)01197-4.

6. Piperno, J. R.; Oxender, D. L., Amino Acid Transport Systems in Escherichia coli K12. *Journal of Biological Chemistry* **1968,** *243* (22), 5914-5920.

7. Neumann, K. D.; Villanueva-Meyer, J. E.; Mutch, C. A.; Flavell, R. R.; Blecha, J. E.; Kwak, T.; Sriram, R.; VanBrocklin, H. F.; Rosenberg, O. S.; Ohliger, M. A.; Wilson, D. M., Imaging Active Infection in vivo Using D-Amino Acid Derived PET Radiotracers. *Scientific Reports* **2017,** *7* (1), 7903. DOI: 10.1038/s41598-017-08415-x.

8. Parker, M. F. L.; Luu, J. M.; Schulte, B.; Huynh, T. L.; Stewart, M. N.; Sriram, R.; Yu, M. A.; Jivan, S.; Turnbaugh, P. J.; Flavell, R. R.; Rosenberg, O. S.; Ohliger, M. A.; Wilson, D. M., Sensing Living Bacteria in Vivo Using d-Alanine-Derived 11C Radiotracers. *ACS Central Science* **2020,** *6* (2), 155-165. DOI: 10.1021/acscentsci.9b00743.

9. Stewart, M. N.; Parker, M. F. L.; Jivan, S.; Luu, J. M.; Huynh, T. L.; Schulte, B.; Seo, Y.; Blecha, J. E.; Villanueva-Meyer, J. E.; Flavell, R. R.; VanBrocklin, H. F.; Ohliger, M. A.; Rosenberg, O.; Wilson, D. M., High Enantiomeric Excess In-Loop Synthesis of d-[methyl-

11C]Methionine for Use as a Diagnostic Positron Emission Tomography Radiotracer in Bacterial Infection. *ACS Infectious Diseases* **2020,** *6* (1), 43-49. DOI: 10.1021/acsinfecdis.9b00196.

10. Haber, A.; Friedman, S.; Lobel, L.; Burg-Golani, T.; Sigal, N.; Rose, J.; Livnat-Levanon, N.; Lewinson, O.; Herskovits, A. A., L-glutamine Induces Expression of Listeria monocytogenes Virulence Genes. *PLoS Pathog* **2017,** *13* (1), e1006161. DOI: 10.1371/journal.ppat.1006161.

11. Klose, K. E.; Mekalanos, J. J., Simultaneous prevention of glutamine synthesis and high-affinity transport attenuates Salmonella typhimurium virulence. *Infection and Immunity* **1997,** *65* (2), 587-596.

12. Zhu, Y., *Staphylococcus aureus* Virulence Factors Synthesis is Controlled by Central Metabolism. *Dissertations & Theses in Veterinary and Biomedical Science* **2010,** *5*.

13. Hassanein, M.; Hight, M. R.; Buck, J. R.; Tantawy, M. N.; Nickels, M. L.; Hoeksema, M. D.; Harris, B. K.; Boyd, K.; Massion, P. P.; Manning, H. C., Preclinical Evaluation of 4-[18F]Fluoroglutamine PET to Assess ASCT2 Expression in Lung Cancer. *Mol Imaging Biol* **2016,** *18* (1), 18-23. DOI: 10.1007/s11307-015-0862-4.

14. Qu, W.; Oya, S.; Lieberman, B. P.; Ploessl, K.; Wang, L.; Wise, D. R.; Divgi, C. R.; Chodosh, L. A.; Thompson, C. B.; Kung, H. F., Preparation and characterization of L-[5-11C]-glutamine for metabolic imaging of tumors. *J Nucl Med* **2012,** *53* (1), 98-105. DOI: 10.2967/jnumed.111.093831.

15. Zhu, L.; Ploessl, K.; Zhou, R.; Mankoff, D.; Kung, H. F., Metabolic Imaging of Glutamine in Cancer. *J Nucl Med* **2017,** *58* (4), 533-537. DOI: 10.2967/jnumed.116.182345.

16. Nasr, K.; Xin, Y.; Rydberg, N.; Hallgren, R.; Cai, H.; Sun, X., Improved Automated Production for Clinical Use of 11C-L-Glutamine. *Journal of Nuclear Medicine* **2017,** *58* (supplement 1), 872.

17. Gleede, T.; Riehl, B.; Shea, C.; Kersting, L.; Cankaya, A. S.; Alexoff, D.; Schueller, M.; Fowler, J. S.; Qu, W., Investigation of SN2 [11C]cyanation for base-sensitive substrates: an

improved radiosynthesis of l-[5-11C]-glutamine. *Amino Acids* **2015,** *47* (3), 525-533. DOI: 10.1007/s00726-014-1883-z.

18. Padakanti, P. K.; Li, S.; Schmitz, A.; Mankoff, D.; Mach, R. H.; Lee, H. S., Automated synthesis of [11C]L-glutamine on Synthra HCN plus synthesis module. *EJNMMI Radiopharmacy and Chemistry* **2019,** *4* (1), 1-9. DOI: 10.1186/s41181-019-0057-4.

19. Rosenberg, A. J.; Nickels, M. L.; Schulte, M. L.; Manning, H. C., Automated radiosynthesis of 5-[11C]l-glutamine, an important tracer for glutamine utilization. *Nuclear Medicine and Biology* **2018,** *67*, 10-14. DOI: 10.1016/j.nucmedbio.2018.09.002.

20. Cruzat, V.; Macedo Rogero, M.; Noel Keane, K.; Curi, R.; Newsholme, P., Glutamine: Metabolism and Immune Function, Supplementation and Clinical Translation. *Nutrients* **2018,** *10* (11). DOI: 10.3390/nu10111564.

21. Taylor, L.; Curthoys, N. P., Glutamine metabolism: Role in acid-base balance. *Biochemistry and Molecular Biology Education* **2004,** *32* (5), 291-304. DOI: 10.1002/bmb.2004.494032050388.

22. van de Poll, M. C.; Soeters, P. B.; Deutz, N. E.; Fearon, K. C.; Dejong, C. H., Renal metabolism of amino acids: its role in interorgan amino acid exchange. *The American Journal of Clinical Nutrition* **2004,** *79* (2), 185-197. DOI: 10.1093/ajcn/79.2.185.

23. Andes, D.; Craig, W. A., Pharmacodynamics of the New Fluoroquinolone Gatifloxacin in Murine Thigh and Lung Infection Models. *Antimicrobial Agents and Chemotherapy* **2002,** *46* (6), 1665-1670. DOI: 10.1128/AAC.46.6.1665-1670.2002.

24. Safdar, N.; Andes, D.; Craig, W. A., In Vivo Pharmacodynamic Activity of Daptomycin. *Antimicrobial Agents and Chemotherapy* **2004,** *48* (1), 63-68. DOI: 10.1128/AAC.48.1.63-68.2004.

25. Weiss, W. J.; Murphy, T.; Lenoy, E.; Young, M., In Vivo Efficacy and Pharmacokinetics of AC98-6446, a Novel Cyclic Glycopeptide, in Experimental Infection Models. *Antimicrobial Agents and Chemotherapy* **2004,** *48* (5), 1708-1712. DOI: 10.1128/AAC.48.5.1708-1712.2004.

26. Evans, S. E.; Ost, D. E., Pneumonia in the neutropenic cancer patient. *Curr Opin Pulm Med* **2015,** *21* (3), 260-271. DOI: 10.1097/MCP.0000000000000156.

27. Lima, S. S.; França, M. S.; Godoi, C. C.; Martinho, G. H.; de Jesus, L. A.; Romanelli, R. M.; Clemente, W. T., Neutropenic patients and their infectious complications at a University Hospital. *Rev Bras Hematol Hemoter* **2013,** *35* (1), 18-22. DOI: 10.5581/1516-8484.20130009.

28. Montecino-Rodriguez, E.; Berent-Maoz, B.; Dorshkind, K., Causes, consequences, and reversal of immune system aging. *J Clin Invest* **2013,** *123* (3), 958-65. DOI: 10.1172/jci64096.

29. Härtel, T.; Klein, M.; Koedel, U.; Rohde, M.; Petruschka, L.; Hammerschmidt, S., Impact of Glutamine Transporters on Pneumococcal Fitness under Infection-Related Conditions. *Infection and Immunity* **2011,** *79* (1), 44-58. DOI: 10.1128/iai.00855-10.

30. Hendriksen, W. T.; Kloosterman, T. G.; Bootsma, H. J.; Estevão, S.; de Groot, R.; Kuipers, O. P.; Hermans, P. W., Site-specific contributions of glutamine-dependent regulator GlnR and GlnR-regulated genes to virulence of Streptococcus pneumoniae. *Infect Immun* **2008,** *76* (3), 1230-8. DOI: 10.1128/iai.01004-07.

31. Kanehisa, M.; Sato, Y.; Kawashima, M.; Furumichi, M.; Tanabe, M., KEGG as a reference resource for gene and protein annotation. *Nucleic Acids Research* **2015,** *44* (D1), D457-D462. DOI: 10.1093/nar/gkv1070.

32. Leisico, F.; V Vieira, D.; Figueiredo, T. A.; Silva, M.; Cabrita, E. J.; Sobral, R. G.; Ludovice, A. M.; Trincão, J.; Romão, M. J.; de Lencastre, H.; Santos-Silva, T., First insights of peptidoglycan amidation in Gram-positive bacteria - the high-resolution crystal structure of Staphylococcus aureus glutamine amidotransferase GatD. *Scientific reports* **2018,** *8* (1), 5313-13. DOI: 10.1038/s41598-018-22986-3.

33. Lupoli, T. J.; Tsukamoto, H.; Doud, E. H.; Wang, T.-S. A.; Walker, S.; Kahne, D., Transpeptidase-Mediated Incorporation of d-Amino Acids into Bacterial Peptidoglycan. *Journal of the American Chemical Society* **2011,** *133* (28), 10748-10751. DOI: 10.1021/ja2040656.

34. Commichau, F. M.; Forchhammer, K.; Stülke, J., Regulatory links between carbon and nitrogen metabolism. *Curr Opin Microbiol* **2006,** *9* (2), 167-172. DOI: 10.1016/j.mib.2006.01.001.

35. Forchhammer, K. Glutamine signalling in bacteria *Front Biosci* [Online], 2007, p. 358-370. PubMed. http://europepmc.org/abstract/MED/17127304 https://doi.org/10.2741/2069 (accessed 2007/01//). DOI: 10.2741/2069.

36. Yuan, J.; Doucette, C. D.; Fowler, W. U.; Feng, X.-J.; Piazza, M.; Rabitz, H. A.; Wingreen, N. S.; Rabinowitz, J. D., Metabolomics-driven quantitative analysis of ammonia assimilation in E. coli. *Molecular Systems Biology* **2009,** *5* (1), 302. DOI: 10.1038/msb.2009.60.

37. Somerville, G. A.; Proctor, R. A., At the Crossroads of Bacterial Metabolism and Virulence Factor Synthesis in Staphylococci. *Microbiology and Molecular Biology Reviews* **2009,** *73* (2), 233-248. DOI: 10.1128/mmbr.00005-09.

38. Erez, A.; Kolodkin-Gal, I., From Prokaryotes to Cancer: Glutamine Flux in Multicellular Units. *Trends in Endocrinology & Metabolism* **2017,** *28* (9), 637-644. DOI: 10.1016/j.tem.2017.05.007.

39. Hassanov, T.; Karunker, I.; Steinberg, N.; Erez, A.; Kolodkin-Gal, I., Novel antibiofilm chemotherapies target nitrogen from glutamate and glutamine. *Scientific Reports* **2018,** *8* (1), 7097. DOI: 10.1038/s41598-018-25401-z.

40. Rinaldo, S.; Giardina, G.; Mantoni, F.; Paone, A.; Cutruzzolà, F., Beyond nitrogen metabolism: nitric oxide, cyclic-di-GMP and bacterial biofilms. *FEMS Microbiology Letters* **2018,** *365* (6). DOI: 10.1093/femsle/fny029.

41. Kallstrom, G., Are Quantitative Bacterial Wound Cultures Useful? *Journal of Clinical Microbiology* **2014,** *52* (8), 2753-2756. DOI: 10.1128/JCM.00522-14.

42. König, C.; Simmen, H. P.; Blaser, J., Bacterial concentrations in pus and infected peritoneal fluid--implications for bactericidal activity of antibiotics. *Journal of Antimicrobial Chemotherapy* **1998,** *42* (2), 227-232. DOI: 10.1093/jac/42.2.227.

43. Kwon, J. H.; Fausone, M. K.; Du, H.; Robicsek, A.; Peterson, L. R., Impact of Laboratory-Reported Urine Culture Colony Counts on the Diagnosis and Treatment of Urinary Tract Infection for Hospitalized Patients. *American Journal of Clinical Pathology* **2012,** *137* (5), 778-784. DOI: 10.1309/ajcp4kvgqzeg1ydm.

44. Lloyd-Price, J.; Abu-Ali, G.; Huttenhower, C., The healthy human microbiome. *Genome Medicine* **2016,** *8* (1), 51. DOI: 10.1186/s13073-016-0307-y.

45. Malla, M. A.; Dubey, A.; Kumar, A.; Yadav, S.; Hashem, A.; Abd_Allah, E. F., Exploring the Human Microbiome: The Potential Future Role of Next-Generation Sequencing in Disease Diagnosis and Treatment. *Frontiers in Immunology* **2019,** *9* (2868). DOI: 10.3389/fimmu.2018.02868.

46. Thursby, E.; Juge, N., Introduction to the human gut microbiota. *Biochem J* **2017,** *474* (11), 1823-1836. DOI: 10.1042/bcj20160510.

47. 2016 Teklad global 16% protein rodent diets. https://www.envigo.com/p/teklad/laboratory-animal-diets/natural-ingredient/rodent/2016-diets.aspx (accessed 4/24/2020).

48. Chen, C. Y.; Nace, G. W.; Irwin, P. L., A 6 x 6 drop plate method for simultaneous colony counting and MPN enumeration of Campylobacter jejuni, Listeria monocytogenes, and Escherichia coli. *Journal of microbiological methods* **2003,** *55* (2), 475.

49. Naghili, H.; Tajik, H.; Mardani, K.; Razavi Rouhani, S. M.; Ehsani, A.; Zare, P., Validation of drop plate technique for bacterial enumeration by parametric and nonparametric tests. *Vet Res Forum* **2013,** *4* (3), 179-183.

50. Woods, A. E.; Ellis, R. C., *Laboratory Histopathology, A Complete Reference*. Churchill – Livingston Press: 1996.

Author contribution statement

X.S., O.K.O., and L.T. conceived of the presented idea. P.J.R. and C.C. carried out the bacterial work. C-Y.W. perform radiosynthesis. P.J.R., A.M., A.S, and J.P. performed the animal work. A.M. A.V. and B.G. conducted the PET imaging study. All authors discussed the results and contributed to the final manuscript

Competing interests

PJR is a shareholder and employee of Smith & Nephew, Inc. The other authors have no competing interests to disclose.[Insert tables here]

Figures

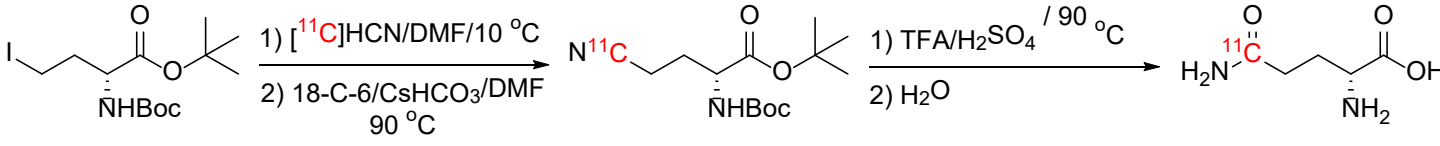

1 **2** **3**

Figure 4. Radiosynthesis of D-5-[11C]-Glutamine. Combination of commercial TRACERlab FXFM radiosynthesis module (GE healthcare) and an in-house developed module was used for the synthesis of D-[11C]-Gln. Automated synthesis involved the following steps: (1) production of [^{11}C]HCN, azeotropic drying of 18-C-6/CsHCO3 solution; (2) [^{11}C]HCN trapping, [^{11}C]cyanation; and (3) in-line transfer to In-house developed module for hydrolysis of intermediate and purification of final product.

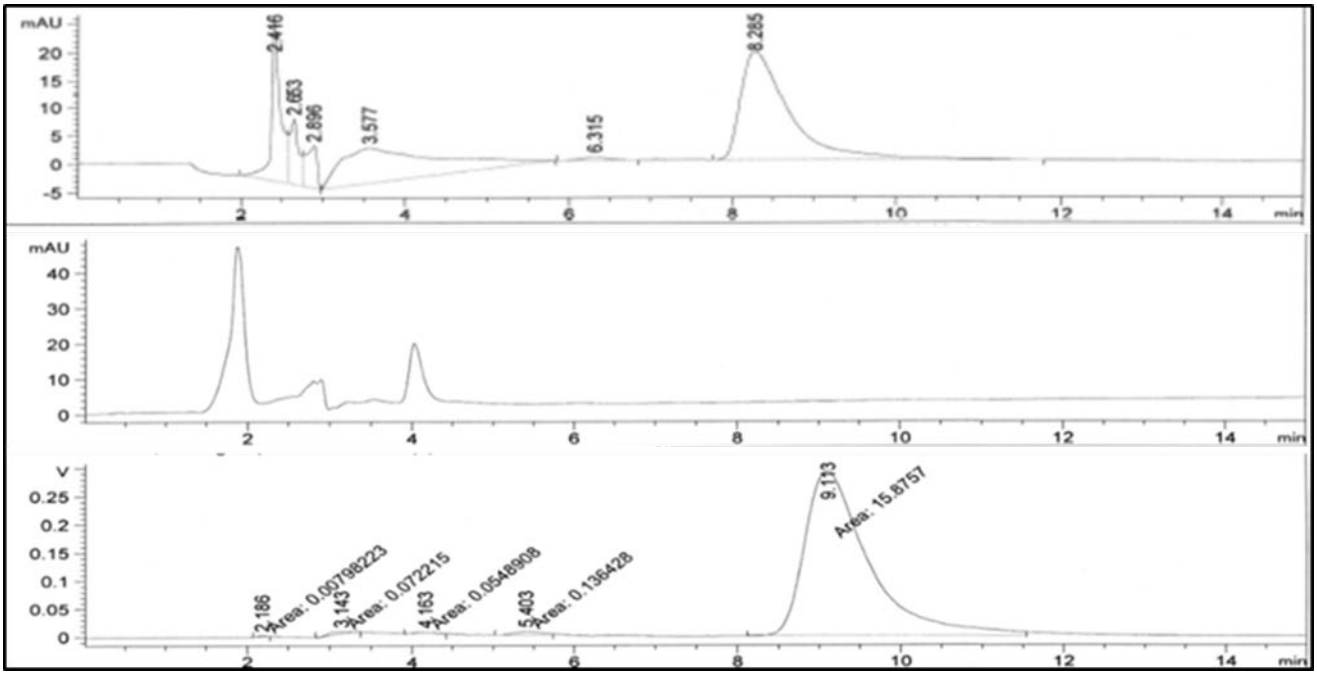

Figure 5. Quality control analysis of D-5-[11C]Gln by radio-HPLC. Supelco Astec ChirobioticTM T Chiral Column, 250 × 4.6 mm, 5 µm column was used for the analysis with 70% ethanol/water as the mobile phase. Flow rate was 1 mL/min, monitored at λ = 210 nm followed by a gamma radioactivity detector. One representative chromatogram has been shown for the radiotracer production. Radiochemical purity of the shown product: 98.3%.

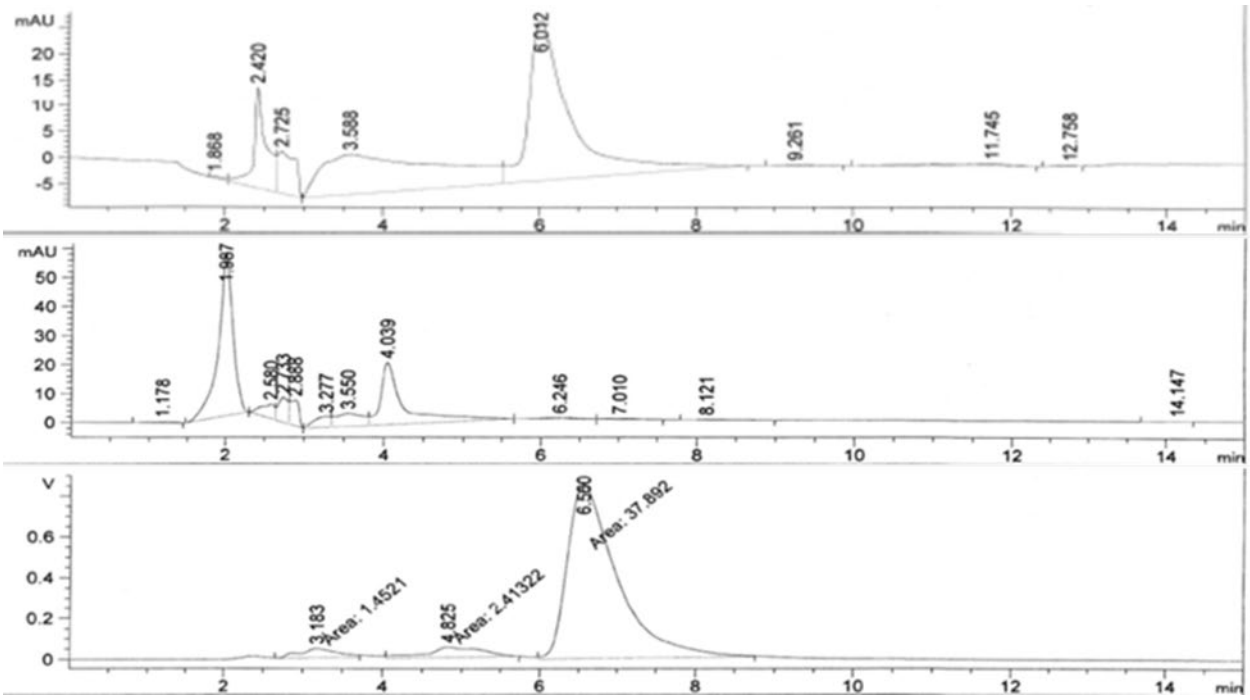

Figure 6. Quality Control analysis of L-5-[11C]-Glutamine by radio-HPLC**.** Supelco Astec ChirobioticTM T Chiral Column, 250 × 4.6 mm, 5 µm column was used for the analysis with 70% ethanol/water as the mobile phase. Flow rate was 1 mL/min, monitored at λ = 210 nm followed by a gamma radioactivity detector. One representative chromatogram has been shown for the radiotracer production. Radiochemical purity of the shown product: 92%.

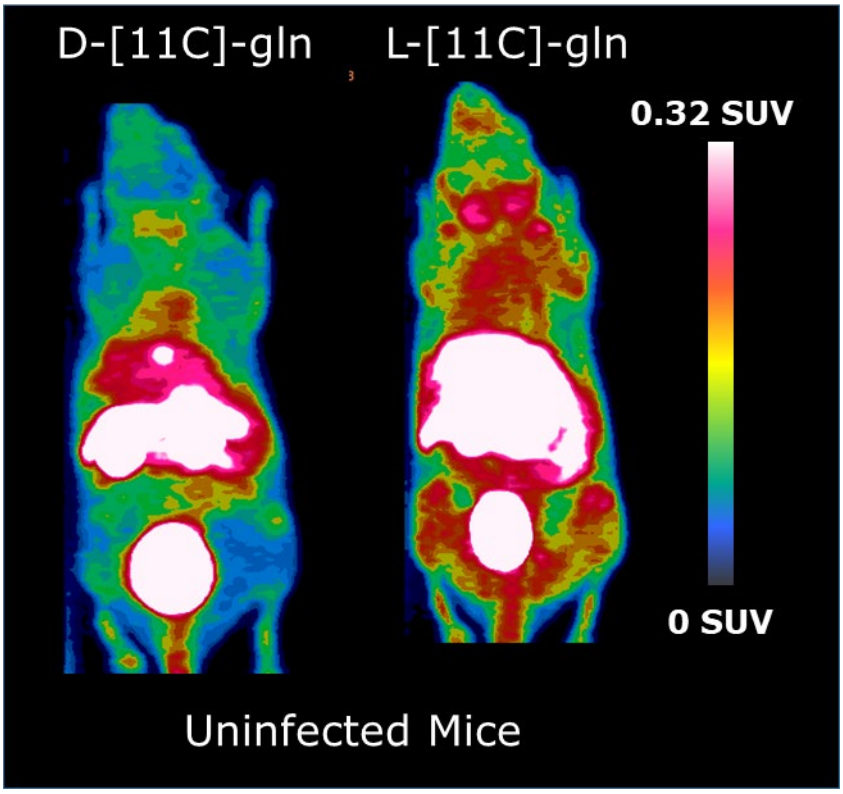
D-[11C]-gln
L-[11C]-gln
0.32 SUV
0 SUV
Uninfected Mice

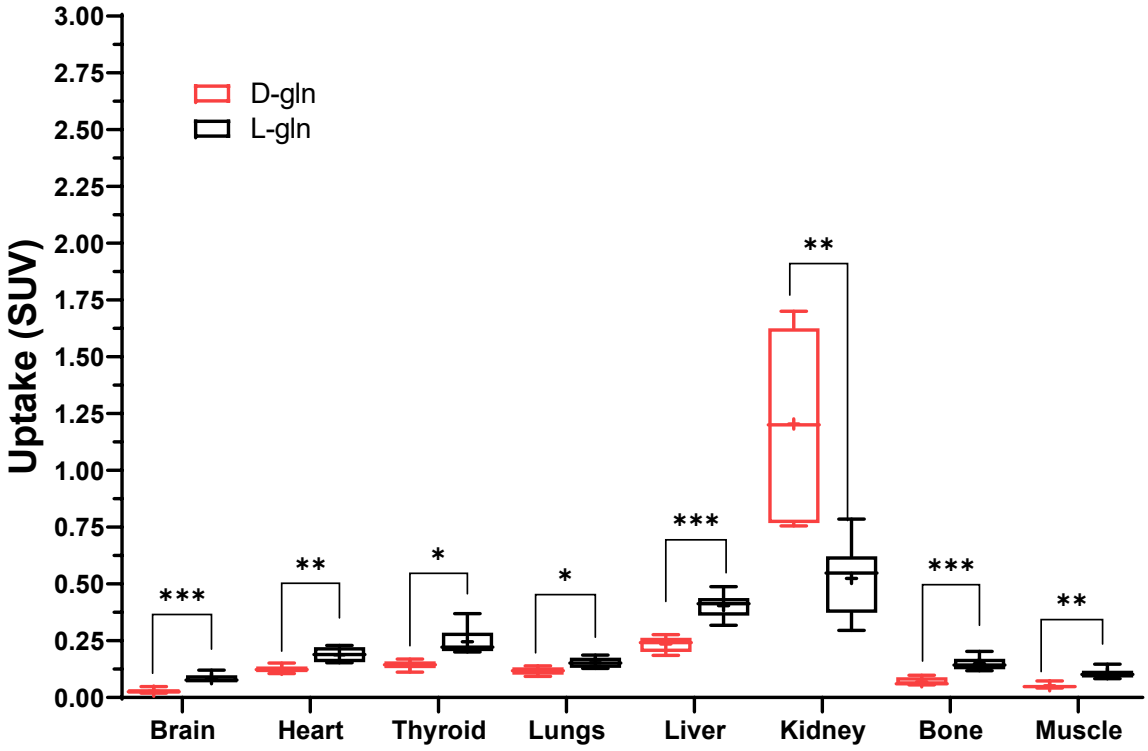
Uptake (SUV)
3.00
2.75
2.50
2.25
2.00
1.75
1.50
1.25
1.00
0.75
0.50
0.25
0.00
D-gln
L-gln
***
**
*
*
***
**
***
**
Brain
Heart
Thyroid
Lungs
Liver
Kidney
Bone
Muscle

Figure 7. Biodistribution of D and L-5-[11C]gln in healthy mice. The top panel shows a representative mouse at 12 hours (D-tracer) and at 18 hours (L tracer). The [11C]-L-gln mouse has a higher background compared to the [11C]-D-gln mouse indicating broad uptake of the L enantiomer by host tissues The bottom panel shows the biodistribution of the tracers in the quantified organs (except muscle). The mice were injected with the radiotracer at 12 hours (D-enantiomer) and then 18 hours (L-enantiomer) after the infection the infection study at a concentration of 8.7 – 13.4 μCi/g weight of the mice. PET imaging was performed 20 min p.i. for 20 min, n = 6 mice. Data are shown as box and whisker plots with error bars representing the min and max values. The symbol in the box represents the mean. Statistical comparative analyses were performed by unpaired t test with Welch's correction, *, **, ***, p-values were < 0.05, 0.01, and 0.005, respectively.

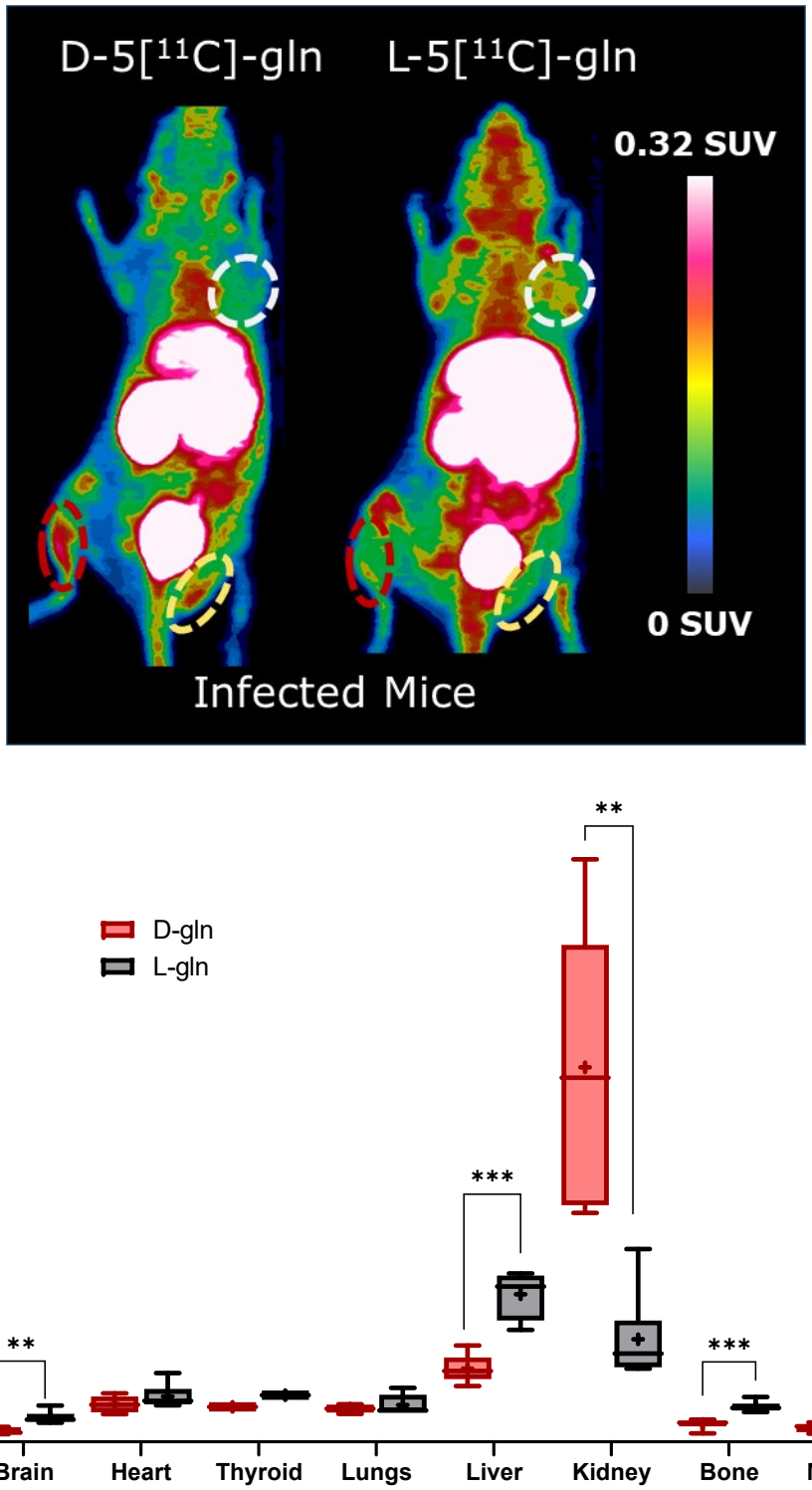

Figure 8. Biodistribution of D and L-5-[^{11}C]gln in Infected Mice**.** The top panel shows a representative mouse scanned with D tracer at 12 hours and L tracer at 18 hours. The levels of

uptake are similar to the healthy mice and but the enhanced contrast between infection foci with the D-5-[^{11}C]gln tracer is evident. The red circle indicates the *E. coli* infection site, the yellow circle the MRSA infection site and the white circle the heat-killed injection site. The D-5-[^{11}C]gln tracer shows no uptake at the heat-killed site. The bottom panel shows the biodistribution of the tracers in the quantified organs (except muscle). The mice were injected with the radiotracer at 12 hours (D-enantiomer) and then the 18 hours (L-enantiomer) after the infection the infection study at a concentration of 8.7 – 13.4 μCi/g weight of the mice. PET imaging was performed 20 min p.i. for 20 min, n = 6 mice. Data are shown as box and whisker plots with error bars representing the min and max values. The symbol in the box represents the mean. Statistical comparative analyses were performed by unpaired t test with Welch's correction, *, **, ***, p-values were < 0.05, 0.01, and 0.005, respectively.

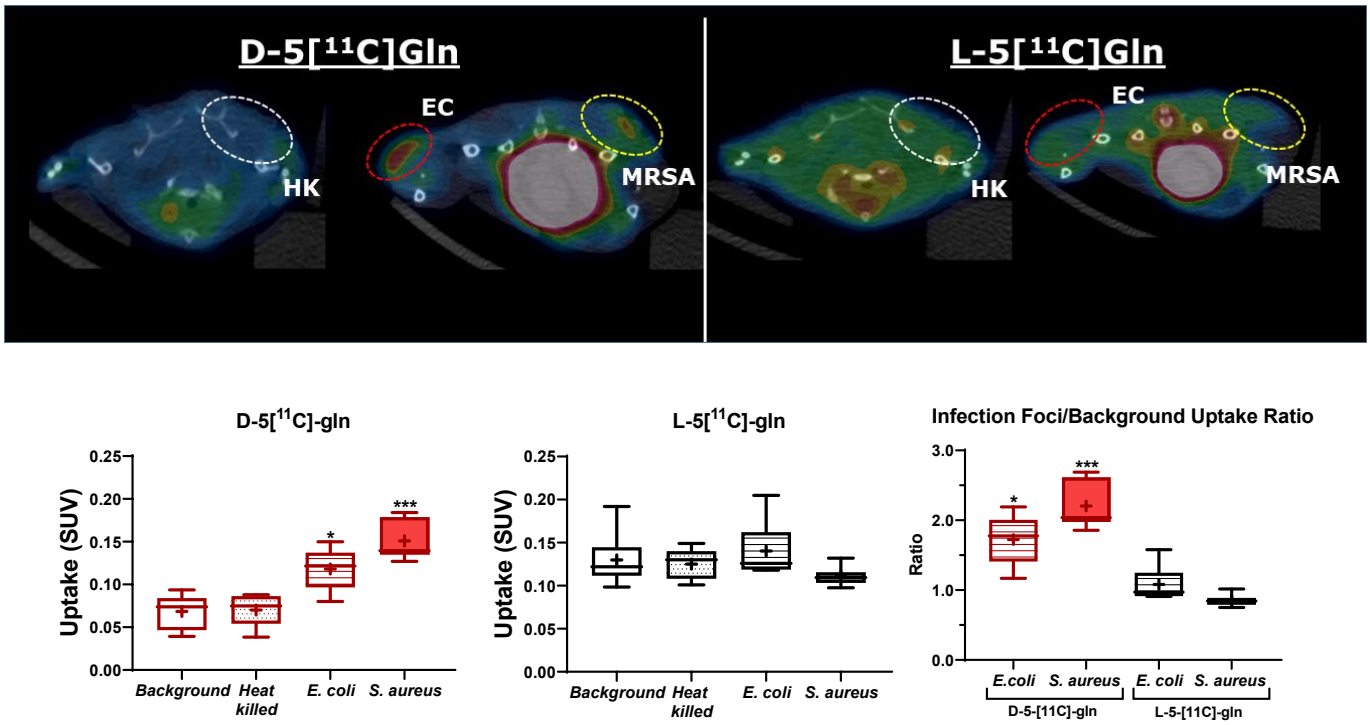

Figure 9. Raw uptake data in infected mice with values for the background (muscle), Heat-killed and bacteria including the uptake ratios versus the muscle background and representative images. The mice were injected with the radiotracer at a concentration of 8.7 – 13.4 µCi/g weight of the mice. PET imaging was performed 20 min p.i. for 20 min, n = 6 mice. Same mice were scanned at 12 – 18 hours post-infection with the D tracer and then the L tracer, respectively. The top panel shows axial PET/CT imaging of one representative mouse infection with *E. coli* (EC, left hind limb, red circle), *S. aureus* (MRSA, right hind limb, gold circle) and Heat-killed pathogen (HK, right shoulder grey shoulder). The bottom panel shows the uptake data and contrast ratios of infection foci by background (A ratio value of 1 indicates no difference between the foci and background uptake). Data are shown as box and whisker plots with min to max value error bars. The symbol in the box represents the mean value. Comparisons of the groups was done using Analysis of Variance with Welch's correction with Dunnett's post-hoc test. Comparisons of the ratios were done using unpaired t tests with Welch's correction. *, **, ***, p-values were < 0.05, 0.01, and 0.005. The data with the D-5-[^{11}C]gln tracer show a significant increase compared to background and heat-killed bacteria while the L-5-[^{11}C]gln tracer show no differences between the means. A similar trend is observed with the uptake ratios the D-enantiomers ratios of 1.7 for E. coli and 2.2 for MRSA.

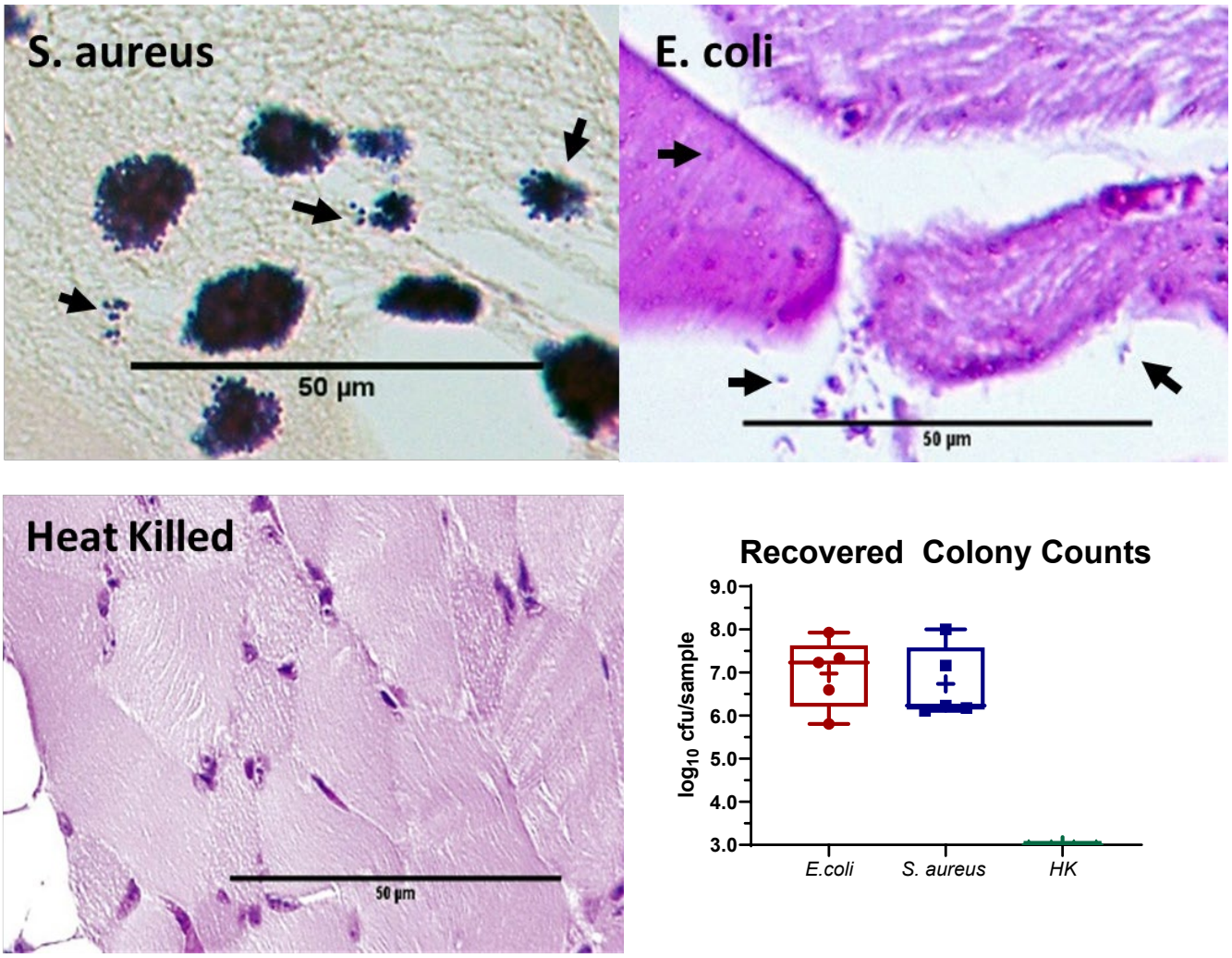

Figure 10. Representative histology images (H&E) of *E. coli* and *S. aureus* infection and representative recovered colony counts in the murine myositis model. Bacteria are indicated by arrows in the *S. aureus* (clusters and individual cocci) and *E. coli* (rods) panels. No bacteria were detected in the heat-killed tissue sections. Scale bars are 50 µm. The lower right panel are the recovered colony counts shown box and whisker plots with error bars representing the min and max recovered counts. The cross symbols are the mean recovered values and the other symbols are the individual recovered counts per mouse (n =5 for infected and 4 for heat killed controls (HK)). Log 6.0-7.0 counts were recovered from the infected foci while there were no counts in the heat-killed samples (below the limit of detection).

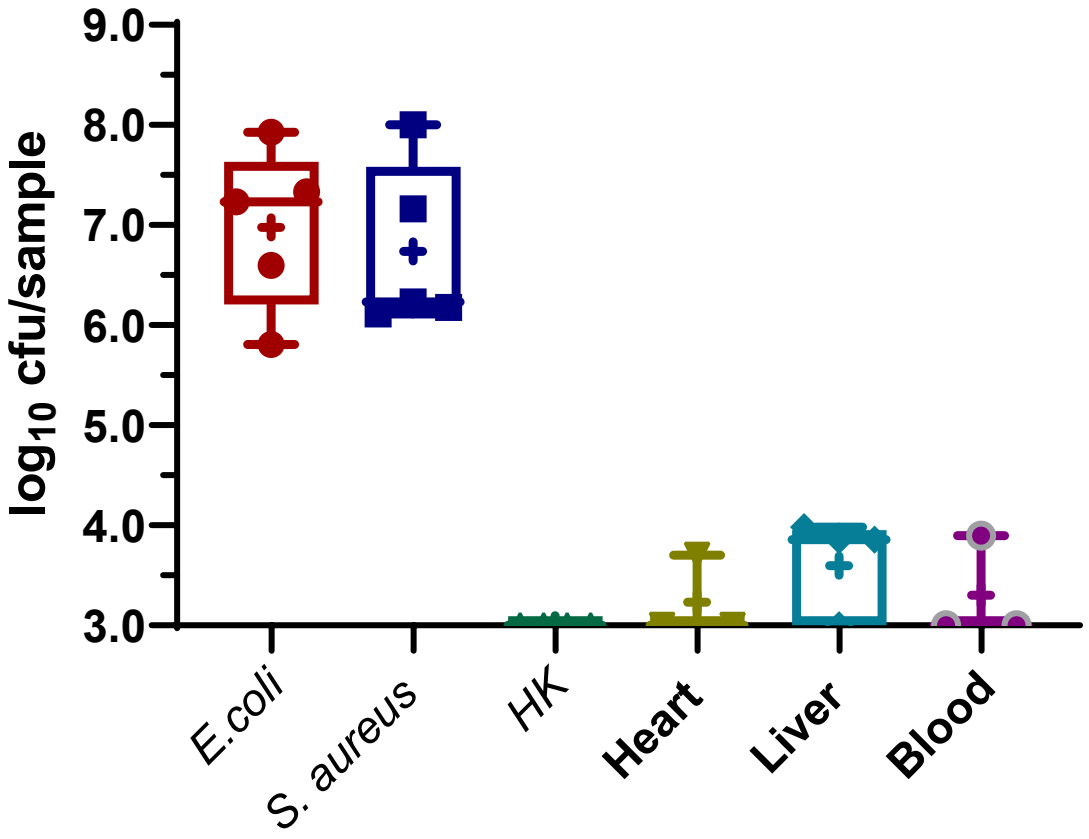

Figure 11. Post-mortem processing of recovered infected tissues collected from the mouse models post-imaging. The measured amount of bacterial CFUs in the collected tissues (infected tissues, inflamed muscle injected with heat-killed bacteria, blood, and other non-infected organs like heart, and liver) from the infected mouse models. Data is represented as box and whiskers plot showing the individual data points, error bar represent the minimum and maximum range. The cross symbol is the mean count. Mean of each dataset has been shown as the data label for each group. n = 5 mice samples processed. For heart, liver, and blood, only 3 – 4 mice data showed any viable counts, suggesting localized infection, rather than systemic entry of the pathogens. The limit of detection for the recoveries was $3 \times \log_{10}$ cfu/sample.

CHAPTER 4

DIAGNOSTICS OF WOUND INFECTIONS[2]

SHUXIN LI, PAUL JAMES RENICK, JON SENKOWSKY, ASHWIN MOHAN NAIR, AND LIPING TANG

LI, S., ET AL. (2020). "DIAGNOSTICS FOR WOUND INFECTIONS." ADVANCES IN WOUND CARE. AHEAD OF PRINT

[2] In Press

Diagnostics of wound infections

Shuxin Li,[1] Paul Renick,[1] Jon Senkowsky,[2] Ashwin Nair,[3]* Liping Tang[1]*

1. Department of Bioengineering, University of Texas at Arlington, Arlington, TX 76019, USA
2. Texas Health Physician's Group, 1001 N Waldrop Dr., # 612, Arlington, TX 76012
3. Progenitec Inc., 7301 W Pioneer Parkway, Suite B, Arlington, Texas 76013-2804

* Corresponding author. Liping Tang, Ph.D., Department of Bioengineering, University of Texas at Arlington, P.O. Box 19138, Arlington, TX 76019-0138, USA. Tel.: +1 817 272 6075; fax: +1 817 272 2251. E-mail address: ltang@uta.edu.

Manuscript Keywords (search terms): Wound Infection Diagnostics, Visual Observation, Wound Culture, Laboratory Diagnostic Kits, Wound Imaging Modalities, Biosensor

Abstract

Significance: Infection is one of the main factors responsible for delayed healing process in chronic wounds and places an enormous economic burden on its treatment. In order to come up with an effective treatment plan, cost-effective, rapid, and accurate diagnostics are highly needed for the wound infection.

Recent Advances: Traditionally, clinicians can suspect wound infection through visual observation of signs and symptoms of wound infection and confirm the diagnosis through wound culture. Nowadays, many laboratory markers including white blood cell count, erythrocyte sedimentation rate, c-reactive protein, procalcitonin, presepsin, and bacterial protease activity have been quantified to assist the diagnosis of wound infection. Moreover, imaging modalities and instrumentations including plain radiography, computed tomography, magnetic resonance imaging, ultrasound imaging, spatial frequency domain imaging, thermography, autofluorescence imaging and biosensor, have emerged for real-time wound infection diagnosis and showed their unique advantages in deeper wound infection diagnosis.

Critical Issues: While the traditional diagnostic approaches provide valuable information, they are costly, time-consuming and dependent on clinicians' experience. Therefore, innovative diagnostics are developed and tested to meet the criteria of wound infection diagnosis which include fast, cheap, non-invasive, high specificity, and no need for special training/facilities.

Future Directions: Many laboratory markers have been studied as potential indicators for wound infection and products that are designed to quantify those markers have been applied in the field of wound infection diagnosis. Imaging modalities as well as instrumentations have also been utilized and developed to detect infection in various type of wounds. This review summarizes and compares all the available diagnostics for wound infection including those are

currently used in clinic and those are still under laboratory development. We hope the paper can serve as an instructional handbook for both clinicians and patients when the wound infection occurs.

SCOPE AND SIGNIFICANCE

Chronic wounds have affected approximately 20 million individuals worldwide and annual cost for their treatment and management is estimated to be over $31 billion [1-3]. There are many factors contribute to the delay healing process of wound including chronic metabolic disease (diabetes), neurological defect, vascular stenosis, nutritional deficiency, aging and infection [4, 5]. Among these factors, infection is the most common factor that delays the wound healing rate and requires immediately treatment. If a wound does not progress through the normal stages of healing within three months or relapses, this can lead to a chronic wound.

There are three stages in the wound infection continuum including contamination, colonization and infection [6]. Wound contamination is the presence of non-replicating bacteria in an open wound. The presence of small numbers of bacteria would not affect normal inflammatory responses and wound healing processes [7]. Wound colonization is further caused by bacterial replication and proliferation. The increased number and persistent presence of microorganisms can prolong the inflammatory phase of wound healing and lead to further tissue damage [8]. When the microorganisms migrate deep into the wound bed and reproduce rapidly, they can trigger either a local or systemic immune reaction with the characteristics of infection [9]. However, some microorganisms can produce a complex protective glycocalyx –also called as biofilm – which makes the infected wounds hard to be detected and treated [10]. The presence of biofilm is ubiquitous in chronic wounds with estimates as high as 80% of chronic wounds containing biofilm[11]. The bacterial phenotype also serves to enhance inflammation leading to further tissue damage and provides protection from antimicrobial therapy as well as the immune system[12, 13]. Invading bacteria have demonstrated the ability to skew early innate immune

responses to allow establishment of the biofilm phenotype[14], which can occur rapidly within less than 24 hours of infection[15].

To diagnose wound infection, most practitioners reply on clinical characteristics 98% of the time, followed by patient-reported symptoms (88%) and wound culturing (70%) [16]. Clinical signs of a superficial infection include increasing drainage, abnormal granulation tissue, abnormal foul odor, increasing temperature, additional breakdown, edema, induration and erythema [17]. Since the signs and symptoms of infected wounds can vary with wound location, onset and type, wound culturing is preferably considered as the gold standard in infection diagnosis. Traditionally, techniques including swab culture (Levine technique), needle aspiration, and tissue biopsy are widely used to identify pathogens in the wound bed [18]. Among them, swab culture is the most widely and frequently applied approach since it is simple, timesaving, cheap, and patient friendly.

Through decades of research and development, tremendous improvements have been made in wound infection diagnosis upon their efficiency and accuracy. In this review, we provide the comprehensive view on different aspects of wound infection diagnostics, ranges from approaches that are actively used in clinic to innovative studies that are undergoing laboratory development, from clinical biological assay to imaging modalities as well as sensor-based instrumentation. The ultimate goal of the paper is to provide both infection-specialized physicians and patients a better evaluation of their choices in wound infection diagnosis.

TRANSLATIONAL RELEVanCE

Many new technologies have been created in recent years to diagnose infected wounds. For example, serological tests such as erythrocyte sedimentation rate, wound fluid biomarkers and procalcitonin have been tested for wound infection diagnosis [19, 20]. In addition to these physiological assays, imaging modalities emerge and are being utilized as wound infection diagnostic tools. Despite of traditional imaging modalities such as radiography and magnetic

resonance imaging, new hybrid imaging techniques including single photon emission computed tomography/computed tomography and positron emission tomography/magnetic resonance imaging [21]. Innovative imaging approaches such as ultrasonography, thermography, and multispectral imaging have arisen to fulfill the need of fast, cost-efficient and accurate diagnosis of wound infection [22].

CLINICAL RELEVANCE

Wound infection is a great burden for wound care and affects millions of people worldwide[2]. Chronic wounds, in addition to being infected, places a severe strain on the patient leading to social isolation, psychological stress, constant pain and immobility[23]. Understanding the pros and cons of the current diagnostics used in clinic can help the development of innovative diagnostics. These emerging diagnostics include quantification of those infection associated biological markers and imaging modalities as well as instrumentations. Unlike the traditional approaches, these new techniques can be used to quickly and accurately diagnose wound infection. There is a great potential to use these techniques to provide additional information of wound infection diagnosis and direct further treatment plans, which may lead to efficient wound management and significant reduction in wound care costs.

DISCUSSION OF FINDINGS AND RELEVANT LIETERATURE

Visual Observations

Ahead of using any diagnostic tool, most clinicians suspect the wound infection through eyeballing the wound and looking for the signs and symptoms of wound infection. Typically, an infected wound shows signs of acute inflammatory responses, [8] which include erythema, edema, changes in type/amount of exudate, bright red granulation tissue, epithelial bridging/pocketing in granulation tissue, peri-wound maceration/excoriation, and delayed wound

healing [24]. However, due to the wound infection continuum, it is vital that clinicians are able to distinguish critical colonization from bacterial infection. Signs like changes in exudate, presence of friable granulation tissue can be caused by critical colonization, discoloration of the wound bed, wound bridging instead of infection. A comprehensive list (Table 4) summarizing signs and symptoms at different stages of the wound infection continuum can be a useful tool for clinicians to assess patients' wounds [25]. As demands on healthcare systems increase, expanding the role of point of care medical personnel (i.e. nurses) in assessing the state of wounds is essential. The Bate-Jensen wound assessment tool[26] can be used for wound diagnosis and captures much of the information listed above. This can help to streamline the diagnosis and move towards implementing therapy in a timelier manner.

Since delayed wound healing process is a promising indicator and outcome for wound infection, wound mapping tools such as wound tracing, scaled photographs, and planimetry can be used to indirectly detect wound infection by monitoring wound size changes [27]. If there is no noticeable improvement of the wound within three weeks, the wound could be infected [28]. It should be noted that the impediment of wound healing can be associated with many factors other than infection. Therefore, further investigation is inevitably needed to confirm the diagnosis.

Odor Sensing and Pain Assessment

Odor sensing and pain assessment are also widely used by the clinicians for wound infection diagnosis. Wound odor (or malodor) is often led by necrosis or extremely poor vascularization of tissues, bacterial colonization or fungal infection in the wound, or a combination of these, and is hence clinically used as an indication for wound infection [29]. Deteriorating, highly exuding and fungating wounds usually possess malodor due to the fermentation of amino acids in anaerobes to malodorous organic amines [30].

Wound pain has been considered as the most frequent sign heralding the onset of infection [31]. The pain mainly comes from the cellular injury and host immunological reactions caused by the growth, multiplication and invasion of the microorganisms [32]. Wound pain assessment tools can help to assess the nature and severity of pain. Thorough and frequent pain assessment is critical for early detection of infection as well as comprehension of the patient's distress and discomfort [33]. Though provide positive prediction of wound infection, both odor sensing and pain assessment cannot identify the microbial species and the quantity of the colonization which are important parameters for instruction of further treatment. Therefore, clinicians need to do further clinical/laboratory assessments to acquire quantitative information within the infected wounds.

Clinical and laboratory assessments

Wound culture

Wound cultures are performed when infection is suspected through visual observation. The culture is used to confirm the initial diagnosis, identify the quantity and species of the present microorganisms, and determine the effective antibiotics [34]. The current literatures provide three techniques on laboratory methods for diagnosing wound infections including deep-tissue biopsy, needle aspiration, and swab culture [35].

Deep-tissue biopsy is a quantitative culture of wound tissue, which is accomplished by using aseptic technique in obtaining a tissue sample via punch biopsy, needle biopsy, or a scalpel [36]. Through microscopic examinations, biopsy results are generally reported as the number of organisms per gram of tissue. Compared with other tests, deep-tissue biopsy result is considered more conclusive and accurate for the detection of microorganisms invading wound tissue which makes the technique the gold standard for identifying wound infection [37]. However, the biopsy procedure itself not only is a time consuming, costly, invasive, painful, and require

special equipment as well as special training, but also has the risk for postsurgical trauma, wound disruption, and bacteremia is fairly high [35]. Therefore, it is usually not the primary choice for wound cultures.

Needle aspiration of wound fluid is a good alternative where the wound has little loss of skin, such as in puncture wounds or postsurgical wounds with suspected abscess. This technique is able to obtain microbes below the surface of the wound via inserting a fine-gauge needle into tissue to aspirate fluid and to quantify the concentrations of microbes [38]. Although needle aspiration is less invasive compared to tissue biopsy, it is still painful and the results are not always reproducible [37].

Swab culture is the most commonly used technique in clinic due to its practical, noninvasive, reproducible, and inexpensive features. It has been reported that swab culture has sufficient correlation with tissue biopsy to identify causative organisms in an infected wound [39-41]. Among the existing approaches, the Levine's technique is considered the best way to obtain a swab culture [42]. Usually, for quantitative swab cultures, the wound fluid stained swab is placed in 1mL of diluent and vortexed to release microorganisms. After incubation under aerobic condition, the type and the number of bacteria is measured and reported as the number of organisms per swab [17]. The major concern associated with swab culture is that only the surface colonizing bacteria will be reflected instead of the pathogenic strain invading deeper tissues. Moreover, upon detection of anaerobic organisms, false-positive and false-negative culture results occurred more often with swab cultures than with tissue biopsies [43]. A comparison of these three wound culture techniques has been listed in Table 5.

Laboratory Markers

In addition to the wound culture techniques, laboratory markers can also be measured to aid diagnosis of wound infection. These makers include white blood cell (WBC) count,

erythrocyte sedimentation rate (ESR), C-reactive protein (CRP), procalcitonin (PCT), presepsin, microbial DNA, and bacterial protease activity (BPA).

Physiologically, when infection occurs, mobilization of neutrophils from the bone marrow will result in the elevation of the neutrophil component of the WBC count [44]. Thus, through regular serological analysis, WBC count can be quantified to indicate the wound infection. However, elevation of WBC count is not always consistently reported with a wound infection [45]. For example, 56% of 189 patients diagnosed with a diabetic foot infection specifically had normal WBC count on admission [46]. Therefore, unless there is a remarkable elevation in WBC count, it cannot be used as a solid evidence for wound infection diagnosis.

ESR is an approach to measure the rate at which erythrocytes fall in the plasma of a randomly drawn anticoagulated blood specimen and can indirectly indicate the activity of acute phase reactants (infection/inflammation) [47]. Theoretically, in response to infection, cytokine-induced elevations in acute-phase proteins are positively charged and thus can induce the aggregation of negatively charged erythrocytes which leads to higher ESR [48]. Nevertheless, the change of ESR levels can also be triggered by chronic inflammation or altered erythrocytes such as sick cell disease [48]. Despite this artificial variation in ESR levels, supportive data from ESR can be utilized in assisting the diagnosis of wound infection [47].

In response to inflammation and infection, CRP, a peptide produced in the liver, is stimulated by cytokines primarily IL-6 and employed in complement binding and phagocytosis by macrophages [49]. By using light scattering from an aggregation of CRP-specific antibody, concentration of CRP can be measured within 15 to 30 minutes [50]. Several studies have included CRP measurement in their study of wound infection. For example, Jeandrot et al. found that higher grade of diabetic foot infection possessed significantly higher level of CRP [51]. Moreover, elevated serum CRP levels were found to correlate well with incisional surgical site infection[52]. Although CRP is frequently found to be elevated due to the acute infection, it is

suggested to be used as supportive data instead of direct indicator towards infection due to its short half-life (4 to 7 hours) [48, 50].

PCT is a peptide hormone secreted by non-neuroendocrine parenchymal cells, can be measured by time-resolved amplified cryptate emission, and serum level of PCT can increase 500~8000 times in patients with severe sepsis compared with healthy individuals [53]. A serial of studies has reported that patients with bacterial infections have elevated PCT levels [54]. Study has shown that PCT values were significantly higher among patients who developed postsurgical infections compared with those who did not [20]. However, due to the relatively low levels of PCT in infected individuals (ng/mL), high-sensitivity PCT is always acquired which makes the procedure costly and limited to facilities [55].

Presepsin, a soluble CD14 subtype, has been considered as a new, emerging, early indicator for diagnosis and prognosis of wound infections. It is secreted by monocytes and functions to stimulate the phagocytosis of monocytes within innate immunity responses [56]. In order to qualitatively and quantitatively measure presepsin, a presepsin assay kit is initially used. Subsequently, a highly sensitive, and fully automated PATHFAST presepsin measurement system was developed for faster processing [57]. Based on the results of several clinical studies, presepsin levels in patients with systemic bacterial infections are significantly higher than those without infections [58-60]. However, there are still several limitations associated to this approach, such as the influence of pathophysiological conditions on its concentration [61], artificial elevation caused by the burn instead of infection [62], and alteration contributed by chronic kidney syndromes [63].

As an adjunct to wound cultures, culture-independent investigation of the microbial DNA applying the pyrosequencing [64], PCR-denaturing gradient gel electrophoresis[65], and quantitative real-time PCR [66] have identified a greater range of bacteria than traditional culture techniques. However, these identification techniques are costly and they require special training as well as the instrument which make them less translational into clinical application. Nowadays,

DxWound, a PCR based microbial DNA analysis system, has been developed to provide accurate and sensitive detection of an array of microbes including aerobic bacteria, anaerobic bacteria, and fungi [67]. Moreover, the procedure is easy to handle and the report can typically come out within one day. This rapid, comprehensive and actionable testing has a great potential to help clinicians diagnose wound infection.

Bacterial protease is a large and diverse group of proteases produced exclusively by all microorganisms and functions mainly in degrading host tissue proteins to sustain the bacteria [68]. Bacterial proteases are often secreted into the infected wound environment and therefore can be utilized as diagnostic markers for wound infection. Moreover, the measurement of bacterial protease activity (BPA) can help to understand the pathological behavior of the microorganisms within the wound and provide information on wound infection prognosis [69]. The most common and basic method to assess the BPA is the incorporation of substrates of bacterial proteases, such as collagen, gelation, and casein, into microbiological agar and a zone of clearance in the agar will appear where extracellular bacterial protease presents [70]. However, this technique is time consuming and lacks specificity. A point-of-care swab-based test, WOUNDCHEK™ Bacterial Status, has been developed by WOUNDCHEK Laboratories to help clinicians to detect EPA within 15 minutes [71]. The product is still undergoing clinic trail and its potential to aid the diagnosis and prognosis of wound infection has yet to be determined. A table that summarizes and compares all the available laboratory markers for wound infection diagnosis is listed for better comprehension (Table 6).

Imaging modalities and instrumentations

Traditional imaging modalities

In clinic, to confirm the diagnosis from visual observation/blood test and to examine the existence of systemic/deep tissue infection, several current imaging modalities are applied to aid wound infection diagnosis from time to time. These imaging modalities include plain

radiography (X-ray), computed tomography (CT), magnetic resonance imaging (MRI), and ultrasound imaging. These imaging modalities are not used as primary diagnostic tools for wound infection due to the facts that they require specific instruments, imaging facility, and are costly.

Plain radiography generally constitutes the initial examination for patients with soft-tissue infections. This approach is widely used to obtain and interpret plain films due to its simple operation, low cost, and wide availability [72]. The radiographs can point out possible inflammatory changes including an effacement of fat planes, swelling, and skin discontinuity in deep ulcers. However, most of the findings are nonspecific and can be misled by other conditions, such as trauma, venous insufficiency, systemic causes of subcutaneous edema, and deep venous thrombosis [73]. Fortunately, plain radiography can distinguish swelling caused by infection from underlying fractures [74].

Computed tomography (CT) plays an important role in the diagnosis of soft-tissue infection and intra-abdominal abscesses due to its wide availability, fast scanning speed, high spatial resolution, and multi-planar reformatting capabilities [75]. Compared with ultrasound imaging which is best for superficial wound infections, CT can evaluate deeper structures and the extent of surrounding inflammations [21]. Moreover, with the application of contemporary contrast protocols, small infected collections, such as internal gas, debris, and peripheral enhancement, can be identified [76].

Magnetic resonance imaging (MRI) has become a domestic imaging tool for the diagnosis of soft-tissue infection due to its high spatial and contrast resolution. Anatomic and pathophysiologic information about the extent of infection within both soft tissue and the underlying bone can be provided by MRI [77]. With the administration of complementary imaging sequences and contrast medium, extent of infection, outline abscess collections and soft-tissue edema can be defined [78]. However, for foreign body detection within superficial wounds, there

are difficulties to distinguish foreign bodies from adjacent structures, such as scar tissue, calcifications, and tendons [21]. Besides, the high cost and low availability of the imaging equipment limit the routine utilization of MRI.

Ultrasound imaging has been widely used and proved to increase diagnostic accuracy in skin and soft tissue infections, such as abscess, wound infection and cellulitis [79]. Ultrasound imaging is standing out among other imaging modalities due to its fast, cost-effective, portable, readily available in many practice settings, and no ionizing radiation properties [80]. Ultrasound imaging has also been applied for evaluation of the suspected radiolucent foreign bodies [81]. As ultrasound imaging can be interfered by the air, when utilized for intra-abdominal infection diagnosis, loops of intestines with intra-luminal gas can obscure its detection [80]. Operator skill is also required to distinguish an abscess from other causes of skin swelling [82].

New imaging modalities

There are several innovative imaging approaches that are still under laboratory development. These imaging approaches include spatial frequency domain imaging (SFDI), thermography, fluorescence imaging and Positron Emission Topography. These fast and noninvasive imaging technologies have a great potential to revolutionize wound infection diagnosis.

Spatial frequency domain imaging (SFDI) is a new noncontact imaging approach that can quantify volume fraction of tissue chromophores, such as oxy-hemoglobin, deoxy-hemoglobin, and water [83]. It can study optical properties of wound tissue by separating and quantifying absorbed and scattered incoherent monochromatic light [84]. The technique has been applied to identify infection in burn wound through quantifying changes in absorption and reduced scattering that correlate with bacterial infection [85]. Although SFDI technology is new to the field of cutaneous wound research, it is promising for diagnosis of burn wound infection and has a great potential to assess infections in diabetic wounds as well as pressure ulcers [86, 87].

Thermography is a technique that applying an infrared camera to measure infrared radiation emitted from the wound tissue[88]. As a marker of inflammation, elevated temperature can be used in multiple studies to diagnose infection around wound site [89]. Recently, smart phone based thermography has been developed for diabetic foot ulcer detection and wound healing prediction which elevated the technique to be simple, portable and cost-effective [90, 91]. Although the technique itself has limited accuracy and specificity [92], it can offer complementary information on wound infection and has a potential to be utilized remotely from the clinic.

Luminescence imaging, an emerging imaging modality that captures visible photons emitted by Cherenkov radiation [93], has recently been used to detect infection in skin wounds [94]. A portable luminescence imaging device for detecting both inflammatory responses and infection in superficial wounds has been developed and tested using a pig full-thickness cutaneous wound model [94]. Since reactive oxygen species (ROS) levels can increase by an order of magnitude in an infected wound [95], this imager can display 2D ROS activity distribution in real time through visualizing ROS-associated luminescence. Moreover, by analyzing ROS intensity and distribution within infected wounds on a pig model, this approach has been developed to distinguish infected wounds from uninfected ones. With unique properties of simple, non-invasive, real-time, and portable, the imager has a great potential to be utilized in clinic as a wound infection diagnostic.

Autofluorescence imaging is becoming an innovative approach for diagnosis of wound infection due to the light absorbing properties of endogenously produced bacterial porphyrins. Bacterial porphyrins are not only important for the metabolism of molecular oxygen and diatomic gases, but also involved in gene regulation [96]. Many clinically relevant bacterial species, such as *S. aureus*, MRSA, *Escherichia coli*, *Enterococcus spp.*, *Proteus spp.*, *Klebsiella pneumonia*, and *Enterobacter spp.*, have been detected using this approach without application of a contrast agent [97, 98]. A handheld portable autofluorescence imaging device has been developed and tested to detect bacterial infection around diabetic foot ulcers in real time [99, 100]. Moreover, a

product, MolecuLight i:XTM, has been commercialized based on the prototype and can not only improve the diagnostic accuracy of identifying wound infection, but also guide more timely and appropriate treatment decisions at the point-of-care [101, 102]. However, it should be noted that this product has many limitations. Briefly, it cannot detect all microorganism which could infect wounds, since not all microorganisms possess porphyrins. In addition, it cannot be used to identify the exact species of the infected microorganisms due to the nonspecific fluorescence from bacterial porphyrins. The wound must also not be actively bleeding or have blood on the wound or periwound areas as this can block the fluorescence signal[103].

Biosensor

A small and inexpensive biosensor has recently been invented to provide clinicians with instant diagnosis of a bacterial infection [104]. A microwave-microfluidic biosensor was recently made available for rapid, contactless and noninvasive quantification of *E. coli* within medium solutions to increase the efficacy of clinical wound infection assessment. Through measuring the variation of resonant amplitude and frequency responses of the microwave system, different concentrations of bacteria can be detected in solutions with different pH values. The minimum prepared optical transparency of bacteria was tested at an OD_{600} value of 0.003 which indicates the poor sensitivity of this device. Moreover, the growth of bacteria can be monitored over time and that reveals the potential to use the device for rapid and real-time monitoring of bacterial infection in the wound. A table that summarizes and compares all the available imaging modalities and instrumentations for wound infection diagnosis is listed for better comprehension (Table 7).

Positron Emission Tomography and Single Photon Emission Computed Tomography

Positron Emission Tomography (PET) relies on developing a three-dimensional image from the accumulation of specific radioisotopes and resulting emission of gamma photons via positron annihilations to construct a three-dimensional image of area of isotope accumulation. Originally, these tracers have been successfully used in the clinic to image tumors since the labels can be

adapted to metabolites that are preferentially taken up by tumors or by immune cells migrating to tumors[105-107]. Many of the same inflammatory modulators and responses are present in infection and these have been used to indirectly detect loci of infection[108-110]. Recently more direct methods to target PET labels specifically for bacteria have been undertaken and are in the process of being validated for use [111-114]. PET can also be coupled with CT scanning to provide a three-dimensional image with underlying anatomical features which can be used to monitor the progress of therapy or provide a clinician with a guide in the event surgical debridement is necessary [108, 109, 115]

The limitations of PET and SPECT/CT in that indirect visualization has to be interpreted correctly to prevent misdiagnosis resulting from sterile inflammation. While this can be resolved by the incorporation of bacterial-specific tracers, in case of combination systems (PET/CT and SPECT/CT) with independent screening modalities must be accounted for in the design of the device[116]. Photon attenuation and correction for scattering with CT must also be accounted for. The equipment to perform these scans and the facility to produce the radioisotope tracers is also expensive and based on the short half-life of the tracers, they must be produced and used within a short timeframe.

Summary

With the growing population of patients whose wounds have a great chance to get infected, there is a great need for a fast, costive, noninvasive, accurate, simple and specific technique to assist clinicians in wound infection diagnosis. Current techniques used in clinical practice including visual observation for clinical signs and symptoms, clinical/laboratory assessments, and imaging modalities/instrumentations are more or less off the target. Based on the recent development of product for diagnostics of wound infection, such as PCR kits DxWound, bacterial protease activity kits WoundChek, and handheld portable bacteria imager MolecuLight i:XTM, there is still giant space for improvement in order to meet the needs of the growing wound care market. Nevertheless, with all these innovative products, the process of the

wound infection diagnosis will become much simpler, faster and cheaper in clinics in the near future.

TAKE-HOME MESSAGES

Wound infection is one of the main factors for delayed wound healing.

Wound infection continuum has three stages including contamination, colonization, and infection.

Current wound infection diagnostics like visual observation of signs and symptoms of wound infection and wound culture are costly, time-consuming, and lack of accuracy.

Pros and cons of the current wound culture techniques.

Multiple laboratory markers have been used for wound infection diagnosis, such as white blood cell count, ESR, CRP, PCT, presepsin, Microbial DNA, and BPA. Pros and cons of using them have been compared.

Other than traditional imaging modalities, new imaging modalities including SFDI, thermography, luminescence imaging, autofluorescence imaging and bacterial specific PET have been used for wound infection diagnosis. Summary and comparison of all the imaging modalities have been listed.

Biosensor has been developed for wound infection diagnosis as well.

ACKNOWLEDEGMENT AND FUNDING SOURCES

This work was supported by a grant from National Institute of Health (AR064650).

AUTHOR DISCLOSURE AND GHOSTWRITING

Conflict of interest: Tang has a potential research conflict of interest due to a financial interest with Progenitec Inc. A management plan has been created to preserve objectivity in research in accordance with UTA policy.

Paul Renick has a potential research conflict of interest due to employment as a full-time staff scientist at Smith & Nephew, plc. and his graduate studies are funded through an employee tuition reimbursement program. A management plan has been created to preserve objectivity in research in accordance with UTA policy.

No competing financial interests exist for the other authors. The content of this article was expressly written by the author(s) listed. No ghostwriters were used to write this article.

ABOUT THE AUTHORS

Shuxin Li – is a bioengineering doctoral student at the University of Texas at Arlington. His research focuses on fabricating probes and probe-loaded gauze for wound monitoring and healing.

Paul Renick –is a quantitative biology doctoral student at the University of Texas at Arlington. His research focuses on the development of bacterial specific PET probes and the development of activated antimicrobial peptides. He is also employed as a Staff Scientist at Smith & Nephew plc.

and has worked in the pharmaceutical industry in the discovery and development of novel antibacterials and biologic therapies.

Jon Senkowsky – is a vascular surgeon with over 30 years of clinical experience in wound management. He provides care for patients with chronic wounds on a daily basis using many techniques and products for the treatment of chronic, non-healing wounds in patients with vascular disease, venous stasis and diabetes.

Ashwin Nair – is a scientist and project leader at Progenitec Inc., with expertise in foreign body reactions to materials and tissue regeneration techniques.

Liping Tang – is a bioengineering professor at the University of Texas at Arlington. His expertise covers a broad area of biocompatibility, biomaterials, tissue engineering, inflammation imaging, infection and stem cell therapies.

References

1. Bumpus K, Maier MA: The ABC's of wound care. *Current cardiology reports.* 2013;15:346.

2. Järbrink K, Ni G, Sönnergren H, et al.: The humanistic and economic burden of chronic wounds: a protocol for a systematic review. *Systematic Reviews.* 2017;6:15.

3. Nussbaum SR, Carter MJ, Fife CE, et al.: An Economic Evaluation of the Impact, Cost, and Medicare Policy Implications of Chronic Nonhealing Wounds. *Value in Health.* 2018;21:27-32.

4. Fonder MA, Lazarus GS, Cowan DA, Aronson-Cook B, Kohli AR, Mamelak AJ: Treating the chronic wound: a practical approach to the care of nonhealing wounds and wound care dressings. *Journal of the American Academy of Dermatology.* 2008;58:185-206.

5. Kirsner RS: The wound healing society chronic wound ulcer healing guidelines update of the 2006 guidelines—blending old with new. *Wound Repair and Regeneration.* 2016;24:110-111.

6. Haesler E, Ousey K: Evolution of the wound infection continuum. *Wounds International.* 2018;9:6-10.

7. Sudharsanan S, Gs S, Sureshkumar S, Vijayakumar C, Sujatha S, Kate V: Does Fine Needle Aspiration Microbiology Offer Any Benefit Over Wound Swab in Detecting the Causative Organisms in Surgical Site Infections? *Wounds: a compendium of clinical research and practice.* 2017;29:255-261.

8. Frykberg RG, Banks J: Challenges in the treatment of chronic wounds. *Advances in wound care.* 2015;4:560-582.

9. Swanson T, Keast D, Cooper R, et al.: Ten top tips: identification of wound infection in a chronic wound. *Wounds Middle East.* 2015;2:20-25.

10. Hurlow J, Couch K, Laforet K, Bolton L, Metcalf D, Bowler P: Clinical biofilms: a challenging frontier in wound care. *Advances in wound care.* 2015;4:295-301.

11. Malone M, Bjarnsholt T, McBain AJ, et al.: The prevalence of biofilms in chronic wounds: a systematic review and meta-analysis of published data. *J Wound Care.* 2017;26:20-25.

12. Flemming H-c, Wingender J, Szewzyk U, Steinberg P, Rice SA, Kjelleberg S: Biofilms: an emergent form of bacterial life. *Nature Reviews. Microbiology.* 2016;14:563-575.

13. Prabhakara R, Harro JM, Leid JG, Harris M, Shirtliff ME: Murine Immune Response to a Chronic Staphylococcus aureus Biofilm Infection. *Infection and Immunity.* 2011;79:1789.

14. Thurlow LR, Hanke ML, Fritz T, et al.: Staphylococcus aureus biofilms prevent macrophage phagocytosis and attenuate inflammation in vivo. *Journal of immunology (Baltimore, Md. : 1950).* 2011;186:6585-6596.

15. Kostakioti M, Hadjifrangiskou M, Hultgren SJ: Bacterial biofilms: development, dispersal, and therapeutic strategies in the dawn of the postantibiotic era. *Cold Spring Harbor perspectives in medicine.* 2013;3:a010306-a010306.

16. Bamberg R, Sullivan P, Conner-Kerr T: Diagnosis of wound infections: current culturing practices of US wound care professionals. *WOUNDS-A COMPENDIUM OF CLINICAL RESEARCH AND PRACTICE.* 2002;14:314-328.

17. Baranoski S, Ayello EA: *Wound care essentials: Practice principles*: Lippincott Williams & Wilkins; 2008.

18. Smith ME, Robinowitz N, Chaulk P, Johnson K: Comparison of chronic wound culture techniques: swab versus curetted tissue for microbial recovery. *British journal of community nursing.* 2014;19:S22-S26.

19. van Asten SA, Jupiter DC, Mithani M, La Fontaine J, Davis KE, Lavery LA: Erythrocyte sedimentation rate and C-reactive protein to monitor treatment outcomes in diabetic foot osteomyelitis. *International wound journal.* 2017;14:142-148.

20. Spoto S, Valeriani E, Caputo D, et al.: The role of procalcitonin in the diagnosis of bacterial infection after major abdominal surgery: Advantage from daily measurement. *Medicine.* 2018;97.

21. Blankenship RB, Baker T: Imaging modalities in wounds and superficial skin infections. *Emergency medicine clinics of North America.* 2007;25:223-234.

22. Li S, Mohamedi AH, Senkowsky J, Nair A, Tang L: Imaging in Chronic Wound Diagnostics. *Advances in Wound Care.* 2019.

23. Walshe C: Living with a venous leg ulcer: a descriptive study of patients'experiences. *Journal of Advanced Nursing.* 1995;22:1092-1100.

24. Swanson T, Angel D: Wound infection in clinical practice update. *Australian Nursing and Midwifery Journal.* 2017;24:33.

25. Brown A: Diagnosing and managing infection in acute and chronic wounds. *Nursing Times.* 2018;114:36-41.

26. Harris C, Bates-Jensen B, Parslow N, Raizman R, Singh M, Ketchen R: Bates-Jensen wound assessment tool: pictorial guide validation project. *J Wound Ostomy Continence Nurs.* 2010;37:253-259.

27. Fette AM: A clinimetric analysis of wound measurement tools. *World Wide Wounds.* 2006.

28. Iqbal A, Jan A, Wajid M, Tariq S: Management of chronic non-healing wounds by hirudotherapy. *World journal of plastic surgery.* 2017;6:9.

29. Ousey K, Roberts D, Gefen A: Early identification of wound infection: understanding wound odour. *Journal of wound care.* 2017;26:577-582.

30. Jones J: Examining the multifactorial nature of wound infection. *Wounds Essentials.* 2012;2:90-97.

31. Gardner SE, Frantz RA, Doebbeling BN: The validity of the clinical signs and symptoms used to identify localized chronic wound infection. *Wound repair and regeneration.* 2001;9:178-186.
32. White R: Wound infection-associated pain. *Journal of wound care.* 2009;18:245-249.
33. Mudge E, Orsted H: Wound infection and pain management made easy. *Wounds International.* 2010;1:1-6.
34. Stotts NA, Whitney JD: Identifying and evaluating wound infection. *Home healthcare nurse.* 1999;17:159-164; quiz 165.
35. Spear M: When and how to culture a chronic wound. *Wound Care Advisor.* 2014;3:23-25.
36. Alavi A, Niakosari F, Sibbald RG: When and how to perform a biopsy on a chronic wound. *Advances in skin & wound care.* 2010;23:132-140.
37. Bonham PA: Swab cultures for diagnosing wound infections: a literature review and clinical guideline. *Journal of Wound Ostomy & Continence Nursing.* 2009;36:389-395.
38. Spear M: Best technique for obtaining wound cultures. *Plastic Surgical Nursing.* 2012;32:34-36.
39. Esposito S, De Simone G, Gioia R, et al.: Deep tissue biopsy vs. superficial swab culture, including microbial loading determination, in the microbiological assessment of Skin and Soft Tissue Infections (SSTIs). *Journal of Chemotherapy.* 2017;29:154-158.
40. Haalboom M, Blokhuis-Arkes MH, Beuk RJ, et al.: Wound swab and wound biopsy yield similar culture results. *Wound Repair and Regeneration.* 2018;26:192-199.
41. Haalboom M, Blokhuis-Arkes M, Beuk R, et al.: Culture results from wound biopsy versus wound swab: does it matter for the assessment of wound infection? *Clinical microbiology and infection.* 2019;25:629. e627-629. e612.
42. Kallstrom G: Are Quantitative Bacterial Wound Cultures Useful? *Journal of Clinical Microbiology.* 2014;52:2753-2756.
43. Aggarwal VK, Higuera C, Deirmengian G, Parvizi J, Austin MS: Swab cultures are not as effective as tissue cultures for diagnosis of periprosthetic joint infection. *Clinical Orthopaedics and Related Research®.* 2013;471:3196-3203.
44. Riley LK, Rupert J: Evaluation of Patients with Leukocytosis. *American family physician.* 2015;92.
45. Ertugrul BM, Savk O, Ozturk B, Cobanoglu M, Oncu S, Sakarya S: The diagnosis of diabetic foot osteomyelitis: examination findings and laboratory values. *Medical Science Monitor.* 2009;15:CR307-CR312.
46. Armstrong DG, Lavery LA, Sariaya M, Ashry H: Leukocytosis is a poor indicator of acute osteomyelitis of the foot in diabetes mellitus. *The Journal of foot and ankle surgery.* 1996;35:280-283.
47. Dinh T, Snyder G, Veves A: Review papers: current techniques to detect foot infection in the diabetic patient. *The international journal of lower extremity wounds.* 2010;9:24-30.
48. Bray C, Bell LN, Liang H, et al.: Erythrocyte sedimentation rate and C-reactive protein measurements and their relevance in clinical medicine. *Wmj.* 2016;115:317-321.
49. Xia D, Samols D: Transgenic mice expressing rabbit C-reactive protein are resistant to endotoxemia. *Proceedings of the National Academy of Sciences.* 1997;94:2575-2580.
50. Litao MKS, Kamat D: Erythrocyte sedimentation rate and C-reactive protein: how best to use them in clinical practice. *Pediatric annals.* 2014;43:417-420.
51. Jeandrot A, Richard J-L, Combescure C, et al.: Serum procalcitonin and C-reactive protein concentrations to distinguish mildly infected from non-infected diabetic foot ulcers: a pilot study. *Diabetologia.* 2008;51:347-352.
52. Fujii T, Tabe Y, Yajima R, Tsutsumi S, Asao T, Kuwano H: Relationship between C-reactive protein levels and wound infections in elective colorectal surgery: C-reactive protein as a predictor for incisional SSI. *Hepatogastroenterology.* 2011;58:752-755.

53. Müller B, Christ-Crain M, Nylen ES, Snider R, Becker KL: Limits to the use of the procalcitonin level as a diagnostic marker. *Clinical infectious diseases.* 2004;39:1867-1868.
54. Becker KL, Snider R, Nylen ES: Procalcitonin assay in systemic inflammation, infection, and sepsis: clinical utility and limitations. *Critical care medicine.* 2008;36:941-952.
55. Aimoto M, Koh H, Katayama T, et al.: Diagnostic performance of serum high-sensitivity procalcitonin and serum C-reactive protein tests for detecting bacterial infection in febrile neutropenia. *Infection.* 2014;42:971-979.
56. Chenevier-Gobeaux C, Borderie D, Weiss N, Mallet-Coste T, Claessens Y-E: Presepsin (sCD14-ST), an innate immune response marker in sepsis. *Clinica Chimica Acta.* 2015;450:97-103.
57. Okamura Y, Yokoi H: Development of a point-of-care assay system for measurement of presepsin (sCD14-ST). *Clinica Chimica Acta.* 2011;412:2157-2161.
58. Endo S, Suzuki Y, Takahashi G, et al.: Usefulness of presepsin in the diagnosis of sepsis in a multicenter prospective study. *Journal of Infection and Chemotherapy.* 2012;18:891-897.
59. Liu B, Chen Y-X, Yin Q, Zhao Y-Z, Li C-S: Diagnostic value and prognostic evaluation of Presepsin for sepsis in an emergency department. *Critical Care.* 2013;17:R244.
60. Topcuoglu S, Arslanbuga C, Gursoy T, et al.: Role of presepsin in the diagnosis of late-onset neonatal sepsis in preterm infants. *The Journal of Maternal-Fetal & Neonatal Medicine.* 2016;29:1834-1839.
61. Claessens Y-E, Trabattoni E, Grabar S, et al.: Plasmatic presepsin (sCD14-ST) concentrations in acute pyelonephritis in adult patients. *Clinica Chimica Acta.* 2017;464:182-188.
62. Hayashi M, Yaguchi Y, Okamura K, et al.: A case of extensive burn without sepsis showing high level of plasma presepsin (sCD14-ST). *Burns Open.* 2017;1:33-36.
63. Nagata T, Yasuda Y, Ando M, et al.: Clinical impact of kidney function on presepsin levels. *PloS one.* 2015;10:e0129159.
64. Cummings PJ, Ahmed R, Durocher JA, Jessen A, Vardi T, Obom KM: Pyrosequencing for microbial identification and characterization. *JoVE (Journal of Visualized Experiments).* 2013:e50405.
65. Liu D, Du L, Yu J, et al.: 16S rDNA PCR-DGGE and sequencing in the diagnosis of neonatal late-onset septicemia. *Molecular medicine reports.* 2015;12:6346-6352.
66. Maurin M: Real-time PCR as a diagnostic tool for bacterial diseases. *Expert review of molecular diagnostics.* 2012;12:731-754.
67. Cantrell S: A feeling for healing Wound-care excellence requires education, evidence, efficacy. *Infection.* 2018;2018.
68. Lebrun I, Marques-Porto R, Pereira A, Pereira A, Perpetuo E: Bacterial toxins: an overview on bacterial proteases and their action as virulence factors. *Mini reviews in medicinal chemistry.* 2009;9:820-828.
69. Kaman W, Hays J, Endtz H, Bikker F: Bacterial proteases: targets for diagnostics and therapy. *European journal of clinical microbiology & infectious diseases.* 2014;33:1081-1087.
70. Suleman L: Extracellular bacterial proteases in chronic wounds: a potential therapeutic target? *Advances in wound care.* 2016;5:455-463.
71. Serena TE: Development of a novel technique to collect proteases from chronic wounds. *Advances in wound care.* 2014;3:729-732.
72. Modjtahedi BS, Rong A, Bobinski M, McGahan J, Morse LS: Imaging characteristics of intraocular foreign bodies: a comparative study of plain film X-ray, computed tomography, ultrasound, and magnetic resonance imaging. *Retina.* 2015;35:95-104.

73. Hayeri MR, Ziai P, Shehata ML, Teytelboym OM, Huang BK: Soft-tissue infections and their imaging mimics: from cellulitis to necrotizing fasciitis. *Radiographics.* 2016;36:1888-1910.
74. Yadavalli S: Radiologic evaluation of musculoskeletal soft tissue infections: a pictorial review. *Current Radiology Reports.* 2015;3:40.
75. Martinez M, Peponis T, Hage A, et al.: The role of computed tomography in the diagnosis of necrotizing soft tissue Infections. *World journal of surgery.* 2018;42:82-87.
76. Ady J, Fong Y: Imaging for infection: from visualization of inflammation to visualization of microbes. *Surgical infections.* 2014;15:700-707.
77. Soldatos T, Durand DJ, Subhawong TK, Carrino JA, Chhabra A: Magnetic resonance imaging of musculoskeletal infections: systematic diagnostic assessment and key points. *Academic radiology.* 2012;19:1434-1443.
78. Harish S, Chiavaras MM, Kotnis N, Rebello R: MR imaging of skeletal soft tissue infection: utility of diffusion-weighted imaging in detecting abscess formation. *Skeletal radiology.* 2011;40:285-294.
79. Pulia MS, Calderone MR, Meister JR, Santistevan J, May L: Update on management of skin and soft tissue infections in the emergency department. *Current infectious disease reports.* 2014;16:418.
80. O'Rourke K, Kibbee N, Stubbs A: Ultrasound for the evaluation of skin and soft tissue infections. *Missouri medicine.* 2015;112:202.
81. Cai X, Kim C, Pramanik M, Wang LV: Photoacoustic tomography of foreign bodies in soft biological tissue. *Journal of Biomedical Optics.* 2011;16:046017.
82. Berger T, Garrido F, Green J, Lema PC, Gupta J: Bedside ultrasound performed by novices for the detection of abscess in ED patients with soft tissue infections. *The American journal of emergency medicine.* 2012;30:1569-1573.
83. Thatcher JE, Squiers JJ, Kanick SC, et al.: Imaging techniques for clinical burn assessment with a focus on multispectral imaging. *Advances in wound care.* 2016;5:360-378.
84. Cuccia DJ: Spatial frequency domain imaging (SFDI): a technology overview and validation of an LED-based clinic friendly device. *Emerging Digital Micromirror Device Based Systems and Applications IV*: International Society for Optics and Photonics; 2012:825405.
85. Nguyen TT, Ramella-Roman JC, Moffatt LT, Ortiz RT, Jordan MH, Shupp JW: Novel application of a spatial frequency domain imaging system to determine signature spectral differences between infected and noninfected burn wounds. *Journal of Burn Care & Research.* 2013;34:44-50.
86. Paul DW, Ghassemi P, Ramella-Roman JC, et al.: Noninvasive imaging technologies for cutaneous wound assessment: A review. *Wound Repair and Regeneration.* 2015;23:149-162.
87. Rowland RA, Ponticorvo A, Baldado ML, et al.: Burn wound classification model using spatial frequency-domain imaging and machine learning. *Journal of biomedical optics.* 2019;24:056007.
88. Hernandez-Contreras D, Peregrina-Barreto H, Rangel-Magdaleno J, Gonzalez-Bernal J: Narrative review: Diabetic foot and infrared thermography. *Infrared Physics & Technology.* 2016;78:105-117.
89. Bharara M, Schoess J, Armstrong DG: Coming events cast their shadows before: detecting inflammation in the acute diabetic foot and the foot in remission. *Diabetes/metabolism research and reviews.* 2012;28:15-20.
90. Fraiwan L, AlKhodari M, Ninan J, Mustafa B, Saleh A, Ghazal M: Diabetic foot ulcer mobile detection system using smart phone thermal camera: a feasibility study. *Biomedical engineering online.* 2017;16:117.

91. Yi S, Lu M, Yee A, Harmon J, Meng F, Hinduja S: Enhance wound healing monitoring through a thermal imaging based smartphone app. *Medical Imaging 2018: Imaging Informatics for Healthcare, Research, and Applications*: International Society for Optics and Photonics; 2018:105791P.

92. Burke-Smith A, Collier J, Jones I: A comparison of non-invasive imaging modalities: Infrared thermography, spectrophotometric intracutaneous analysis and laser Doppler imaging for the assessment of adult burns. *Burns.* 2015;41:1695-1707.

93. Ruggiero A, Holland JP, Lewis JS, Grimm J: Cerenkov luminescence imaging of medical isotopes. *Journal of Nuclear Medicine.* 2010;51:1123-1130.

94. Dacy A, Haider N, Davis K, Hu W, Tang L: Design and evaluation of an imager for assessing wound inflammatory responses and bioburden in a pig model. *Journal of Biomedical Optics.* 2019;25.

95. Kim M-H, Liu W, Borjesson DL, et al.: Dynamics of neutrophil infiltration during cutaneous wound healing and infection using fluorescence imaging. *Journal of Investigative Dermatology.* 2008;128:1812-1820.

96. Shu M, Kuo S, Wang Y, et al.: Porphyrin metabolisms in human skin commensal propionibacterium acnes bacteria: potential application to monitor human radiation risk. *Current medicinal chemistry.* 2013;20:562-568.

97. Richards-Kortum R, Sevick-Muraca E: Quantitative optical spectroscopy for tissue diagnosis. *Annual review of physical chemistry.* 1996;47:555-606.

98. DaCosta RS, Andersson H, Wilson BC: Molecular Fluorescence Excitation–Emission Matrices Relevant to Tissue Spectroscopy¶. *Photochemistry and photobiology.* 2003;78:384-392.

99. Wu YC, Smith M, Chu A, et al.: Handheld fluorescence imaging device detects subclinical wound infection in an asymptomatic patient with chronic diabetic foot ulcer: a case report. *International wound journal.* 2016;13:449-453.

100. Ottolino-Perry K, Chamma E, Blackmore KM, et al.: Improved detection of clinically relevant wound bacteria using autofluorescence image-guided sampling in diabetic foot ulcers. *International wound journal.* 2017;14:833-841.

101. Serena TE, Harrell K, Serena L, Yaakov RA: Real-time bacterial fluorescence imaging accurately identifies wounds with moderate-to-heavy bacterial burden. *Journal of wound care.* 2019;28:346-357.

102. Rennie MY, Dunham D, Lindvere-Teene L, Raizman R, Hill R, Linden R: Understanding real-time fluorescence signals from bacteria and wound tissues observed with the MolecuLight i: XTM. *Diagnostics.* 2019;9:22.

103. FAQ MolecuLight i:X. 2019; https://moleculight.com/faq/.

104. Narang R, Mohammadi S, Ashani MM, et al.: Sensitive, Real-time and Non-Intrusive Detection of Concentration and Growth of Pathogenic Bacteria using Microfluidic-Microwave Ring Resonator Biosensor. *Scientific reports.* 2018;8:15807.

105. Granov A, Tiutin L, Schwarz T: *Positron Emission Tomography*. 1. Aufl.;1st; ed. Berlin, Heidelberg: Springer Berlin Heidelberg; 2013.

106. Koglin N, Mueller A, Berndt M, et al.: Specific PET Imaging of x_c^-Transporter Activity Using a 18F-Labeled Glutamate Derivative Reveals a Dominant Pathway in Tumor Metabolism. *Clinical Cancer Research.* 2011;17:6000-6011.

107. Krasikova RN, Kuznetsova OF, Fedorova OS, et al.: 4-[18F]Fluoroglutamic Acid (BAY 85-8050), a New Amino Acid Radiotracer for PET Imaging of Tumors: Synthesis and in Vitro Characterization. *Journal of Medicinal Chemistry.* 2011;54:406-410.

108. Erba PA, Israel O: SPECT/CT in infection and inflammation. *Clinical and Translational Imaging.* 2014;2:519-535.

109. Horger M, Eschmann SM, Pfannenberg C, et al.: The value of SPET/CT in chronic osteomyelitis. *European Journal of Nuclear Medicine & Molecular Imaging.* 2003;30:1665-1673.
110. Palestro CJ, Love C: Role of Nuclear Medicine for Diagnosing Infection of Recently Implanted Lower Extremity Arthroplasties. *Seminars in Nuclear Medicine.* 2017;47:630-638.
111. Neumann KD, Villanueva-Meyer JE, Mutch CA, et al.: Imaging Active Infection in vivo Using D-Amino Acid Derived PET Radiotracers. *Scientific Reports.* 2017;7:7903.
112. Ordonez AA, Jain SK: Pathogen-Specific Bacterial Imaging in Nuclear Medicine. *Seminars in Nuclear Medicine.* 2018;48:182-194.
113. Vallabhajosula S, Solnes L, Vallabhajosula B: A Broad Overview of Positron Emission Tomography Radiopharmaceuticals and Clinical Applications: What Is New? *Seminars in Nuclear Medicine.* 2011;41:246-264.
114. Weinstein EA, Ordonez AA, DeMarco VP, et al.: Imaging Enterobacteriaceae infection in vivo with ^{18}F-fluorodeoxysorbitol positron emission tomography. *Science Translational Medicine.* 2014;6:259ra146-259ra146.
115. Sathekge MM, Ankrah AO, Lawal I, Vorster M: Monitoring Response to Therapy. *Seminars in Nuclear Medicine.* 2018;48:166-181.
116. Livieratos L: Technical Pitfalls and Limitations of SPECT/CT. *Seminars in Nuclear Medicine.* 2015;45:530-540.

Tables:

Table 4. Signs and symptoms within wound infection continuum

Contamination	All open wounds may contain microorganisms. They will not multiply or persist until suitable nutritive and physical conditions are available for each microbial species, or they successfully evade host's defenses. Consequently, their presence is only transient and wound healing is not delayed.
Colonization	Microbial species successfully grow and divide, but do not cause damage to the host or initiate wound infection.
Local infection	Covert (subtle) signs of local infection: Hypergranulation (excessive 'vascular tissue'); Bleeding, friable granulation; Epithelial bridging and pocketing in granulation tissue; Wound breakdown and enlargement; Delayed wound healing beyond expectations; New or increasing pain; Increasing malodor.
	Overt (classic) signs of local infection: Erythema; Local warmth; Swelling; Purulent discharge; Delayed wound healing beyond expectations; New or increasing pain; Increasing malodor.
Spreading infection	Extending in duration +/- erythema; Lymphangitis; Crepitus; Wound breakdown/dehiscence with or without satellite lesions; Malaise/lethargy or nonspecific general deterioration; Loss of appetite; Inflammation, swelling of lymph glands.
Systemic infection	Severe sepsis; Septic shock; Organ failure; Death.

International Wound Infection Institute (IWII) Wound infection in clinical practice. Wounds International 2016

Table 5. Comparisons among wound culture techniques

	Descriptions	Advantages	Disadvantages
Deep-tissue biopsy	Obtain tissue sample via punch/needle biopsy or a scalpel; Quantitative results acquired by microscopic examinations.	Conclusive and accurate result for detecting invading microorganisms; Gold standard for wound infection diagnosis.	Time-consuming, costly, invasive, painful, require special equipment and special training; High risk for postsurgical trauma, wound disruption, and bacteremia.
Needle aspiration	Obtain microbes below the surface of the wound via inserting a fine-gauge needle into tissue to aspirate fluid.	Feasible for small open wound and detecting subcutaneous microorganisms; Less invasive.	Time-consuming, painful; May underestimate bacterial isolates.
Swab culture	Press sterile culture swab against the wound base to extract wound fluid, Using eluent for incubation and quantification.	Practical, noninvasive, reproducible, and inexpensive; Has sufficient correlation with tissue biopsy outcome.	Time-consuming; Can't detect pathogenic strain invading deeper tissues; Weak in detection of anaerobic organisms.

Directly sampling of infected sights can be performed by swab culture, needle aspiration and tissue biopsy and result in the detection of pathogenic microorganisms. While these methods are widely used there are drawbacks, notably the time to culture the microorganisms (especially anaerobes), swab culture is a superficial procedure and can miss deep tissue pathogens. Both the needle aspiration and biopsy are painful and can induce pain additional trauma through wound disruption. All the methods are only capable of identifying actively growing pathogens. Molecular processing of sample via molecular techniques (PCR) can identify pathogens but are limited by sample quality and ability to obtain a sample.

Table 6. Laboratory markers for wound infection diagnosis

	Descriptions	Pros and cons
White blood cell count	Elevated neutrophil population can be considered as a sign of infection.	Simple, fast, non-invasive, cost effective; Low specificity, can't determine microbial species.
Erythrocyte sedimentation rate (ESR)	In response to infection, cytokine-induced elevations in acute-phase proteins are positively charged and thus can induce the aggregation of negatively charged erythrocytes which leads to higher ESR.	Simple, fast, non-invasive, cost effective; Artificial variation exists, low specificity, can't determine microbial species.
C-reactive protein (CRP)	In response to inflammation and infection, CRP is stimulated by cytokines primarily IL-6. By using light scattering from aggregation of CRP-specific antibody, concentration of CRP can be measured.	Simple, fast, non-invasive; Short half-time, can't determine microbial species.
Procalcitonin (PCT)	PCT is a peptide hormone secreted by non-neuroendocrine parenchymal cells and can be measured by time-resolved amplified cryptate emission. patients with bacterial infections have elevated PCT levels.	Fast, non-invasive; Costly, require high-sensitivity facilities, can't determine microbial species.
Presepsin	Presepsin is a soluble CD14 subtype secreted by monocytes and stimulates the phagocytosis of monocytes within innate immunity responses. It can be quantified by either an assay kit or PATHFAST presepsin measurement system.	Fast, non-invasive, high sensitivity, prognosis. Alterations can be contributed by other pathophysiological conditions, can't determine microbial species.
Microbial DNA	Culture-independent investigation of the microbial DNA can identify a greater range of bacteria than traditional culture techniques. It can be detected by DxWound, a PCR based microbial DNA analysis system.	Accurate, sensitive, non-invasive, can determine microbial species. Costly, require special training and instruments.
Bacterial protease activity (BPA)	Bacterial proteases are often secreted into the infected wound environment to degrade host tissue proteins for bacterial sustenance. BPA can be quantified with WOUNDCHEK™ Bacterial Status, a point-of-care swab-based test under clinic trial.	Fast, non-invasive, prognosis. Lacks specificity, can't determine microbial species.

Table 7. A summary of imaging modalities and instrumentations for wound infection diagnosis

	Descriptions	Pros and cons
Plain radiography	Initial examination for patients with soft-tissue infections; Can reveal inflammatory changes and distinguish swelling caused by infection from underlying fractures.	Simple operation, low cost, wide availability; Radioactive, most of the findings are nonspecific, can be misled by other conditions.
Computed tomography (CT)	Can diagnose soft-tissue infection and intra-abdominal abscesses; Can evaluate deeper structures and the extent of surrounding inflammations; Can identify small, infected collections.	Wide availability, fast scanning speed, high spatial resolution, multiplanar reformatting capabilities, high penetration depth; Radioactive, sometimes requires contrast agent.
Magnetic resonance imaging (MRI)	A domestic imaging tool for the diagnosis of soft-tissue infection; Can provide anatomic and pathophysiologic information about the extent of infection within both soft tissue and the underlying bone.	High spatial/contrast resolution, non-radioactive; Costly, low availability, require special training/facility, hard to distinguish foreign bodies from adjacent structures within superficial wounds.
Ultrasound imaging	Can increase diagnostic accuracy in skin and soft tissue infections; Can evaluate the suspected radiolucent foreign bodies.	Fast, cost-effective, portable, readily available in many practice settings, no ionizing radiation; Can be interfered by the air, low penetration depth, rely on operator's skill.
Spatial frequency domain imaging (SFDI)	A new noncontact imaging approach that can quantify volume fraction of tissue chromophores; Can identify infection in burn wound.	Noncontact, can distinguish infection and noninfected burn wounds; Limited scanning area, limited wound types.
Thermography	Use an infrared camera to measure infrared radiation emitted from the wound tissue; Smart phone-based thermography has been developed for diabetic foot ulcer detection and wound healing prediction.	Simple, portable, cost-effective, real time imaging, noninvasive, feasible for remote diagnosis; Limited accuracy, limited specificity.
Luminescence imaging	Using a CCD camera to capture visible photons emitted by Cherenkov radiation; Based on intensity and distribution, a portable imager has been developed to distinguish infected wounds from uninfected ones on a pig model.	Simple, portable, cost-effective, real time imaging, noninvasive, feasible for remote diagnosis; Limited specificity, still under laboratory investigation.
Autofluorescence imaging	An innovative approach for diagnosis of wound infection due to the light absorbing properties of endogenously produced bacterial porphyrins; A handheld portable device has been developed and tested to detect bacterial infection around diabetic foot ulcers in real time.	Simple, portable, cost-effective, real time imaging, sensitive, feasible for remote diagnosis. Low specificity, can't determine microbial species.
Biosensor	A microwave-microfluidic biosensor for quantification of E. coli within medium solutions to increase the efficacy of clinical wound infection assessment; The growth of bacteria can be monitored over time.	Small, cost-effective, rapid, contactless, noninvasive, real time measurement, high sensitivity; Limited detectable bacterial species, still under laboratory investigation.

CHAPTER 5

BACTERIAL ACIDITY-TRIGGERED ANTIMICROBIAL ACTIVITY OF SELF-ASSEMBLING PEPTIDE NANOFIBERS[3]

WEIKE CHEN, SHUXIN LI, PAUL RENICK, SU YANG, NIKHIL PANDY, CARA BOUTTE, KYTAI T. NGUYEN LIPING, TANG AND HE DONG

CHEN, W., ET AL. (2019). "BACTERIAL ACIDITY-TRIGGERED ANTIMICROBIAL ACTIVITY OF SELF-ASSEMBLING PEPTIDE NANOFIBERS." JOURNAL OF MATERIALS CHEMISTRY B 7(18): 2915-2919.

[3] Reproduced by permission of The Royal Society of Chemistry, July 2020

ABSTRACT

A self-assembling peptide nanofiber was developed to sense the microenvironmental pH change associated with bacterial growth. Using a near-infrared probe, a strong correlation was observed between the local pH reduction of bacterial colonies with the degree of peptide disassembly, which led to their enhanced antimicrobial activity against anaerobic bacteria.

Introduction

Trigger-responsive nanomaterials have tremendous promise for targeted therapeutic delivery strategies that improve the treatment of a variety of diseases.[1] Among various approaches, self- assembly has been proven as an effective bottom-up approach to construct functional nanomaterials. A wide range of molecular building blocks, including amphiphilic polymers, lipids, proteins and peptides can be custom-designed and assembled into ‘‘smart’’ nanomaterials that can sense various disease-specific micro- environmental conditions.[2] Self-assembled nanomaterials can easily change their physicochemical properties in response to the environmental change and lead to local release of therapeutics with enhanced drug potency and reduced side effects on healthy tissues and cells. In recent years, great levels of success have been achieved for nanomaterials designed for targeted cancer therapy.[3] However, the development of self-assembled nanomaterials for targeted antimicrobial delivery is just getting underway for infectious disease treatment.[4]

Similar to some of the tumor tissues, certain bacteria can reduce the local pH of the infectious tissues through low oxygen triggered anaerobic fermentation.[5] Host immune response can further lower the local pH where bacteria reside through the mechanism of production of lactic acids during phagocytosis.[6] While the acidic pH is considered as an undesirable factor

causing the reduction of the antimicrobial activity of several classes of antibiotics,[7] it can be utilized as a natural physiological cue for the design of antimicrobial nanomaterials for targeted antimicrobial delivery. Recent reports have demonstrated advances in the design of acid-sensitive nanoparticles for targeting the bacterial membrane and delivery of small molecule antibiotics to treat bacterial infections in acidic conditions.[4a] Acid-dependent helical polypeptides were also reported to selectively target and eradicate pathogenic *H. pylori* without affecting commensal bacteria in the stomach.[4d] These successful examples provide the inspiration and highlight the feasibility of using pH as a physiological trigger to achieve targeted antimicrobial therapy.

In this work, we sought to develop a novel acid-activatable antimicrobial therapy by capitalizing on our recent development of self-assembling nanofibers (SANs) for bacterial acidity triggered antimicrobial delivery. SANs are supramolecular assemblies of *de novo* designed multidomain peptides (MDPs) that have been explored as highly cytocompatible antimicrobial and cell penetrating nanomaterials.[8] The first generation of MDPs has a general formula of $K_x(QL)_yK_z$ (amino acid single code letter K: Lysine, Q: Glutamine, L: Leucine) to mimic natural cationic antimicrobial peptides (AMPs). Unlike most conventional AMPs that exist as monomers in solutions, MDPs can form supramolecular b-sheet nanofibers in which the hydrophobic residues and non-polar surface are partially masked between the two sheets, which has been proven as an important factor to minimize the cytotoxicity of MDPs toward mammalian cells.[9] The cytocompatibility of SANs was greatly enhanced compared to that of traditional monomeric AMPs. However, the confinement of the hydrophobic moiety within the assembly can also reduce their antimicrobial activity while monomeric AMPs are more potent to kill bacteria. As such, the current study by developing SANs that undergo pH-responsive disassembly combines the advantages of both self-assembled peptides in terms of their cytocompatibility and monomeric

AMPs in terms of their antimicrobial activity to treat acidity- associated bacterial infections. The central hypothesis is SANs under the physiological condition are bio-inert because the membrane-interacting hydrophobic moieties of SANs are buried inside the assembly and not accessible to the cell membrane. At the bacterial colonization site with an acidic pH, MDPs become charged and the increased charge density triggers SANs disassembly and subsequent release of activated peptides to effectively interact with the cell membrane and kill bacteria (Figure 12).

Three MDPs with the sequences of $WH_5(QL)_6K_2$, $WH_7(QL)_6K_2$, and $WH_9(QL)_6K_2$ abbreviated as WH_5, WH_7 and WH_9 (H: Histidine, W: Tryptophan) were initially explored as the building units to fabricate SANs. The sequences were chosen based on the following considerations. First, the central repeating (QL) domain provides the driving force for SANs formation under the neutral physiological condition as discussed in our previous studies.[8b] Second, oligo-histidine with different lengths was incorporated at the N-terminus to endow pH-responsiveness to SANs. At a pH below the pK_a of histidine, peptides become charged. The electro- static repulsion among the positively charged MDPs would destabilize SANs and lead to the release of activated MDPs that can effectively eradicate bacteria. Third, the number of histidine residues are varied to integrate and achieve a good balance between self-assembly under the neutral condition and disassembly upon acidification. MDPs with different numbers of histidine would render a small library to explore the effect of charge on SANs stability, disassembly efficiency and their resulting biological activities. Lastly, two lysine residues were appended at the C-terminus to ensure sufficient solubility of SANs and minimize lateral fiber aggregation through electro- static repulsion. All peptides contained a tryptophan residue for accurate determination of the peptide concentration by UV spectroscopy. Elucidating the physicochemical properties of MDPs as a function of pH is critical to tailor their biological activities. Critical assembly concentration (CAC) measurements were first

conducted to investigate their ability to assemble under different pH conditions. As shown in Figure 13 ~~Fig. S2~~ (ESI†), a non-linear relationship was observed for all three MDPs at pH 7.4 (Tris buffer, 20 mM) suggesting the formation of higher ordered assemblies as the concentration increased. At an acidic pH (MES buffer, pH 5.7, 20 mM), a linear correlation was found between the fluorescence intensity and peptide concentrations, suggesting most peptides do not self-assemble and rather remain isolated. It is worth noting that we chose pH 5.7 as the acidic condition for this study to achieve a good balance between the protonation degree of histidine (pKa = B6) and bacterial growth under the acidic condition. The pH-dependent self-assembly and disassembly were further investigated and confirmed by circular dichroism (CD) spectroscopy. At pH 7.4, all three peptides exhibited predominant b-sheet structures as characterized by a minimum peak between 210–220 nm (Figure 14a S3a, ESI†) indicating the formation of SANs. When the pH was reduced to 5.7, which was below the pKa point of histidine, the presumed increase in positive charges and electrostatic repulsion triggered disassembly and unfolding of b-sheets to random coils and/or weak helices. As shown in Figure 14b S3b (ESI†), all three MDPs unfolded upon pH reduction, but to different degrees. WH7 and WH9 exhibited more disordered structures thanWH5 given the larger blue shifts of the minimum absorption down to B203 nm indicating a greater tendency to disassemble. To quantitatively determine the extent of SANs disassembly, spin dialysis was used to estimate the amounts of disassembled MDPs upon pH reduction. Centrifugal filters with molecular weight (MW) cutoff at 10 kDa and 30 kDa were used to separate the monomeric MDP and any potential non-specific aggregates (up to 9 mers) (due to their amphiphilic nature) from the residual higher ordered assemblies, respectively. As shown in Table 8, no materials were detected in the filtrate for all three MDPs through spin dialysis suggesting the stability and integrity of SANs at the neutral pH. At the acidic pH, disassembly occurred as shown by the increased concentrations of MDPs in the filtrate using both filters. It was estimated that 24.60% of WH5, 34.70% of WH7 and 41.00% of WH9 were disassembled to monomers based on the dialysis result using the filter with a MW cutoff at 10

kDa. Using a 30 kDa filter, the percentage of MDPs in the filtrate increased to 37.77%, 62.56% and 71.46% for WH5, WH7 and WH9, respectively. The filtrate of WH9 at pH 5.7 was analyzed by CD spectroscopy showing highly disordered random coil structures (Figure 14c, ESI†), thus excluding the possibility of the presence of b-sheet oligomers in the filtrate. The oligomeric species present in the filtrate is likely due to the non-specific aggregation between the amphiphilic MDPs. Transmission electron microscopy (TEM) revealed the morphological change of MDPs under different pH treatments.

For TEM characterization and the following biological evaluation, we primarily focused on WH9 because it is the most sensitive to pH change giving a higher extent of disassembly upon solution acidification. At pH 7.4, WH9 spontaneously self-assembled to form elongated fibers (Figure 15a). Reducing the pH to 5.7 led to a significant reduction of the fiber density and the formation of non-specific spherical aggregates (Figure 15b). We suspect that these spherical aggregates were formed from disassembled MDPs due to the drying effect during TEM sample preparation process. The disassembly of SANs was verified by dynamic light scattering (DLS) measurements showing a dramatically reduced particle size to below 2 nm when pH was reduced (Figure 15c and Figure 16, ESI†). Although the number mean of the hydrodynamic diameter generated by DLS does not represent the actual size of these nanofibers due to their non-spherical shape, the dramatic size reduction suggests the effectiveness of solution acidity to trigger the disassembly of SANs.

Acidity-triggered SANs disassembly was further studied in the context of bacterial inoculation on an agar plate. We chose Bacteroides fragilis as a model bacterium that undergoes anaerobic growth leading to the acidification of the surrounding environment. We first determined whether the growth of B. fragilis would influence the pH immediately adjacent to the bacterial colony. Using a pH ratiometric near infrared probe developed recently,10 we measured the change of fluorescent intensity of the probe with time using an in vivo Kodak imager. The results allow us to calculate the pH nearby the colony on an agar plate at 0.5, 2.5, 7, and 22.5 h upon bacterial

inoculation. Interestingly, we found that growth of B. fragilis released metabolites which can cause the surrounding environment to become acidic (from pH 7.5 to pH 6.3 in less than 24 h) (Figure 17, ESI†). To test whether the in situ low pH can induce SANs disassembly, we synthesized and prepared rhodamine (Rho)-labeled WH9. Rho-WH9 had very low fluorescent intensity due to fluorescent quenching upon self-assembly. By reducing the local pH, WH9 disassembled leading to the recovery of rhodamine fluorescence. Therefore, the fluorescence intensity of the peptide reflects the degree of peptide disassembly and can be used to correlate with the microenvironmental pH change associated with bacterial growth. To determine whether the acidic environment nearby bacterial colonies causes SANs to disassemble, Rho-WH9 was applied on both the bacterial colonies and non-inoculated agars as controls after 24 h of bacterial inoculation. The fluorescence intensity was monitored immediately using an in vivo Kodak imager. The results showed an average of 88% increase of the fluorescence intensity for peptides deposited on the bacteria colonies than those on the agar media without bacteria (Figure 18a), suggesting a local acidic pH can trigger the disassembly of SANs, leading to the recovery of self-quenched fluorescence. The fluorescence intensity of the peptide across the bacterial colony was further plotted as a function of imaging pixels (B0.1 mm per pixel) starting from the outermost of a colony (shown as 0 on the *x*-axis of Figure 18b), while moving toward the center (shown as 10 on the *x*-axis of Figure 18b). The local bacterial pH change across a single colony was measured by the radiometric fluorescence probe described above and plotted in the same manner. A good correlation was observed between the reduced pH and the increased fluorescence of Rho-WH_9, further confirming local bacterial acidity can trigger SANs disassembly. The antimicrobial activities of WH_9 were tested against both Gram-negative bacteria, *Escherichia coli* and *B. fragilis* and Gram-positive bacteria, *Staphylococcus aureus* under the anaerobic condition where bacterial cultures became acidic over time peptides were co-incubated with *E. coli*, *B. fragilis* and *S. aureus* for 48 h and the UV absorbance at 600 nm was measured for the estimation of the minimum inhibitory concentration (MIC) values.

As shown in Table 9, WH_9 was effective against all three bacterial strains in the anaerobic condition where the bacterial culture gradually became acidic to pH 6.4. The MIC values of WH_9 were determined at 10 mM against *E. coli*, 5 mM against *B. fragilis* and 5 mM against *S. aureus*. In contrast, the MIC of WH_9 was estimated at 40 mM against *E. coli* in the aerobic condition where the culture pH remained neutral (pH was between 7.2 and 7.5 during culture). For aerobic bacterial cultures with a starting pH at 5.7, the MIC was determined as 10 mM comparable to that determined in the anaerobic condition. In comparison, the MICs of WH_5 and WH_7 were determined at 40 mM and 20 mM in the acidic aerobic *E. coli* cultures showing less potency to inhibit the growth of bacteria. The antimicrobial activity also correlates well with the peptide's ability to dissemble as detailed in the spin dialysis experiment (Table 8).

The mode of antimicrobial action was investigated by epifluorescence microscopy. WH_9 was co-incubated with *E. coli* aerobically so that the culture pH can be adjusted and maintained either acidic or neutral during the entire culture. A live–dead assay was performed wherein *E. coli* was incubated with WH_9 for 3 h, followed by staining with SYTO9 and Propidium Iodide (PI). As shown in (Figure 19a), a much higher fraction of *E. coli* cells fluoresced red at the acidic pH due to pH-triggered disassembly and release of peptides that can increase the membrane permeability of PI. At the neutral pH (Figure 19b), the peptide was confined within the SANs and did not have sufficient freedom to access to and further permeate the bacterial cell membrane. The live–dead assay was also performed in Gram-positive *S. aureus* culture showing the same trend of pH-dependent antimicrobial activity (Figure 20, ESI†).

The physical interaction between WH_9 and bacteria was also studied by fluorescence microscopy upon incubation of FITC- labelled WH_9 with *E. coli* followed by PI staining. The binding affinity of WH_9 toward bacteria was greatly improved upon acidification as demonstrated by the numbers of bacterial cells that were attached by peptides showing green fluorescence on the cell membrane (Figure 21a, ESI†) while at the neutral condition

much less binding occurred between the peptides and bacteria (Figure 21b, ESI†). Scanning electron microscopy (SEM) was used to visualize any morphological change induced in bacteria by exposure to WH_9 at the acidic condition. As compared to control bacteria without peptide treatment (Figure 22a, ESI†), *E. coli* incubated with WH_9 under the acidic culture condition showed significant membrane damage (Figure 22b, ESI†), suggesting the mode of action is through bacterial membrane disruption by the disassembled peptides.

A critical challenge associated with conventional AMPs is their moderate to severe cytotoxicity and hemolytic activity.[11] We have recently demonstrated that self-assembly can be an effective approach to reduce the non-polar membrane-contact area of AMPs leading to greatly improved cytocompatibility and bacterial cell selectivity.[9] To evaluate the cytotoxicity of the newly designed WH_9 toward mammalian cells during blood circulation, NIH/3T3 fibroblasts were incubated with peptides at various concentrations and the cell viability was quantified by the MTT assay. 80 mM was selected as the upper concentration threshold to avoid potential precipitate formation as the peptide concentration increased in the mammalian culture media. As shown in Figure 23 (ESI†), dose-dependent cell viability was measured showing ~80% of cell viability up to 40 mM and 72% cells were still alive upon incubation with peptides at 80 mM. The hemocompatibility was evaluated by incubating human red blood cells (RBCs) with WH_9 at different concentrations for 1 h and released haemoglobin was measured by UV spectroscopy (Figure 24, ESI†). Within the tested peptide concentrations up to 160 mM (16 times of the MIC) less than 5% of hemolysis was observed with peptide-treated RBCs compared to the positive control group of RBCs treated with Triton-100. Taken together, the pH-triggered antimicrobial activity and excellent cytocompatibility and hemocompatibility of self- assembled WH_9 highlight their great potential as a new anti- microbial strategy to effectively treat bacterial infections associated with acidity.

In summary, we have demonstrated a new pH-responsive antimicrobial nanomaterial based on the self-assembly of *de novo* designed MDPs for acid-responsive antimicrobial delivery at the site of infection associated with bacterial acidity. The MDP can be designed to form stable nanofibrous structure in neutral pH with excellent cytocompatibility and hemocompatibility. The pH-triggered disassembly was demonstrated in both the aqueous solution and on a bacteria-inoculated agar plate and shown to be important factors for their antimicrobial activity. This new antimicrobial strategy while awaiting more extensive *in vitro* evaluation and *in vivo* studies holds great promise to treat bacterial infections in which acidity plays an important role in bacterial pathogenesis. For future studies, SANs based on custom- designed non-natural amino acids may offer diverse chemical functionality and broader pH-tunability to suit various clinical needs in the combat of infectious diseases.

Materials and methods

Materials

Fmoc-protected amino acids, 2-(6-Chloro-1-H-benzotriazole-1-yl)-1,1,3,3-tetramethylaminium hexafluorophosphate (HCTU), MBHA rink amide resin, were purchased from Novabiochem. Piperidine, diisopropylethylamine (DIPEA) 5(6)-Carboxyfluorescein (FAM), 5(6)-carboxy-tetramethyl-rhodamine, Mueller Hinton Broth (MHB), MTT assay kit were purchased from Sigma-Aldrich. LIVE/DEADTM BacLightTM Bacterial Viability Kit, Centrifugation filters with molecular weight cutoff at 10 kDa and 30 kDa, Agar, TritonTM X- 100, Blood agar (TSA with 5% sheep blood) were purchased from Fisher Scientific. Dulbecco's modified Eagle medium (DMEM) culture medium was purchased from Life Technologies. Fetal Bovine Serum (FBS) was purchased from VWR. TEM staining reagent, uranium acetate dihydrate and TEM grid were purchased from TED PELLA, INC. Escherichia coli (ATCC 25922), Bacteroides fragilis (ATCC

25285) and Staphylococcus aureus (ATCC 29213) were purchased from ATCC.

Synthesis and purification of peptides

Multidomain peptides were synthesized on a Prelude® peptide synthesizer using standard FMOC-solid phase peptide synthesis procedures. Fmoc groups were deprotected by 20% (V/V) piperidine in N, N-dimethylformamide (DMF) for 5 min (2 times). HCTU was used as the coupling reagent and mixed Fmoc protected amino acids in the presence of DIPEA with a molar ratio of 1:1:2.5 (amino acid: HCTU: DIPEA). Upon the completion of the synthesis, the N- terminus of the peptides were acetylated in the presence acetic anhydride and DIPEA in DMF. The acetylated peptides were cleaved from the resin using a mixture of trifluoroacetic acid (TFA) / triisopropanolsilane (TIS) / H2O (95/2.5/2.5 by volume) for 3 hours. The cleavage solution was collected through filtration and neat TFA was used to wash the resin twice. TFA solution was evaporated under moderate air flow. The residual peptide solution was precipitated in cold diethyl ether, followed by centrifugation and washing with cold diethyl ether for four times. The crude peptide was dried under vacuum overnight for HPLC purification. The peptide was purified using a preparative reversed phase C4 column with a linear gradient of water/acetonitrile containing 0.05% TFA. Elution was monitored at 230 nm and 280 nm. The mass of the three peptides were confirmed by MALDI. WH5: expected [M+H]+: 2634, observed [M+H]+: 2634; WH7: expected [M+H]+: 2908, observed [M+H]+: 2908; WH9: expected [M+H]+: 3182, observed [M+H]+: 3182. Fluorescein and rhodamine terminated peptides were synthesized as follows. After final deprotection of the peptide, the N-terminus was coupled with 4 equivalents of 5(6)-carboxyl fluorescein or 5(6)-carboxy-tetramethyl-rhodamine using a combination of 4 equivalents of HCTU and 8 equivalents of DIPEA in DMF. The reaction mixture was stirred overnight. The completion of the coupling reaction was confirmed by the Kaiser test. If necessary, the coupling of 5-(6)-

carboxyl- fluorescein or 5(6)-carboxy-tetramethyl-rhodamine was repeated once. The cleavage and purification procedure followed the same procedure as described for the nonlabelled peptides. The molecular weight was confirmed by MALDI. FITC-WH9: expected [M+H]+: 3499, observed [M+H]+: 3500; Rho-WH9: expected [M+H]+: 3553, observed [M+H]+: 3554 (Figure 25).

Structural Characterization

Circular Dichroism (CD) Spectroscopy

Samples were prepared by dilution from the peptide stock solution to a concentration at 50 μM in either Tris buffer (pH 7.4, 20 mM) or MES buffer (pH 5.7, 20 mM). The samples were incubated at 4°C overnight. Data were collected from 250 nm to 190 nm at room temperature (RT) using a 1 mm cuvette, a bandwidth at 1 nm, scan rate at 100 nm/min and a response time of 2 sec. Each spectrum was averaged from three scans. The mDeg of rotation was converted to molar residual ellipticity via the formula $\theta=(mDeg*1000)/(c*n*l)$, where c is the concentration of the peptide solution expressed in mM, n is the number of amino acids in the peptide sequence and l is the path length of the cell used in mm.

Transmission Electron Microscopy (TEM)

Sample preparation was the same as that used in the CD experiment. Peptide solution (10 □L) was dropped onto a holey carbon grid (TED PELLA 01824). After 2 minutes, excess solution was carefully removed with filter paper. 10 μL of 2 wt % uranyl acetate aqueous solution was dropped onto the grid for negative staining. After 2 minutes, excess staining solution was removed and the TEM samples were dried for overnight before imaging.

Critical aggregation concentration (CAC) measurement

Peptide solution (160 μM) was added in either 200 μL Tris buffer (20 mM, pH 7.4) or 200 μL MES buffer (20 mM, pH 5.7) with an increment of 2 μL each time. Fluorescence spectra were acquired after each peptide addition by monitoring the emission of peptides from 295 nm to 440 nm using an excitation wavelength at 280 nm. Fluorescence intensity at 350 nm was plotted as a function of the peptide concentrations. The CAC was determined to be the concentration at which nonlinearity started to develop as shown in Figure 13.

Minimum inhibitory concentration (MIC) determination

For the MIC test in the aerobic condition, *E. coli* was cultured in MHB media under constant shaking at 100 rpm at 37 °C to reach the mid-exponential growth phase. The bacterial solution was plated on an agar plate for colony forming unit (CFU) counting. Bacterial suspensions were diluted to approximately 2x105 CFU/mL in MHB media at either pH 7.4 or 5.7. Peptide solutions at various concentration (80, 40, 20, 10, 5, 2.5 μM) were prepared in either Tris buffer (pH 7.4, 20 mM) or MES buffer (pH 5.7, 20 mM) through filter sterilization and exposed under UV light for at least 30 mins. 50 μL of each peptide solution was mixed with 50 μL of bacterial solution in a 96-well plate and the experiments were performed in triplicates. The plates were incubated at 37°C under constant shaking at 100 rpm for 18 hrs and the optical density (OD) at 600 nm was measured on a plate reader. The MIC was determined at the peptide concentration in which OD reading is below 0.06 and no cloudiness was visible to naked eyes. For the MIC test in the anaerobic condition, *E. coli* (ATCC 25922), *B. fragilis* (ATCC 25285) and *S. aureus* (ATCC 29213) inocula were prepared using the BBL Prompt Inoculation System to generate an approximate 1.5 x 10^8 CFU/mL that was further diluted to

generate an inoculum at 1.0 x 10^6 CFU/mL in MHB media at pH 7.4. Peptide solutions with various concentration (80, 40, 20, 10, 5, 2.5 μM) were prepared in Tris buffer (pH 7.4, 20 mM). All the reagents for the anaerobic test were reduced under anaerobic conditions for at least 2 hrs prior to the initiation of testing and care was taken to minimize all bacterial strains to oxygen exposure. 50 μL of each peptide solution was mixed with 50 μL of bacterial solution in a 96- well plate and the experiments were performed in triplicates. The plates were incubated 48 hrs under constant shaking at 100 rpm. The MIC was determined at the peptide concentration in which OD reading is below 0.06 and no cloudiness was visible to naked eyes. For all MIC tests, bacterial culture without peptides (with equal volume mixing of Tris buffer) was used as a negative control. Gentamicin was used as the positive control that helps validate the MIC assay. The aerobic control plates only and against the control drugs (Gentamicin and Moxifloxacin) have MIC values within the CLSI control ranges and MBCs consistent with known bactericidal modes of action. Gentamicin is efficacious against *E. coli* and *S. aureus* although the MIC is shifted higher in anaerobic versus aerobic conditions.[1]

Scanning electron microscopy to examine the morphology of the bacterial membrane

400 μL bacterial suspensions (*E. coli,* 10^8 CFU/mL) were added to a 24-well plate with a cover glass (d=12 mm) placed on the bottom of each well. After 24 hrs of incubation, bacterial suspension was removed, and the plates were washed with PBS buffer (pH 7.4) to remove any non-adherent bacteria. 100 μL of fresh MHB media (pH 5.7) and 100 μL of 40 μM peptide solution in MES buffer (pH 5.7, 20 mM) were mixed and added in each well and incubated at 37 °C for 1 hr. The media were removed, and the cover glasses were washed with Tris buffer for three times. Bacteria were fixed using 4% glutaraldehyde solution for overnight. The cover glasses were further dehydrated using a series of graded ethanol solutions from 35, 50, 75, 90, 95 and 100% (contents of

ethanol volume). Samples were placed on a carbon tape and further coated with a 5 nm-thick gold layer. The morphology of the bacteria with and without peptide treatments were observed using a field emission scanning electron microscope operated at an accelerating voltage of 1.0 kV and a working distance of 5.8 mm.

Live and dead bacterial assay

400 μL of bacterial suspensions (*E.coli*, 10^8 CFU/mL) was added to confocal dish and incubated at 37 °C for 24 hrs. Bacterial suspensions were removed from the confocal dish and washed with PBS buffer (pH 7.4) for three times to remove any non-adherent bacteria. 100 μL of fresh MHB media and 100 μL of 40 μM peptide solution in either Tris buffer (pH 7.4, 20 mM) or MES buffer (pH 5.7, 20 mM) was added sequentially in the confocal dish. After incubation at 37 °C for 3 hrs, the culture media were removed and washed with PBS buffer (pH 7.4) for three times. Bacteria were stained with live/dead bacteria assay kit solution at room temperature for 15 min. Finally, bacteria were washed with PBS buffer (pH 7.4) for three times. Images were captured with epifluorescence and processed with ImageJ software.

Membrane localization assay

Bacterial suspensions (*E. coli*, 10^8 CFU/mL) were added to a confocal dish. After 24 hrs of incubation, bacterial suspensions were removed, and confocal dish was washed with PBS buffer (pH 7.4) for three times to remove any non-adherent bacteria. Next, 100 μL of MHB media and 100 μL of 7% FITC-labeled peptides were added to confocal dish to reach a concentration at 40 μM. After 3 hrs of incubation, bacteria were washed with PBS (pH 7.4) for three times. Bacteria were stained with PI at room temperature for 15 min. Finally, bacteria were washed with PBS buffer (pH 7.4) for three times. Images were captured using a fluorescence microscope and processed with ImageJ software.

Hemolytic activity test

Human red blood cells (RBCs) were donated from a volunteer and 4% of human RBCs were prepared in PBS buffer (pH 7.4). 20 μL of peptide solution at various concentrations (1600, 800, 400, 200, 100, 50, and 25 μM) were prepared in PBS buffer (pH 7.4). Peptides were mixed with 180 μL of RBC suspensions in a 1.5 mL Eppendorf tube. The mixtures were incubated at 37 °C for 1 hr, followed by centrifugation at 3000 g for 5 mins. 100 μL of the supernatant was taken out and transferred to a 96-well plate. Hemoglobin release was determined by measuring the absorbance of the supernatant at 540 nm on a microplate reader (Vitor2 1420 Multilabel Counter, PerkinElmer). RBCs treated with 1% Triton-X served as positive controls and untreated RBCs served as a negative control group. Each sample was tested in three replicates. The percentage of hemolysis remained is calculated using the following equation:

% hemolysis = (A peptide-A negative control)/ (A Triton X-A negative control) x 100

in which the negative control group contains RBC suspension mixed with PBS buffer without peptides.

Cytotoxicity measurement

NIH/3T3 cells were seeded onto a 96-well plate at a density of 104 cells/well and incubated for 24 hrs at 37 °C in an incubator with 5% of CO2. After 24 hrs, the culture medium was removed. 10 μL of peptide solution at various concentrations (800, 400, 200, 100, 50, 25, 12.5 μM) was mixed with 90 μL fresh culture medium in a 96-well plate. After 24 hrs of incubation, the MTT assay was performed to quantify the cell viability by monitoring the UV absorbance at 490 nm. Cell culture without peptides were used as a negative control. All the experiments were performed in four replicates.

Measurement of the microenvironmental pH in bacterial colonies

The pH value of the *B. fragilis* living milieu was measured using a pH ratiometric fluorescence imaging probe based on our previous publication with minor modification.2 First, probes in PBS (0.5mg/mL) with different pH values were dropped on surface of the blank TSAB (Trptic Soy Agar with 5% sheep blood) plate, imaged with an in vivo Kodak imager (Ex 630nm, Em 700 nm, Exposure time 10s; Ex 760nm, Em 830 nm, Exposure time 10s). The results were analyzed to acquire a correlation curve between fluorescence ratio and indicated pH value and further plotted as a standard curve. Secondly, probes suspended in DI water (0.5mg/mL) were dropped on individual B. fragilis colonies on a TSAB plate and the plate without bacteria (as a control) and were imaged with the same protocol. The pH around bacterial colonies was determined based on the standard curve established above.

Statistical analysis

Student's t-test was used to analyze the cell viability and hemolytic activity of peptides at different concentrations. Experiments were performed in three replicates. A p-value of less than 0.05 was considered to be statistically significant.

This study was supported by the National Science Foundation
(DMR 1824614) and the start-up funds from the University of Texas at Arlington.

Conflicts of interest

There are no conflicts to declare.

Notes and references

1 (*a*) V. P. Torchilin, *Nat. Rev. Drug Discovery*, 2014, 13, 813; (b)O. Veiseh, B. C. Tang, K. A. Whitehead, D. G. Anderson and R. Langer, *Nat. Rev. Drug Discovery*, 2014, 14, 45; (*c*) E. J. Chung, L. B. Mlinar, K. Nord, M. J. Sugimoto, E. Wonder, F. J. Alenghat, Y. Fang and M. Tirrell, *Adv. Healthcare Mater.*, 2015, 4, 367; (*d*) L. L. Lock, Z. Tang, D. Keith, C. Reyes and H. Cui, *ACS Macro Lett.*, 2015, 4, 552; (*e*) Y. Wang and D. S. Kohane, *Nat. Rev. Mater.*, 2017, 2, 17020; (*f*) D. Rosenblum, N. Joshi, W. Tao, J. M. Karp and D. Peer, *Nat. Commun.*, 2018, 9, 1410.

2 (*a*) H. J. Chung and T. G. Park, *Nano Today*, 2009, 4, 429; (*b*) H. Hosseinkhani, P.-D. Hong and D.-S. Yu, *Chem. Rev.*, 2013, 113, 4837; (*c*) L. Zhang, J. M. Chan, F. X. Gu, J.-W. Rhee, A. Z. Wang, A. F. Radovic-Moreno, F. Alexis, R. Langer and O. C. Farokhzad, *ACS Nano*, 2008, 2, 1696.

3 (*a*) L. Gu and D. J. Mooney, *Nat. Rev. Cancer*, 2015, 16, 56; (b) D. A. Scheinberg, C. H. Villa, F. E. Escorcia and M. R. McDevitt, *Nat. Rev. Clin. Oncol.*, 2010, 7, 266; (*c*) J. A. Barreto, W. O'Malley, M. Kubeil, B. Graham, H. Stephan and L. Spiccia, *Adv. Mater.*, 2011, 23, H18; (*d*) Q. Sun, Z. Zhou, N. Qiu and Y. Shen, *Adv. Mater.*, 2017, 29, 1606628.

4 (*a*) A. F. Radovic-Moreno, T. K. Lu, V. A. Puscasu, C. J. Yoon, R. Langer and O. C. Farokhzad, *ACS Nano*, 2012, 6, 4279; (*b*) M. Hughes, S. Debnath, C. W. Knapp and R. V. Ulijn, *Biomater. Sci.*, 2013, 1, 1138; (*c*) B. Horev, M. I. Klein, G. Hwang, Y. Li, D. Kim, H. Koo and D. S. W. Benoit, *ACS Nano*, 2015, 9, 2390; (*d*) M. Xiong, Y. Bao, X. Xu, H. Wang, Z. Han, Z. Wang, Y. Liu, S. Huang, Z. Song, J. Chen, R. M. Peek, L. Yin, L.-F. Chen and J. Cheng, *Proc. Natl. Acad. Sci. U. S. A.*, 2017, 114, 12675.

5 (a) S. Fuchs, J. Pane´-Farre´, C. Kohler, M. Hecker and S. Engelmann, J. Bacteriol., 2007, 189, 4275; (b) B. Marteyn, F. B. Scorza, P. J. Sansonetti and C. Tang, Cell. Microbiol.,2011, 13, 171.

6 (a) R. Dubos, Lancet, 1955, 266; (b) A. S. Trevani, G. Andonegui, M. Giordano, D. H. Lo´pez, R. Gamberale, F. Minucci and J. R. Geffner, J. Immunol., 1999, 162, 4849; (c) B. J. Marsland and E. S. Gollwitzer, Nat. Rev. Immunol., 2014, 14, 827; (d) M. Kilian, I. L. C. Chapple, M. Hannig, P. D. Marsh, V. Meuric, A. M. L. Pedersen, M. S. Tonetti, W. G. Wade and E. Zaura, Br. Dent. J., 2016, 221, 657.

7 R.-C. Mercier, C. Stumpo and M. J. Rybak, J. Antimicrob. Chemother., 2002, 50, 19.

8 (a) D. Xu, D. Dustin, L. Jiang, D. S. K. Samways and H. Dong, Chem. Commun., 2015, 51, 11757; (b) D. Xu, L. Jiang, A. Singh, D. Dustin, M. Yang, L. Liu, R. Lund, T. J. Sellati and H. Dong, Chem. Commun., 2015, 51, 1289.

9 D. Xu, W. Chen, Y. J. Tobin-Miyaji, C. R. Sturge, S. Yang, B. Elmore, A. Singh, C. Pybus, D. E. Greenberg, T. J. Sellati,W. Qiang and H. Dong, ACS Infect. Dis., 2018, 4, 1327.

10 Y.-T. Tsai, J. Zhou, H. Weng, J. Shen, L. Tang and W.-J. Hu, Adv. Healthcare Mater., 2014, 3, 221.

11 W. Aoki, K. Kuroda andM.Ueda, J. Biosci. Bioeng., 2012, 14, 365.

Figures

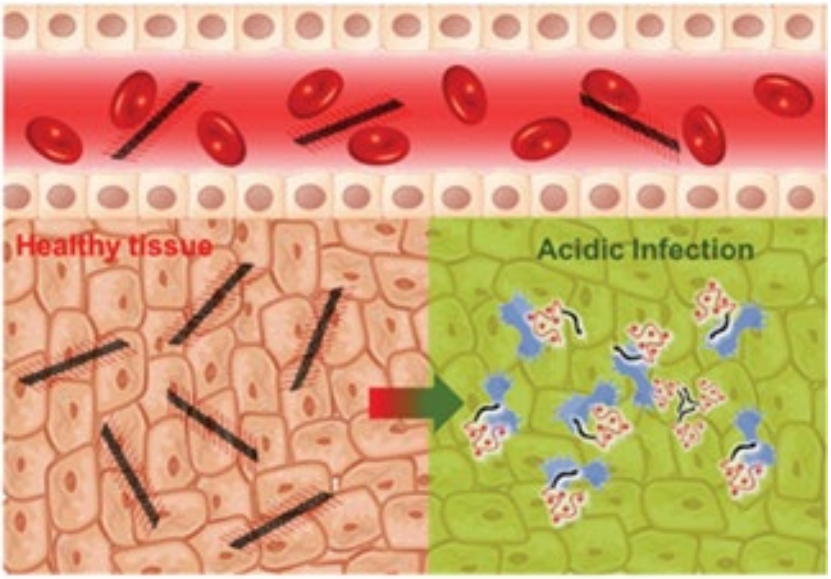

Figure 12. Cartoon representation of cytocompatible and hemocompatible SANs formed by pH responsive MDPs and their disassembly triggered by local bacterial acidity for the delivery of activated MDPs to eradicate bacteria.

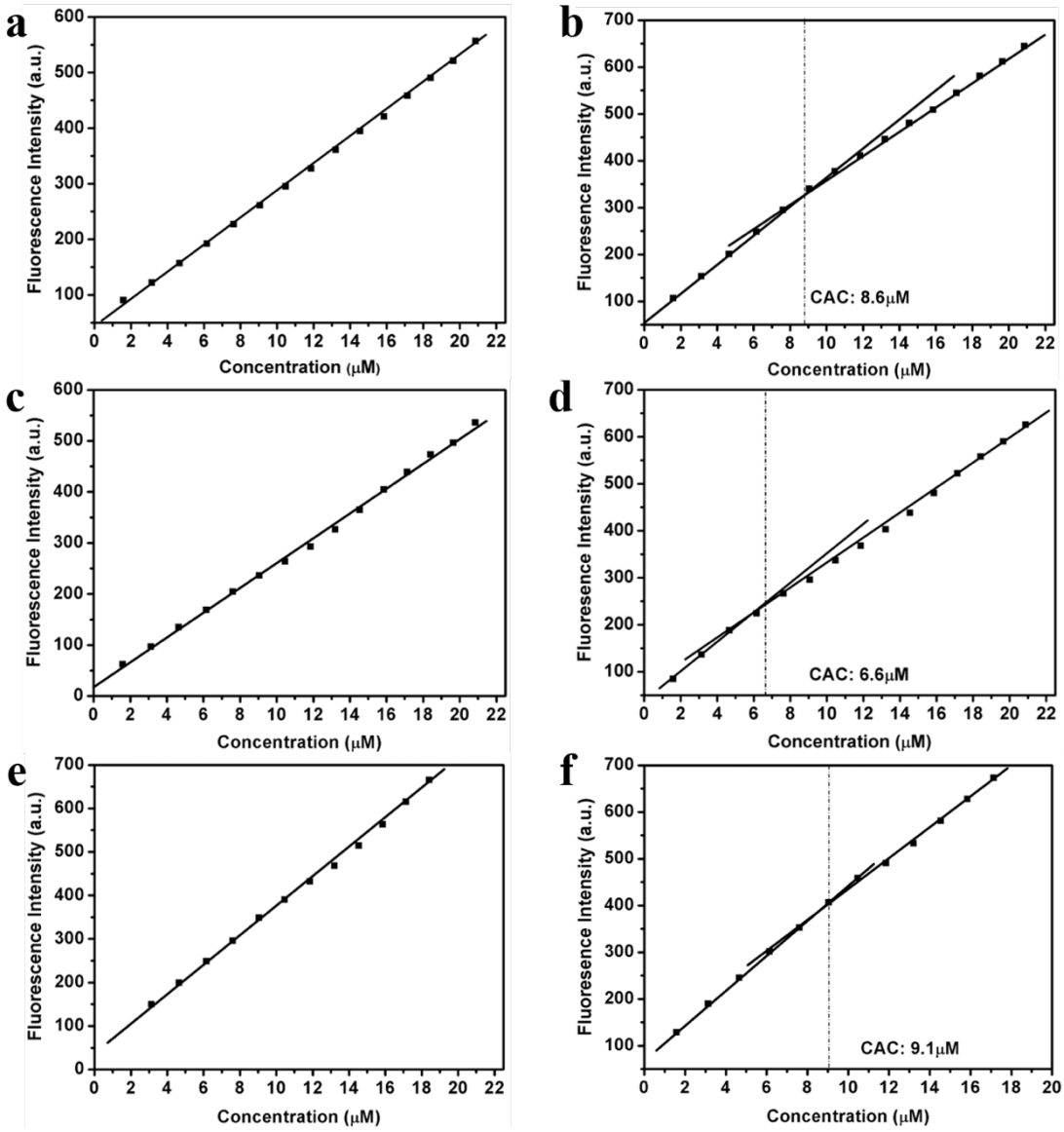

Figure 13. CAC determination by monitoring the tryptophan fluorescence at various peptide concentrations at pH 7.4 and pH 5.7. WH5 at (a) and pH 5.7 (b) pH 7.4; WH7 at (c) pH 5.7 and (d) pH 7.4; WH9 at (e) pH 5.7 and (f) pH 7.4.

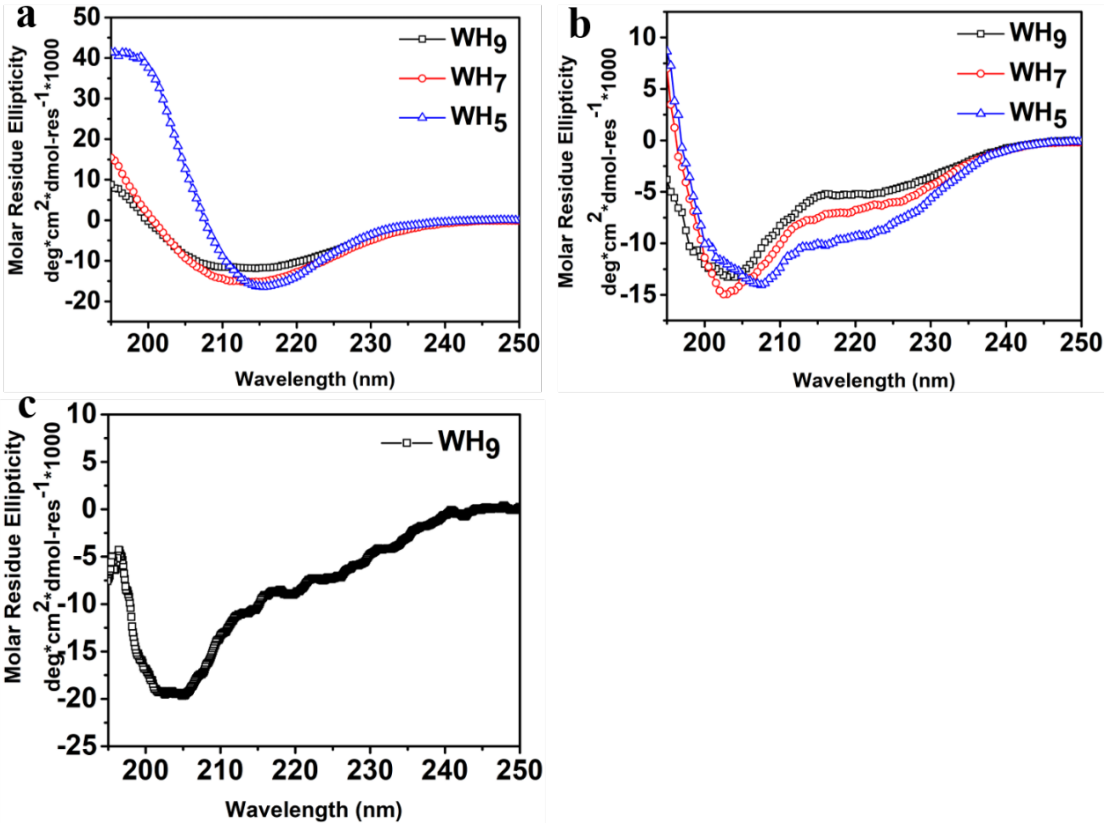

Figure 14. pH-dependent peptide secondary structures by CD spectroscopy at RT. (a) CD spectra of peptides showing predominant β-sheet secondary structures in Tris buffer (pH 7.4, 20 mM); (b) CD spectra of peptides in MES buffer (pH 5.7, 20 mM) showing weak helices/random coils; (c) CD spectrm of the filtrate of WH9 in MES buffer (pH 5.7, 20 mM) showing a random coiled strcuture. Peptide concentration: 50 μM.

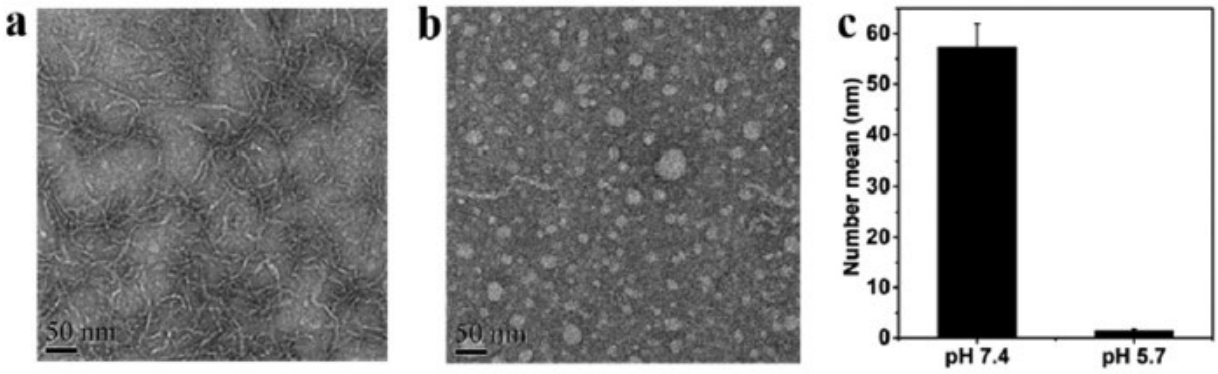

Figure 15. Negatively stained TEM images of WH_9 at (a) pH 7.4 showing SANs formation and (b) at pH 5.7 showing SANs disassembly. (c) pH-Dependent hydrodynamic size measurement by DLS. Peptide concentration: 100 μM in Tris buffer (pH 7.4, 20 mM) and MES buffer (pH 5.7 20 mM)

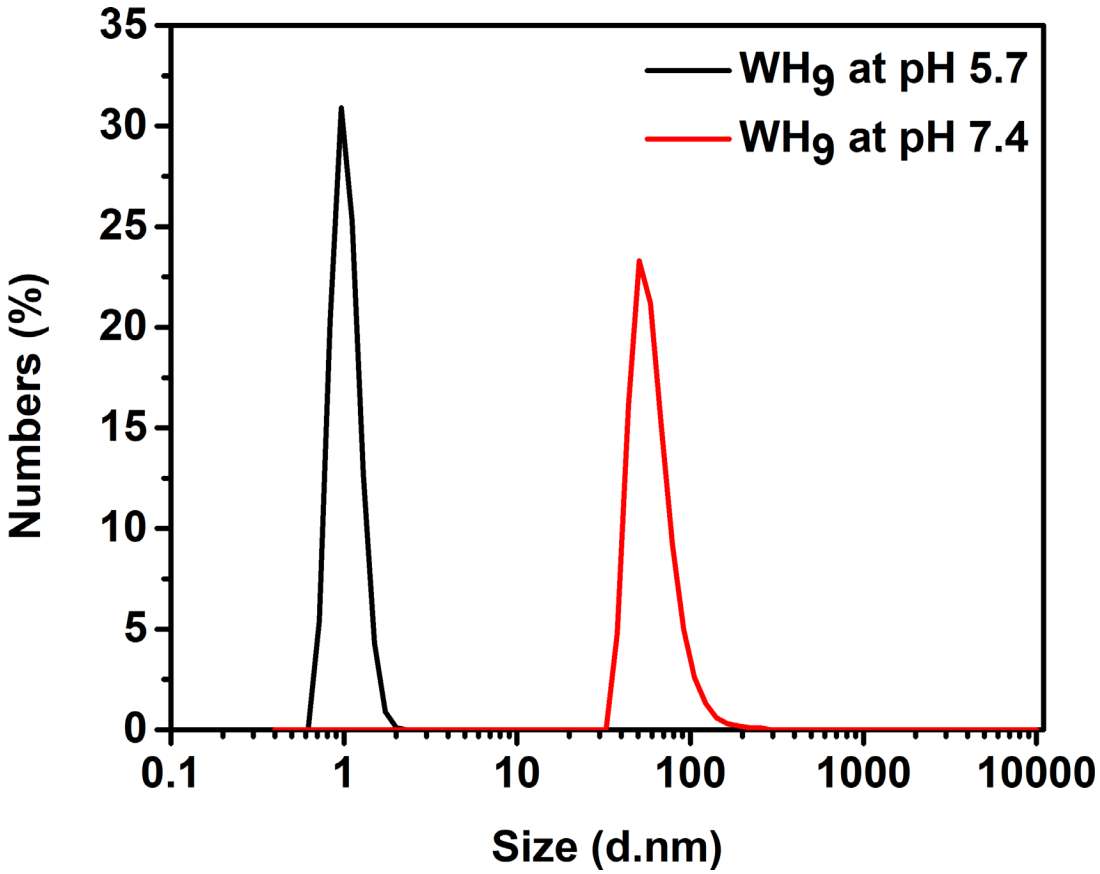

Figure 16. Particle size distribution by numbers (%) of WH9 at neutral and acidic condition.

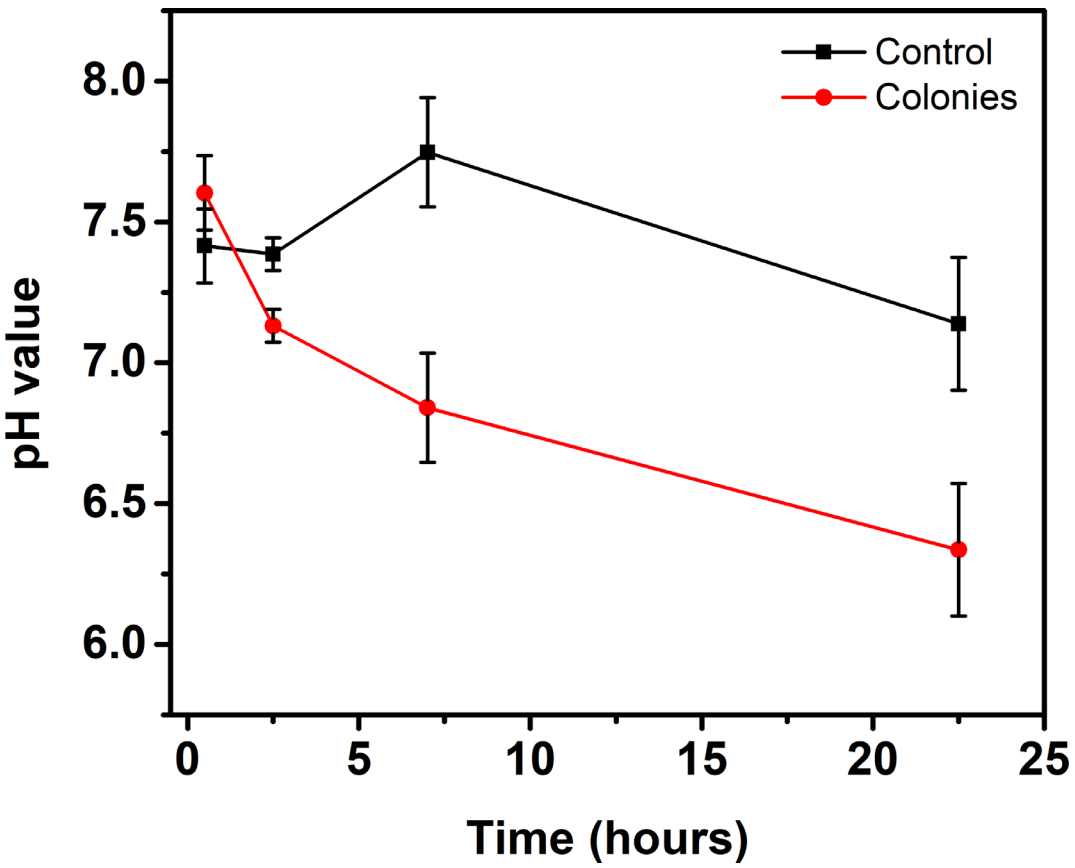

Figure 17. Time-dependent local pH of B. fragilis on the agar plate.

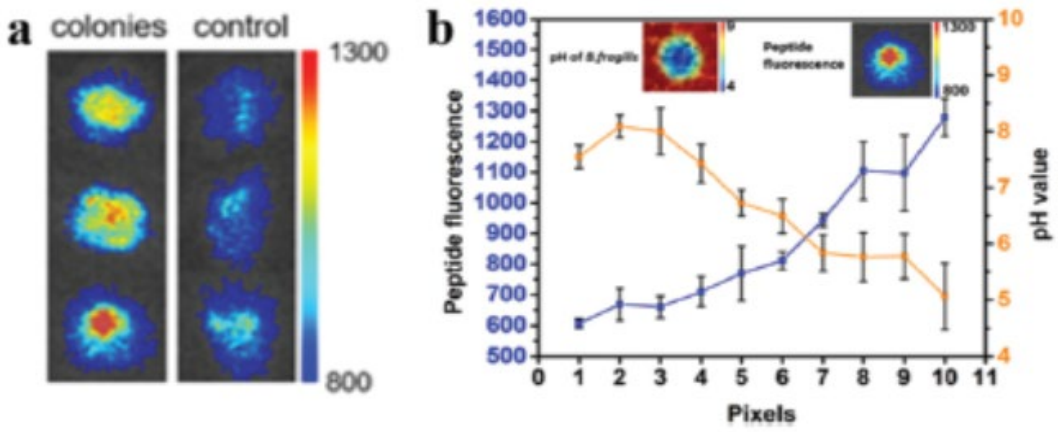

Figure 18. Local bacterial acidity triggered peptide disassembly as determined by in situ fluorescence microscopy (a) Fluorescence intensity of Rho-labeled WH_9 deposited on 3 bacterial colonies (3 spots on the left panel) compared to those on agar media (right panel) without bacteria showing that the acidic bacterial environment induces SANs disassembly that led to the recovery of the self-quenched rhodamine fluorescence. (b) Correlation of the local bacterial pH (orange line) with the fluorescence intensity of the Rho-labeled WH_9 (blue lines) applied on bacterial colonies. The inset pictures are fluorescent microscopic images of bacterial colonies upon Rho-labeled peptide treatment (right) and colonies containing the near infrared pH probe (left).

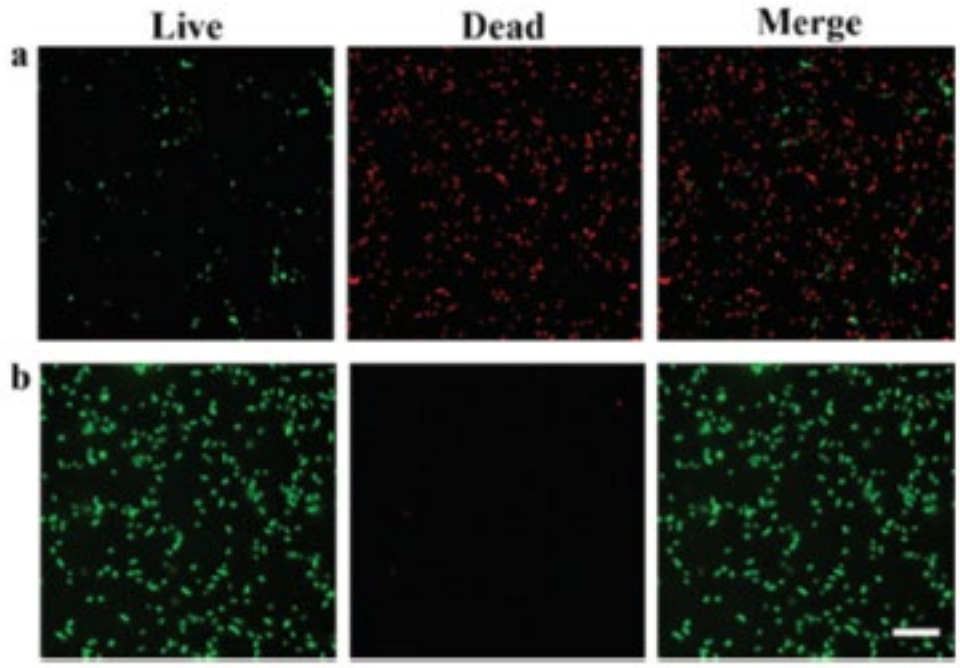

Figure 19. Fluorescence images of live/dead bacterial assay results (*E. coli*). Top panel: *E.coli* treated with 20 μM WH_9 at (a0 pH 5.7 and (b) pH 7.4 for 3 h. Live bacteria were stained with SYTO9 (green) and dead bacteria were stained with PI (red). Scale bar: 20 μM

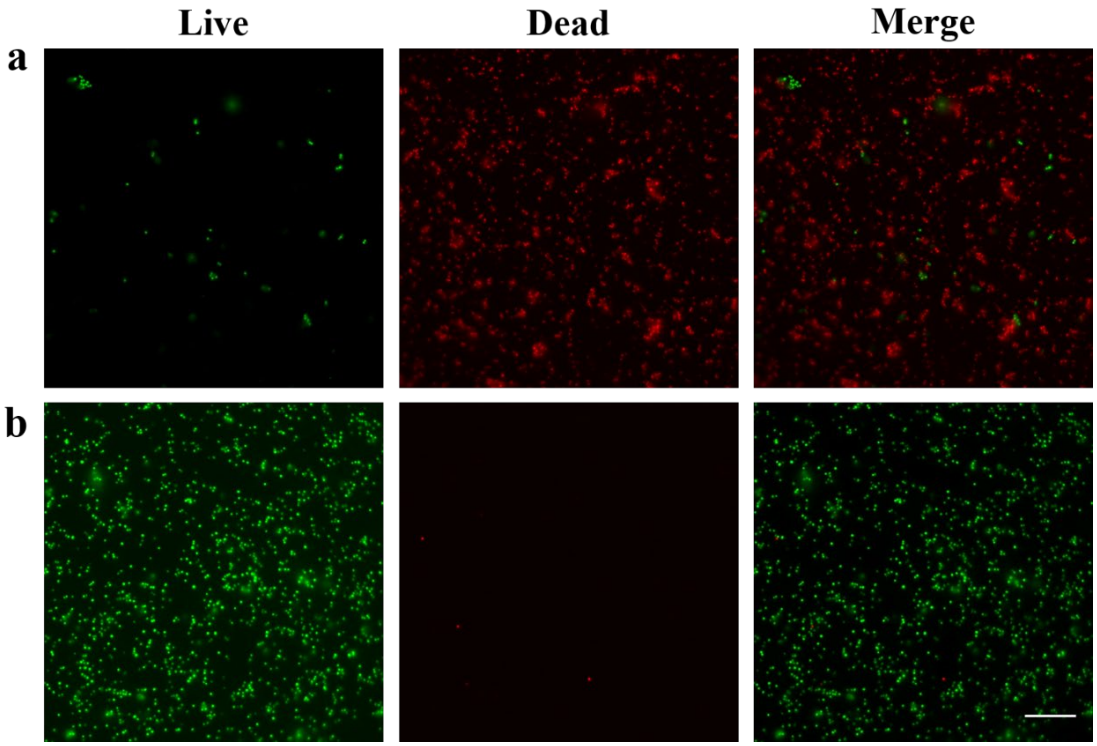

Figure 20. Fluorescence images of Live/dead bacterial assay results (*S. aureus*). Top panel: *S. aureus* treated with 10 μM WH9 at (a) pH 5.7 and (b) pH 7.4 for 3hrs. Live bacteria were stained with SYTO9 (green) and dead bacteria was stained with PI (red). Scale bar: 20 μm.

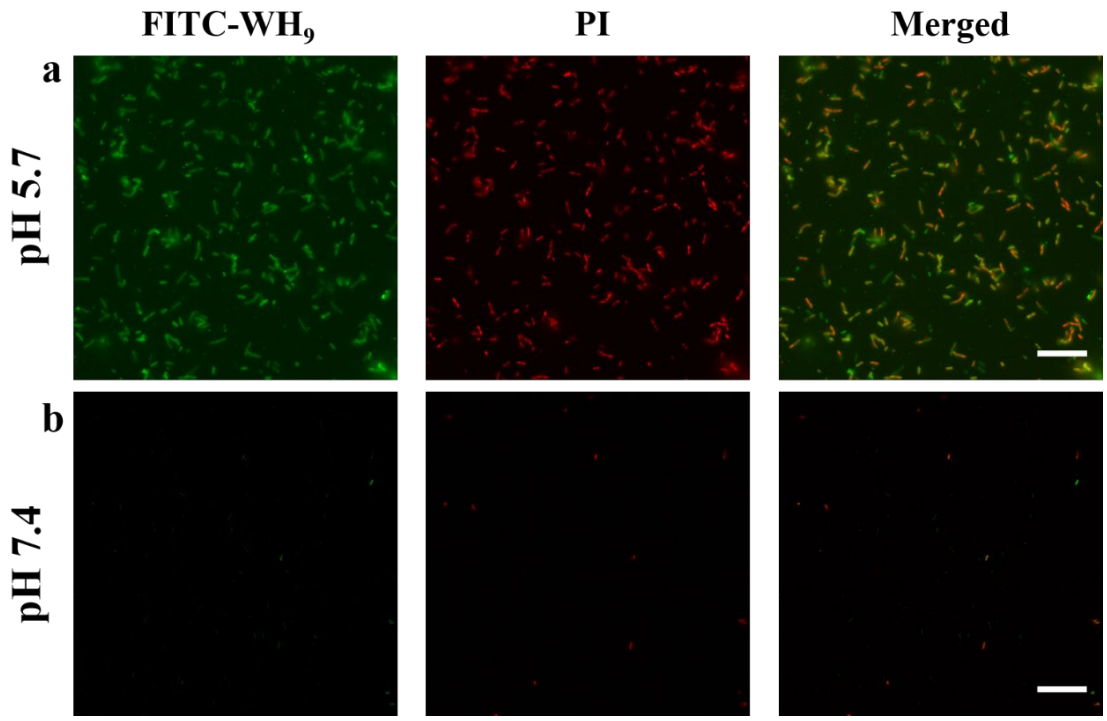

Figure 21. Fluorescence images of *E.coli* treated with FITC-WH9 followed by PI staining in (a) acidic (pH 5.7) and (b) neutral culture condition (pH 7.4). FITC-WH9 was found to attach on the bacterial membrane in the acidic condition, causing membrane disruption and bacterial death as stained by PI. Scale: 20 μm.

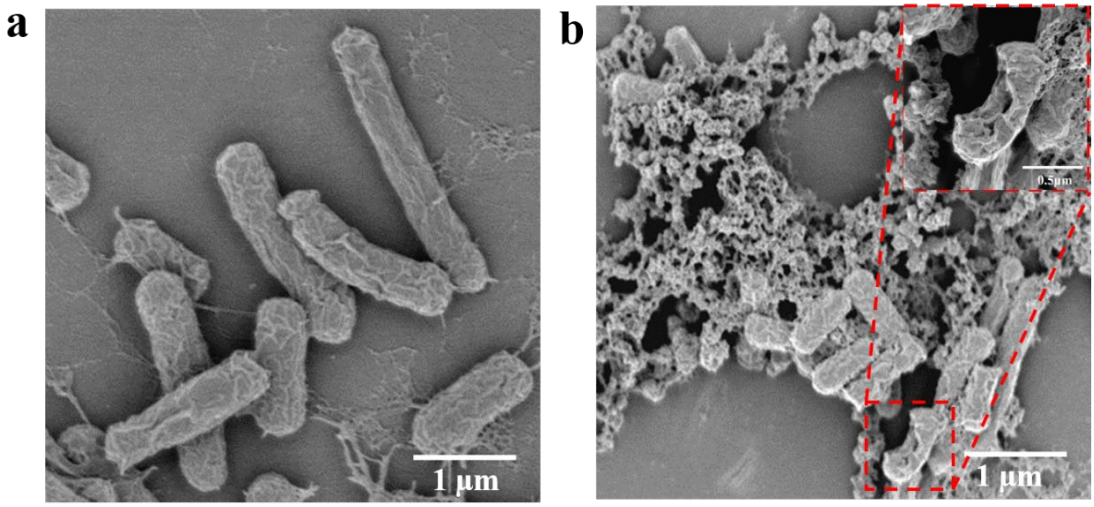

Figure 22 SEM images showing the morphological change of *E. coli* with and without peptide treatment in the acidic condition. a) E. coli without peptide treatment at pH 5.7. b) *E. coli* upon WH_9 incubation (2x MIC) for 1 hr at pH 5.7. The inset picture shows the damage of bacterial membrane upon peptide treatment.

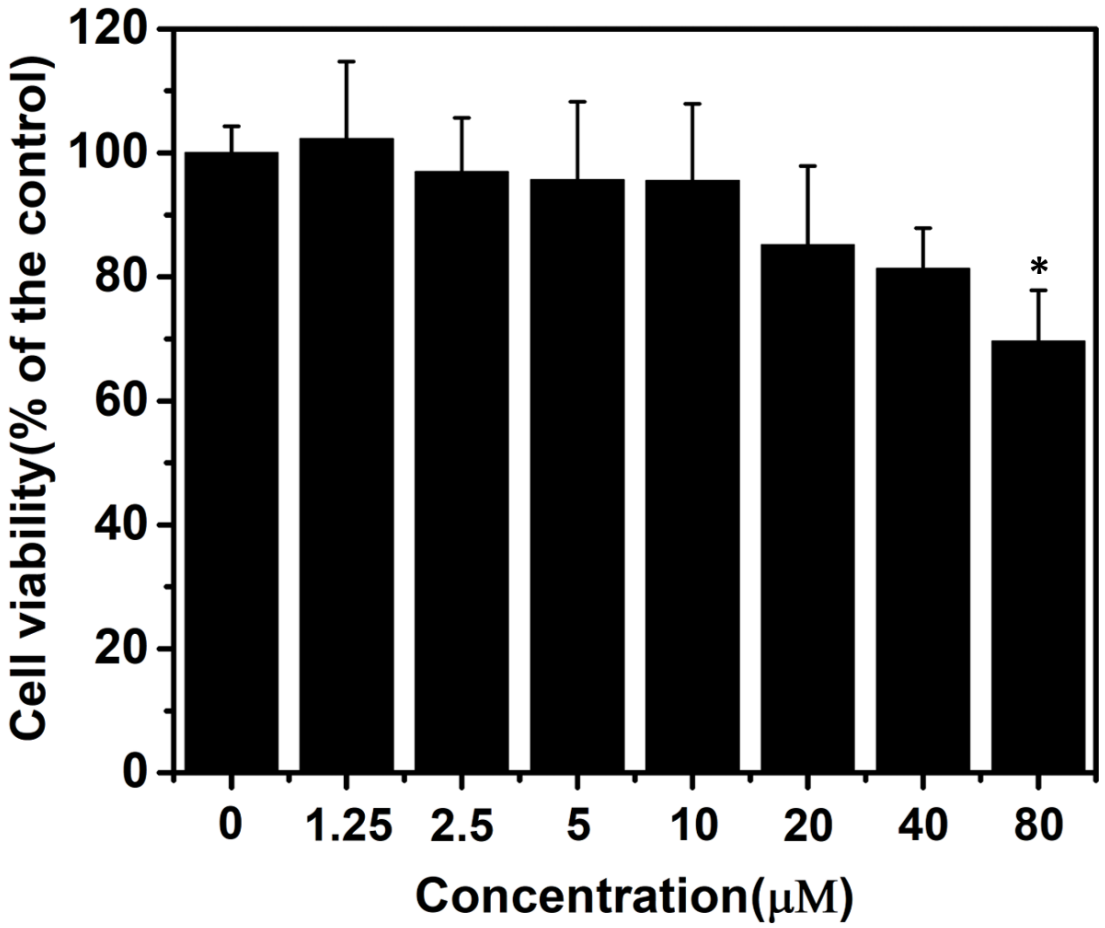

Figure 23. NIH/3T3 cell viability of peptide-treated cells in relative to the control group without peptide after 24 hrs of incubation with WH_9 at various concentrations. Statistically significant differences are indicated by * P< 0.05.

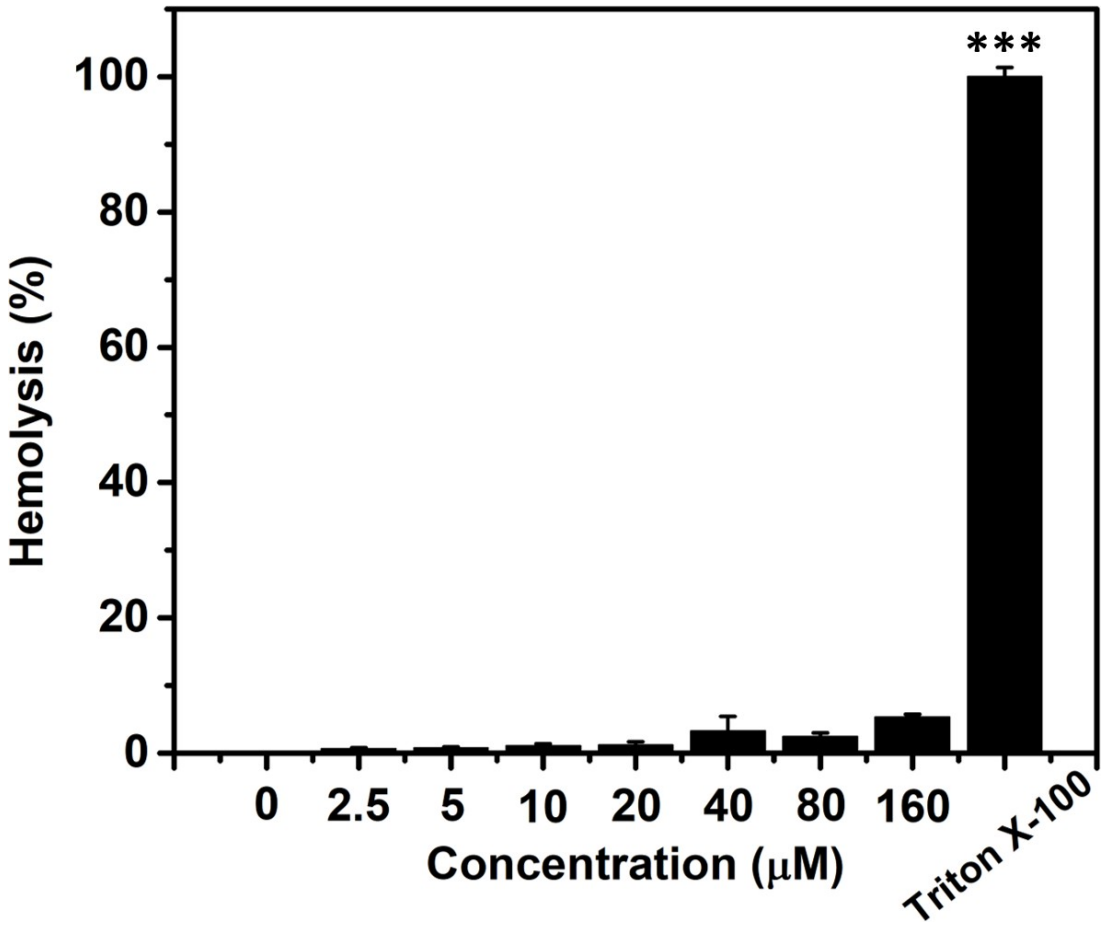

Figure 24. The percentage of hemolysis induced by WH_9 at various peptide concentrations. Statistically significant differences are indicated by *** $p < 0.001$

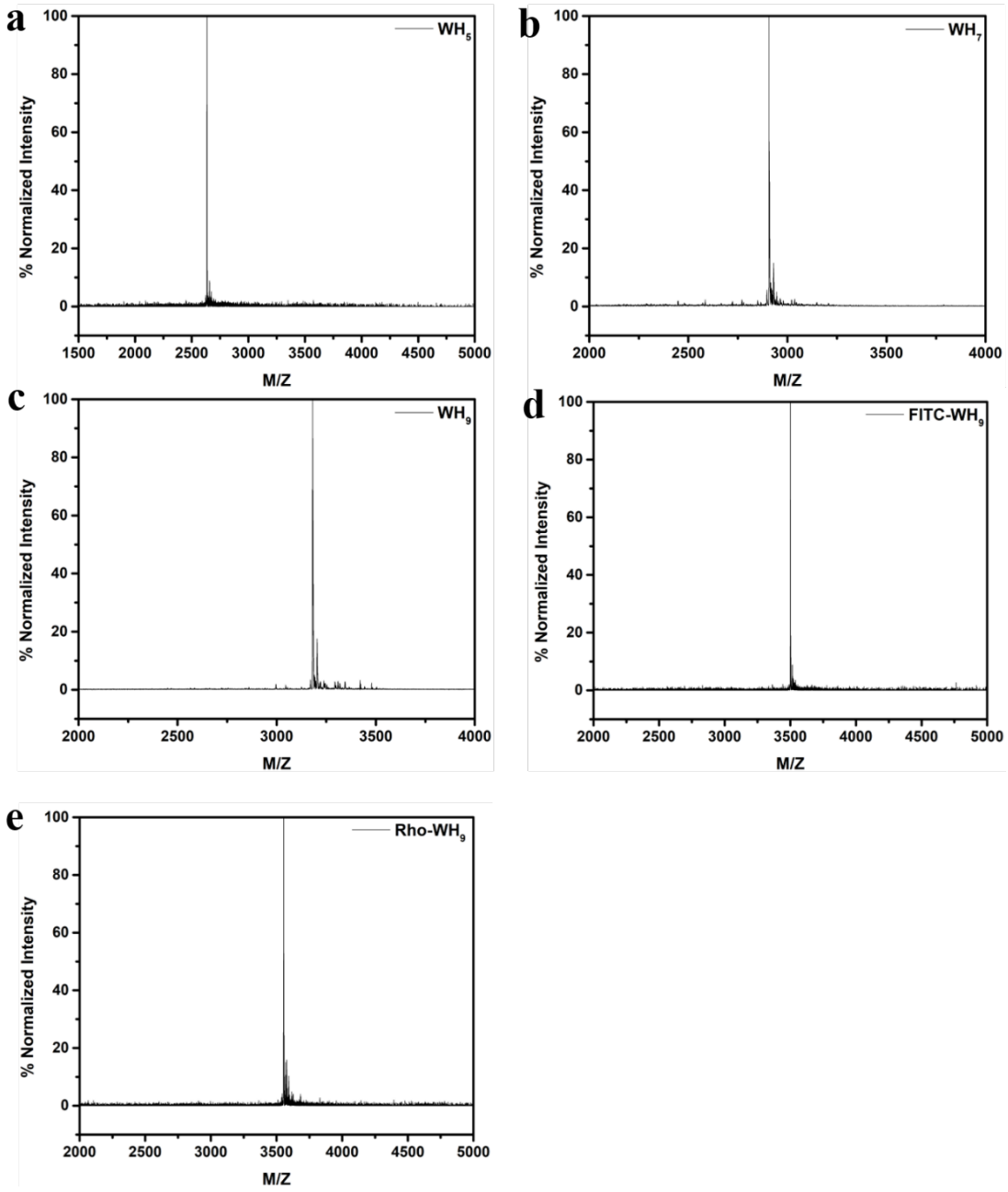

Figure 25. MADLI spectra of WH_5 (a), WH_7 (b), WH_9 (c), FITC-WH_9 (d) and Rho-WH_9 (e)

Tables

Table 8. Quantification of disassembled MDPs

	10 kDa filter		30 kDa filter	
Peptides	pH 7.4	pH 5.7	pH 7.4	pH 5.7
WH_5	0	24.60 ± 0.08%	0	37.77 ± 0.56%
WH_7	0	34.70 ± 0.08%	0	62.56 ± 3.55%
WH_9	0	41.00 ± 0.49%	0	71.64 ± 0.27%

Standard deviation is calculated based on 3 measurements for each sample.

Table 9. Antimicrobial activity, cytotoxicity and hemolytic activity

MIC (μM)					IC_{50} (μM)	HC_{10} (μM)
Anaerobic			Aerobic			
E. coli	*B. fragilis*	*S. aureus*	*E. coli*			
			pH 7.4	pH 5.7		
10	5	5	>40	10	>80	>160

CHAPTER 6

CONCLUSIONS AND DISCUSSION

While the discussion of biofilm infection on devices in Chapter 2 illustrates the challenges and importance of controlling biofilm infection, it represents only one instance of biofilm infection. Bacterial biofilms have been implicated in a variety of chronic human infections (1-3). The diverse location of these infections presents its own challenges for treatment that must account for anatomical location, host factors and the bacterial populations and phenotypes present in these biofilms. By better understanding the biofilm life cycle, new interventions can be developed to stop this type of infection. There are four key strategies that can be applied to this goal: prevention, weakening, disruption and killing. The prevention of biofilm formation can incorporate material science to develop materials that inhibit biofouling by modification of the surface properties or activate under certain conditions exposing pharmacophores to kill colonizing bacteria. A growing body of evidence also supports a variety of life-style factors and co-morbidities that may predispose the host to infection, including obesity, diabetes and smoking (4) much like factors that predispose people to chronic conditions like diabetes and heart disease. This raised the possibility that by changing habits and modifying lifestyle behaviors could play a role in reducing the incidence of biofilm infections. Traditional treatment for infection involves antimicrobial chemotherapy and the unique nature of biofilm infections due to their emergent resistance makes this a challenge (5, 6). The current three pharmacokinetic and pharmacodynamic (PK/PD) parameters used to assess the drivers of efficacy, AUC/MIC, Cmax/MIC and Time/MIC all share a fundamental weak point: each of these parameters incorporate planktonically derived MIC value to set the therapeutic dose (7-9). A concerted effort to examine these parameters considering experimental values that indicate kill biofilm cells need to be undertaken. To combat resistance and to target subpopulations of bacteria within biofilms, cocktails of antibiotics with different classes are currently used. With the use of antibiotics comes the risk of resistance development so strategies are required to overcome this limitation. Intrinsically, the use of antibiotic cocktails help suppress resistance this based on the

different targets for given agents. The development of novel antibacterial agents will help add to the options available clinically.

Chapter 4 describes the development of peptide nanofibers that activate in acidic microenvironments driven by the presence of bacteria. The advantage of antibacterials like this, besides the membrane disruptive activity, is that the agent becomes activated under specific conditions. An advantage of this targeted activation would be to prevent the host microbiome from being exposed to sub-MIC concentrations of antibacterial, thus selecting to resistant phenotypes and placing commensals under the same selective pressure as the pathogens. In this instance the normal flora in the body can act as a reservoir of antibiotic resistance (via horizontal gene transfer) and, as many of these commensals are opportunistic pathogens, a source of drug-resistant infection. The responsive assembling nanofibers become more active under conditions driven by the bacteria, resulting in a *de facto* delivery system not only targeting pathogens but activating in the environment generated by them. By coupling a mode of action that is non-specific against bacteria (e.g. membrane disruption) with a delivery system, this reduces the chances that resistant mutants will arise outside the infection environment or in normal flora. This leads to the idea of responsive agents or formulations that would activate under different physiological conditions to deliver antibiotics in a precisely targeted manner. The development of this responsive AMP couples this targeted delivery with an antibacterial class used by virtually every life form on the planet and thus has a proven track record of efficacy. Such a targeting approach should also not be limited strictly to AMPs. This technology could also be applied to other therapeutics, including EPS targeting agents, quorum sensing inhibitors or disruptors and anti-virulence factor agents. These strategies represent new approaches to interfere the establishment of biofilm or aid in the disruption of existing biofilm

While such approaches are innovative and can lead to new treatments, the lack of cidality of some of these new technologies could prove challenging from a regulatory and safety

perspective. It would probably be necessary to use these agents in conjunction with proven antibacterial agents to prevent re-seeding of the biofilm or systemic infections as these agents do not “kill”. It would also require the development of new techniques to determine the efficacy of these agents in pre-clinical models as antibacterial efficacy is not a study endpoint. While there would be regulatory hurdles to developing such agents, a precedent exists in the form of β-lactamase inhibitors used to stop the inactivation of β-lactam antibiotics by these enzymes.

Finally, the detection of infection and determining an exact location of infectious foci are extremely helpful in the initiation and guiding of antibacterial chemotherapy. The PET method described in Chapter 3 will be able to provide highly detailed location information and, when coupled with CT, highly precise anatomical information. Being able to pinpoint the locations or presence of infection can determine the type of intervention needed, particularly in some circumstances, the type antibacterial agent used. For example, prosthetic device infections are predominantly caused by coagulase-negative staphylococci, *Staphylococcus epidermidis* and *Staphylococcus aureus*. In cystic fibrosis infections, early in life the pathogens isolated are *Staphylococcus aureus* and *Hemophilus influenza*, while in later life *Pseudomonas aeruginosa* becomes the prominent pathogen. This information is factored into empiric therapy matrices that are implemented during the initiation of antibacterial chemotherapy and being able to add a spatial confirmation of the location of infection will help refine this process. Knowing the location of an infection coupled with information on the most prevalent pathogens from clinical experience can guide the selection of agents used to treat these infections. If surgical interventions are required for debridement and cleaning of wounds or infection foci, these imaging generated by the PET methods in Chapter 3 would provide the surgeon with a highly accurate map of site ideally limiting the amount of trauma and ensuring the removal of infected tissue. The directly labeling of pathogens using D-glutamine PET tracers will also help more confidently confirm the presence of infection. The direct imaging ability of the D-gln tracers also

will allow physicians to monitor the effectiveness of therapy in a clinical setting and aid scientists in the development of new and refinement of older technologies when targeting infectious foci. This tool will immensely help in the preclinical development of antibacterial agents by monitoring the efficacy of experimental agents and confirmation of PK/PD parameters in the treatment of infection.

For chronic wounds, while sharp debridement is the “gold standard” for care of infected chronic wounds(10, 11), it remains critical to determine what pathogens are present to guide the appropriate therapy. The diagnostic tools presented in Chapter 4 provide this information. One complicating variable with *in-situ* measurement is differentiation of normal flora from pathogens. Tracers like the D-glutamine tracer in Chapter 3 would be lost in the background of the gut normal flora and possibly on the skin as well. This does not necessarily rule out nuclear medicine in the use of diagnosing wound infection. A hypothetical situation where it could prove useful is if the infected wounds contain a higher signal than background or uninfected wounds. Establishing these benchmarks through further experimentation would be necessary to confirm the use of PET tracers for wound infection diagnosis.

An additional point of interest is the ability of the molecular and culture methods used in wound infection diagnosis to identify the bacteria present. There is a growing body of literature that points to microbiomes that stimulate healing and those that are present in non-healing chronic wounds(12-14). The implication here is that the clinician could intervene with targeted agents against certain microbes or through a combination of antimicrobials followed by probiotics, restore or establish a “healing microbiome” in these chronic wounds (15-17).

The information and technologies presented here will help guide the development of new therapies and treatment strategies. The increasing knowledge about biofilm infections will generate new ideas to intervention and prevention. The use of nuclear medicine, specifically D-glutamine PET tracers will allow the visualization of infection facilitating diagnosis, development

of new agents and assessment of treatment. The development of targeted environmentally activated antibacterial agents will help to reduce the development of drug resistance and inhibit the spread of resistance to commensal bacteria. This increased body of knowledge and application is occurring at an ideal time to help us prevent the emergence of the post-antibiotic age.

References

1. Donlan RM. 2002. Biofilms: microbial life on surfaces. Emerging infectious diseases 8:881-890.
2. Høiby N, Bjarnsholt T, Moser C, Bassi GL, Coenye T, Donelli G, Hall-Stoodley L, Holá V, Imbert C, Kirketerp-Møller K, Lebeaux D, Oliver A, Ullmann AJ, Williams C, Biofilms ESGf, Consulting External Expert Werner Z. 2015. ESCMID guideline for the diagnosis and treatment of biofilm infections 2014. Clinical Microbiology and Infection 21:S1-S25.
3. Malone M, Bjarnsholt T, McBain AJ, James GA, Stoodley P, Leaper D, Tachi M, Schultz G, Swanson T, Wolcott RD. 2017. The prevalence of biofilms in chronic wounds: a systematic review and meta-analysis of published data. J Wound Care 26:20-25.
4. Stewart PS, Parker AE. 2019. Measuring Antimicrobial Efficacy against Biofilms: A Meta-Analysis. Antimicrobial agents and chemotherapy doi:10.1128/AAC.00020-19.
5. Davies D. 2003. Understanding biofilm resistance to antibacterial agents. Nature Reviews Drug Discovery 2:114-122.
6. Stewart P. 2018. How Bacteria in Biofilms Withstand Antibiotics. Montana Biofilm Science and Technology Meeting 2018.
7. Craig WA. 1998. Pharmacokinetic/Pharmacodynamic Parameters: Rationale for Antibacterial Dosing of Mice and Men. Clinical Infectious Diseases 26:1-10.
8. Drusano GL. 2004. Antimicrobial pharmacodynamics: critical interactions of 'bug and drug'. Nature reviews Microbiology 2:289-300.
9. Mouton JW, Dudley MN, Cars O, Derendorf H, Drusano GL. 2005. Standardization of pharmacokinetic/pharmacodynamic (PK/PD) terminology for anti-infective drugs: an update. Journal of antimicrobial chemotherapy 55:601-607.
10. Nusbaum AGBS, Gil JBS, Rippy MKDVMPD, Warne BDPM, Valdes J, Claro ABS, Davis SCBS. 2012. Effective Method to Remove Wound Bacteria: Comparison of Various

Debridement Modalities in an In Vivo Porcine Model. Journal of Surgical Research 176:701-707.

11. Schultz GS, Barillo DJ, Mozingo DW, Chin GA, Wound Bed Advisory Board M. 2004. Wound bed preparation and a brief history of TIME. International wound journal 1:19-32.
12. Ammons MCB, Morrissey K, Tripet BP, Van Leuven JT, Han A, Lazarus GS, Zenilman JM, Stewart PS, James GA, Copié V. 2015. Biochemical Association of Metabolic Profile and Microbiome in Chronic Pressure Ulcer Wounds. PloS one 10:e0126735.
13. Gardner SE, Hillis SL, Heilmann K, Segre JA, Grice EA. 2012. The Neuropathic Diabetic Foot Ulcer Microbiome Is Associated With Clinical Factors. Diabetes (New York, NY) 62:923-930.
14. Grice EA, Snitkin ES, Yockey LJ, Bermudez DM, Liechty KW, Segre JA. 2010. Longitudinal shift in diabetic wound microbiota correlates with prolonged skin defense response. Proceedings of the National Academy of Sciences doi:10.1073/pnas.1004204107:201004204.
15. Lolou V, Panayiotidis MI. 2019. Functional Role of Probiotics and Prebiotics on Skin Health and Disease. Fermentation (Basel) 5:41.
16. Lukic J, Chen V, Strahinic I, Begovic J, Lev-Tov H, Davis SC, Tomic-Canic M, Pastar I. 2017. Probiotics or pro-healers: the role of beneficial bacteria in tissue repair. Wound repair and regeneration 25:912-922.
17. Peral MC, Rachid MM, Gobbato NM, Martinez MAH, Valdez JC. 2010. Interleukin-8 production by polymorphonuclear leukocytes from patients with chronic infected leg ulcers treated with Lactobacillus plantarum. Clinical Microbiology and Infection 16:281-286.